

EIGHTEENTH INTERNATIONAL CONFERENCE
ON
LIQUID AND AMORPHOUS METALS

LAM 18

JMS DASTER PLAZA
Hiroshima International Youth House

September 4-7

&

Online September 8-9, 12

2022



EIGHTEENTH INTERNATIONAL CONFERENCE
ON
LIQUID AND AMORPHOUS METALS

LAM 18

JMS & ASTER PLAZA
Hiroshima International Youth House

September 4-7

&

Online September 8-9, 12

2022

CONFERENCE ORGANIZATION

ORGANIZING COMMITTEE

Chair (General): M. Inui (Hiroshima Univ.)
Chair (Program): F. Shimojo (Kumamoto Univ.)
Co-Chair: S. Hosokawa (Kumamoto Univ.)
Co-Chair: H. Kato (Tohoku Univ.)

Y. Kajihara (Hiroshima Univ.)	S. Munejiri (Hiroshima Univ.)
S. Ohmura (Hiroshima Inst. Tech.)	S. Kohara (NIMS)
H. Masai (AIST)	T. Morishita (AIST)
Y. Kawakita (J-PARC)	K. Matsuda (Kumamoto Univ.)
S. Tahara (Univ. of Ryukyus)	H. Shimakura (Niigata Univ. of PALS)
T. Usuki (Yamagata Univ.)	T. Iwashita (Oita Univ.)
J. Saida (Tohoku Univ.)	T. Otomo (KEK)
K. Fuchizaki (Ehime Univ.)	K. Kimura (Univ. of Tokyo)
A. Chiba (Keio Univ.)	

INTERNATIONAL ADVISORY BOARD

A. Di Cicco (Italy)	C. D. Dalian (China)
B. Gelchinski (Russia)	D. J. Gonzalez (Spain)
S. Hosokawa (Japan)	M. Inui (Japan)
H. Liu (China)	W. C. Pilgrim (Germany)
P. Popel (Russia)	J. F. Wax (France)
K. F. Kelton (USA)	D. L. Price (France)
P. S. Salmon (UK)	F. Shimojo (Japan)
T. Scopigno (Italy)	M. Vasin (Russia)

INTERNATIONAL PROGRAM COMMITTEE

T. Bryk (Ukraine)	F. Demmel (UK)
S. De Panfilis (Italy)	V. Giordano (France)
D. Holland-Moritz (Germany)	N. Jakse (France)
J. Z. Jiang (China)	K. Khishchenko (Russia)
B. Ruta (France)	W. Schirmacher (Germany)
V. Sidorov (Russia)	M.-L. Saboungi (France)
P. Svec (Slovak Republic)	H. Kato (Japan)

SPONSOR

THE KAJIMA FOUNDATION

(鹿島学術振興財団)

JSMS Committee on Metallic Glasses

(日本材料学会金属ガラス部門委員会)

ELECTRIC TECHNOLOGY RESEARCH FOUNDATION OF CHUGOKU

(中国電力技術研究財団)

SPONSOR Company

Heraeus K.K.

MAKABE R&D Co.,LTD

SCOPE OF CONFERENCE

Since the 60s the state-of-the-art in the field of liquid and amorphous metals and alloys is the focus of an international conference, the “Liquid and Amorphous Metals conference” (LAM), which is in its 18th conference. Born as a conference on liquid metals in 1966 at Brookhaven, since 1980 it has been renewed including amorphous metals (1980, Grenoble, France) and then has continued a three years basis, with the last three editions held in Beijing, China, in 2013, in Bonn, Germany, in 2016 and in Lyon, France, in 2019.

The aim of the LAM conferences is to bring together scientists working in the field of liquid and amorphous metals in order to discuss new advances and future directions in this intriguing field of condensed matter physics, chemistry and materials sciences. Although primarily aimed at discussing the hottest topics in liquid and amorphous metals including semiconductors, molten salts, quasicrystals, complex systems, and some non-metallic systems such as molecular glasses, polymers, and colloids have in the past found their place in the conference, with the aim of stimulating discussions and brainstorming.

The conference includes the following topics:

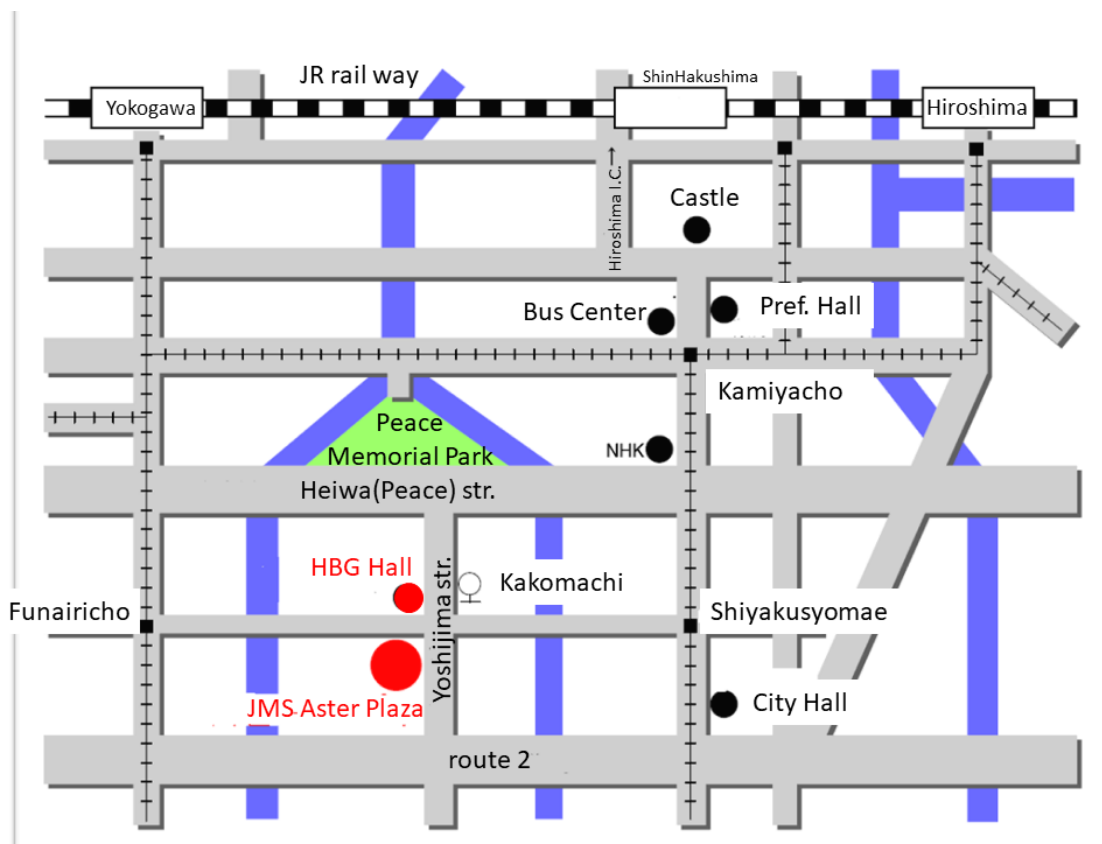
- Structure
- Dynamics
- Atomic transport and diffusion phenomena
- Microstructure – heterogeneities
- Modelling and simulations
- Electronic structure and transport
- Thermodynamics.
- Surface and interfacial properties
- Magnetic properties
- Mechanical properties
- Solidification
- Glass transition
- Metal-nonmetal transition
- Amorphous and quasicrystals
- Exotic phenomena
- Experiments performed in space
- Hyper-order investigation
- Industrial applications

INFORMATION ON LOCAL CONFERENCE

CONFERENCE VENUE

JMS Aster Plaza Hiroshima International Youth House
Kakomachi 4-17, Naka-ku, Hiroshima City, Hiroshima pref. 730-0812, Japan
TEL: 082-244-8000

HBG Hall (Welcome party, Buffet Lunch)



From JR Hiroshima station

Street Car (190 JPY) : ① to Kamiyacho-keiyu Ujina : getting off at Shiyakusyomae and 600 m
: ⑥ to Eba : getting off at Funairicho and 400 m

Bus (190 JPY) Line 24 of Hiroshima Bus
: to Yoshijima eigyosyo or to Yoshijima Byoin: getting off at Kakomachi and 200 m

Taxi (about 1,200 JPY) : about 15 min

From Bus Center

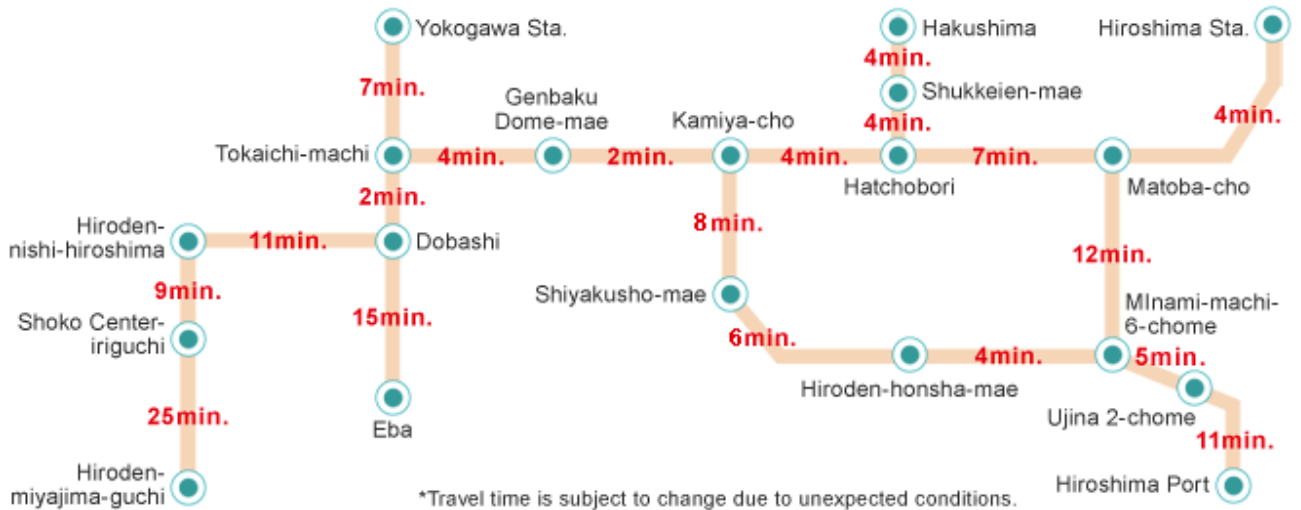
1.5 km on foot

Taking Street Car or Bus above at Kamiyacho (Be careful, several stops to different destinations)

Hiroden (Street Car) route map



Example of required time



JMS Aster Plaza Hiroshima International Youth House



Attention: Please come to Registration desk at first before going to Welcome Party open at 18:00 (close at 20:00).

REGISTRATION

Registration desk at JMS Aster Plaza (ground floor) will be open during the following times:

September 4	15:00-18:00
September 5-6	09:00-18:00
September 7	09:00-16:00

MEALS

Buffet Lunch is included in the registration fee.

COFFEE BREAK

Coffee break is supplied at Citizen's Gallery (poster session room) on the ground floor in Aster Plaza.

ORAL SESSIONS

Oral presentations are conducted at Medium Hall upstairs in JMS Aster Plaza.

Please keep your allocated time that includes discussion & comments.

Total duration:

Plenary Speaker	: 40 min
Invited Speaker	: 30 min
Committee Member Talk	: 30 min
Local Committee Member Talk	: 25 min
General	: 20 min

Online participants can watch live stream of oral session but please send the questions and comments to the presenter by e-mail.

POSTER SESSION

Poster session is conducted at Citizen's Gallery on the ground floor in JMS Aster Plaza. The area for each poster is about 1200 mm × 1800 mm. We are assuming a poster size of about 900 mm × 1200 mm. The poster can be mounted at the allocated area from 15:00 on 4th September till 15:00 on 7th September. We provide permitted tapes to fix a poster on the wall. **Never use pushpins and your own tapes to do it.**

SOCIAL PROGRAM

WELCOME-RECEPTION-PARTY

Date	: Sunday, September 4, 2022
Time	: 18:00-20:00
Place	: Café & Restaurant in HBG Hall

CONFERENCE DINNER (BANQUET)

Date	: Wednesday, September 7, 2022
Boarding Time	: 18:35-
Time	: 18:50-21:00
Place	: Cruising by Ginga
Fee	: 11,000 yen

INFORMATION ON ONLINE CONFERENCE

ORAL SESSIONS

We are preparing zoom for the online presentation. Please see notes in ORAL SESSIONS above.

POSTER SESSIONS

Online poster session includes online posters plus most of posters in Local conference. We are preparing the web site to upload a poster of about 900 mm × 1200 mm whose size is 20 MB maximum. Files of pdf and jpeg per poster (the name should be poster number.pdf and poster number.jpg) should be submitted to a file exchanged system whose URL will be announced to each presenter. When your file becomes larger than 20 MB, please contact us. Short presentation (within 5 min, within 5 slides including a cover sheet) is programmed for every poster. The short presentation is conducted using zoom of oral presentation. Please prepare slides for short presentation. Discussion of each poster can be done using breakout room in zoom or the zoom prepared by the presenter.

MANUSCRIPTS

The special issue on 18th International Conference on Liquid and Amorphous Metals (LAM18) is published by J. Phys.: Condensed Matter, similarly to LAM17. The deadline of the submission will be in November after LAM18 conference. All relevant researchers, regardless of whether they participated in LAM18 or not, are eligible to present their research in the special issue.

Memo

Local Conference Programme at a Glance

Monday 5th, September	
9:20- 9:30	Introduction
9:30-10:10	Plenary Xun-Li Wang
	Session A1
10:10-10:40	Invited Giancarlo Jug
10:40-11:00	Masato Ohnuma
11:00-11:20	Coffee Break
	Session A2
11:20-11:45	Committee Junji Saida
11:45-12:05	Yusuke Ohashi
12:05-14:00	Lunch
	Session A3
14:00-14:30	Invited Noel Jakse
14:30-14:50	Eloi Pineda
14:50-15:10	Peter Michael Derlet
15:10-15:30	Rui Yamada
15:30-15:50	Coffee Break
15:50-17:50	Poster Session PS1

Tuesday 6th, September	
9:20-10:00	Plenary Takeshi Egami
	Session A4
10:00-10:30	Invited Alfred Q.R. Baron
10:30-10:50	Ari Paavo Seitsonen
10:50-11:10	Coffee Break
	Session A5
11:10-11:35	Committee Yukio Kajihara
11:35-11:55	Junpei T. Okada
11:55-12:15	Hiroki Naruta
12:15-14:00	Lunch
	Session A6
14:00-14:30	Invited Jens Rüdiger Stellohm
14:30-14:55	Committee Ayano Chiba
14:55-15:15	Yoshifumi Sakaguchi
15:15-15:35	Coffee Break
	Session A7
15:35-16:00	Committee Yukinobu Kawakita
16:00-16:20	Kohei Shimamura
16:20-16:40	Coffee Break
16:40-18:40	Poster Session PS2

Wednesday 7th, September	
9:20-10:00	Plenary Yang Ren
	Session A8
10:00-10:30	Committee Andrea Di Cicco
10:30-10:55	Committee Satoshi Ohmura
10:55-11:15	Yoichi Nakajima
11:15-11:35	Coffee Break
	Session A9
11:35-12:05	Committee Jean-François Wax
12:05-12:25	Fabio Iesari
12:25-12:45	Hinata Hokyo
12:45-14:00	Lunch
	Session A10
14:00-14:30	Invited László Pusztai
14:30-15:00	Invited Robert Maaß
15:00-15:30	Invited Takeshi Wada
15:30-15:50	Coffee Break
	Session A11
15:50-16:20	Invited Wolf -C. Pilgrim
16:20-16:40	Akihide Koura
16:40-17:00	Hikaru Kitamura
18:35-	Boarding / Dinner

Online Conference Programme at a Glance

Thursday 8th, September	
JST CEST	
	Session R1
16:00-16:30 9:00-9:30	Invited Luis E. González
16:30-17:00 9:30-10:00	Committee Taras Bryk
17:00-17:10 10:00-10:10	Coffee Break
	Session R2
17:10-17:40 10:10-10:40	Committee Dirk Holland Moritz
17:40-18:00 10:40-11:00	Neta Ellert
18:00-18:20 11:00-11:20	Nicolai Lukas Grund
18:20-20:00 11:20-13:00	Meal Break
	Session R3
20:00-20:30 13:00-13:30	Invited Chuang Dong
20:30-20:50 13:30-13:50	Shuang Zhang
20:50-21:10 13:50-14:10	Kazuki Mitsui
21:10-21:20 14:10-14:20	Coffee Break
	Session R4
21:20-21:50 14:20-14:50	Invited Yohei Onodera
21:50-22:10 14:50-15:10	Xinguo Hong
22:10-22:30 15:10-15:30	Katsuki Hayashi
22:30-22:40 15:30-15:40	Coffee Break
	Session R5
22:40-23:00 15:40-16:00	Dmitri V. Louzguine
23:00-23:20 16:00-16:20	Xiao-Dong Wang
23:20-23:40 16:20-16:40	Paul Laffont

Friday 9th, September	
JST CEST	
16:00-16:40 9:00-9:40	Plenary Jian-Zhong Jiang
	Session R6
16:40-16:55 9:40-9:55	Corporate Webinar
16:55-17:15 9:55-10:15	Fan Yang
17:15-17:25 10:15-10:25	Coffee Break
	Session R7
17:25-18:20 10:25-11:20	Poster Short Presentation
18:20-19:00 11:20-12:00	Poster Session RPS1
19:00-20:00 12:00-13:00	Meal Break
	Session R8
20:00-20:20 13:00-13:20	Shuai Wei
20:20-20:40 13:20-13:40	Loicia Gaudilliere
20:40-21:00 13:40-14:00	Tianding Xu
21:00-21:10 14:00-14:10	Coffee Break
	Session R9
21:10-21:30 14:10-14:30	Shuang Ma
21:30-21:50 14:30-14:50	Vadim B. Vorontsov
21:50-22:10 14:50-15:10	Yanhui Li
22:10-22:20 15:10-15:20	Coffee Break
	Session R10
22:20-22:40 15:20-15:40	Dmitrii Fleita
22:40-23:00 15:40-16:00	G. M. Bhuiyan

Monday 12th, September	
JST CEST	
	Session R11
16:00-16:30 9:00-9:30	Invited Jörg Behler
16:30-17:00 9:30-10:00	Invited Nikolay Chtchelkatchev
17:00-17:10 10:00-10:10	Coffee Break
	Session R12
17:10-18:00 10:10-11:00	Poster Short Presentation
18:00-18:40 11:00-11:40	Poster Session RPS2
18:40-20:00 11:40-13:00	Meal Break
	Session R13
20:00-20:30 13:00-13:30	Invited Michele Ceriotti
20:30-20:50 13:30-13:50	Ayu Irie
20:50-21:00 13:50-14:00	Coffee Break
	Session R14
21:00-21:30 14:00-14:30	Invited Takashi Odagaki
21:30-22:00 14:30-15:00	Invited Kostya Trachenko
22:00-22:10 15:00-15:10	Coffee Break
	Session R15
22:10-22:40 15:10-15:40	Invited Osamu Yamamuro
22:40-23:00 15:40-16:00	Nico Neuber
23:00-23:10 16:00-16:10	Closing

LAM-18 Conference

Local Conference Programme

Day 1 - Monday 5th, September 2022

9:20-9:30	Welcome/Introduction	Organizers
9:30-10:10	Plenary Session I Plenary Talk Medium-range Order and Cluster Connectivity	Chair: Masanori Inui Xun-Li Wang PL1 City University of Hong Kong, China
10:10-11:00	Session A1 Structural Properties of Glasses	Chair: Junji Saida
10:10-10:40	Invited Talk The Intermediate-Range Structure of Glasses as seen from their Magnetic Properties and Under an Optical Microscope	Giancarlo Jug IL1 Università dell'Insubria, Italy
10:40-11:00	Structural Origin of Temperature Memory Effect of Quenched Strain in Metallic Glasses	Masato Ohnuma O1 Hokkaido University, Japan
11:00-11:20	Coffee Break	
11:20-12:05	Session A2 Synthesis of Metallic Glasses	Chair: Noel Jakse
11:20-11:45	Local Committee Member Talk Synthesis and Mechanical Property of Highly Structure Controlled Metallic Glasses by Thermal Rejuvenation Technique	Junji Saida CL1 Tohoku University, Japan
11:45-12:05	High-entropy design and its influence on glass-forming ability in Zr–Cu-based metallic glass	Yusuke Ohashi O2 Tohoku University, Japan
12:05-14:00	Lunch	
14:00-15:30	Session A3 Dynamic Properties of Metallic Glasses	Chair: Giancarlo Jug
14:00-14:30	Invited Talk Dynamic heterogeneities in undercooled metallic alloys	Noel Jakse IL2 Université Grenoble-Alpes, France

14:30-14:50	Relaxation dynamics of glass forming metals: Study of aging anelasticity and supercooled liquid behavior in a ZrTiCuNiBe alloy	Eloi Pineda Universitat Politècnica de Catalunya, Spain	O3
14:50-15:10	Emergent structural heterogeneity and it's effect on viscosity and transport in a model binary metallic glass	Peter Michael Derlet Paul Scherrer Institute, Switzerland	O4
15:10-15:30	Creation of Three-Dimensional Relaxation State Gradient in Zr ₅₀ Cu ₄₀ Al ₁₀ Metallic Glass Through a Thermal Process	Rui Yamada Tohoku University, Japan	O5

15:30-15:50 Coffee Break

15:50-17:50 Poster Session PS1

Day 2 - Tuesday 6th, September 2022

9:20-10:00	Plenary Session II Plenary Talk How the Liquid Structure is Formed; Bottom-up, Top-down, or Both?	Chair: Shinya Hosokawa Takeshi Egami University of Tennessee, USA	PL2
10:00-10:50	Session A4 Dynamic Properties	Chair: Yukio Kajihara	
10:00-10:30	Invited Talk Hydrodynamic Interaction Between Quasi-elastic and Acoustic Modes Observed by Inelastic X-Ray Scattering	Alfred Q.R. Baron RIKEN SPring-8 Center, Japan	IL3
10:30-10:50	<i>Ab initio</i> Study of Collective Excitations in Liquid Sb	Ari Paavo Seitsonen École Normale Supérieure, France	O6
10:50-11:10	Coffee Break		
11:10-12:15	Session A5 Phase Transition in Liquids	Chair: Alfred Q.R. Baron	
11:10-11:35	Local Committee Member Talk Interpretation of thermodynamic anomalies of liquid water in terms of critical fluctuations	Yukio Kajihara Hiroshima University, Japan	CL2

11:35-11:55	Phase relation between supercooled liquid and amorphous Silicon	Junpei T. Okada Tohoku University, Japan	O7
	Cancelled		O8

11:55-14:00 Lunch

14:00-15:15 Session A6
Structure I

Chair: Yukinobu Kawakita

14:00-14:30 **Invited Talk**
Structure of amorphous Cu-Ge-Te and the implications for its functionality

Jens Rüdiger Stellhorn **IL4**
Hiroshima University, Japan

14:30-14:55 **Local Committee Member Talk**
X-ray and neutron diffraction of semi-crystalline isotactic poly (4-methyl-1-pentene) with alkane absorption

Ayano Chiba **CL3**
Keio University, Japan

14:55-15:15 Direct observation of concentration fluctuations in Au-Si eutectic liquid by small-angle neutron scattering

Yoshifumi Sakaguchi **O9**
Comprehensive Research Organization for Science and Society (CROSS), Japan

15:15-15:35 Coffee Break

15:35-16:20 Session A7
Dynamic and Transport Properties

Chair: Jens R. Stellhorn

15:35-16:00 **Local Committee Member Talk**
Structural Relaxation in Complex Liquid Metals Antimony and Bismuth by Means of Coherent Quasi-Elastic Neutron Scattering and Time -Space Correlation Function

Yukinobu Kawakita **CL4**
Japan Atomic Energy Agency, Japan

16:00-16:20 Estimating Thermal Conductivity of Silver Chalcogenides Using Machine-Learning Interatomic Potentials

Kohei Shimamura **O10**
Kumamoto University, Japan

16:20-16:40 Coffee Break

16:40-18:40 Poster Session PS2

Day 3 - Wednesday 7th, September 2022

9:20-10:00	Plenary Session III Plenary Talk Supercritical Elasticity and Structural Entanglement of Multicomponent alloys	Chair: Hidemi Kato Yang Ren City University of Hong Kong, China	PL3
10:00-11:15	Session A8 Liquids and Glasses under Pressure	Chair: Jean-François Wax	
10:00-10:30	Committee Member Talk Investigation of local structural changes in GeSe ₂ glass under ultra-high pressure	Andrea Di Cicco University of Camerino, Italy	CL5
10:30-10:55	Local Committee Member Talk Bonding and structure of liquid iron-light-element-oxygen ternary alloys under high pressure: molecular dynamics simulations	Satoshi Ohmura Hiroshima Institute of Technology, Japan	CL6
10:55-11:15	Inelastic X-ray scattering measurements of liquid Fe-S at high pressure	Yoichi Nakajima Kumamoto University, Japan	O11
11:15-11:35	Coffee Break		
11:35-12:45	Session A9 Properties under Pressure and Shear Strain	Chair: Andrea Di Cicco	
11:35-12:05	Committee Member Talk Simulation study of the collective excitations in liquid sodium under high pressure	Jean-François Wax Université de Lorraine, France	CL7
12:05-12:25	Structure of liquid Cd under high-pressure condition	Fabio lesari Aichi Synchrotron Radiation Center, Japan	O12
12:25-12:45	<i>Ab initio</i> simulation for the ductility mechanism of silver chalcogenides	Hinata Hokyo Kumamoto University, Japan	O13
12:45-14:00	Lunch		

14:00-15:30	Session A10 Properties of Metallic Glasses	Chair: Wolf -C. Pilgrim
14:00-14:30	Invited Talk Reverse Monte Carlo modeling: state of affairs and applications to metallic glasses	László Pusztai IL5 Wigner Research Centre for Physics, Hungary
14:30-15:00	Invited Talk Long-time and intermittent structural evolution of metallic glasses	Robert Maaß IL6 Federal Institute for Materials Research and Testing (BAM), Germany
15:00-15:30	Invited Talk Decoupling between thermodynamic and dynamical glass transitions in high-entropy metallic glasses	Takeshi Wada IL7 Tohoku University, Japan
15:30-15:50	Coffee Break	
15:50-17:00	Session A11 Structure II	Chair: László Pusztai
15:50-16:20	Invited Talk Structure Determination in a new Type of Amorphous Molecular Solids with Extreme Nonlinear Optical Properties	Wolf -C. Pilgrim IL8 Philipps-University of Marburg, Germany
16:20-16:40	Static Structure of Liquid Ag ₂ Se Based on Molecular Dynamics Simulations Using Artificial Neural Network Potential	Akihide Koura O14 Kumamoto University, Japan
16:40-17:00	Semianalytic Formula for Multiphonon Thermal Diffuse Scattering in Solids	Hikaru Kitamura O15 Kyoto University, Japan
17:00-18:35	Free time	
18:35-	Boarding	
18:50-	Dinner	

LAM-18 Conference

Online Conference Programme

Day 4 - Thursday 8th, September 2022

JST
CEST

16:00-17:00 9:00-10:00	Session R1 Structure and Dynamics of Liquids I	Chair: Kazuhiro Matsuda	
16:00-16:30 9:00-9:30	Invited Talk Dynamic properties of liquids of interest in nuclear energy production: liquid Li-Pb alloys and molten UO ₂	Luis E. González Universidad de Valladolid, Spain	RIL1
16:30-17:00 9:30-10:00	Committee Member Talk Origin of Positive Sound Dispersion in Simple Liquids and Liquid Alloys	Taras Bryk Institute for Condensed Matter Physics of NASU, Ukraine	RCL1
17:00-17:10 10:00-10:10	Coffee Break		
17:10-18:35 10:10-11:35	Session R2 Structure and Dynamics of Liquids II	Chair: Tomoko Mizuguchi	
17:10-17:40 10:10-10:40	Committee Member Talk Chemical short-range order in undercooled Cu-Ni melts	Dirk Holland Moritz Institute of Materials Physics in Space, Germany	RCL2
17:40-17:55 10:40-10:55	Corporate Webinar Talk Company Introduction and Gas Atomization Technology	Teppei Ishikawa MAKABE R&D Co.,LTD	RCW0
17:55-18:15 10:55-11:15	The Short-Range Order in Liquid Water	Neta Ellert Ben-Gurion University of the Negev, Israel	RO1
18:15-18:35 11:15-11:35	Impact of sulfur addition on the structure and dynamics of Ni-Nb alloys	Nicolai Lukas Grund Institute of Materials Physics in Space, Germany	RO2
18:35-20:00 11:35-13:00	Meal Break		
20:00-21:10 13:00-14:10	Session R3 Structure and Dynamics of Non-Crystalline Materials I	Chair: Tetsuya Morishita	
20:00-20:30 13:00-13:30	Invited Talk Cluster-plus-glue-atom Model and the Thus-obtained Composition Genes for Metallic Glasses	Chuang Dong Dalian Jiaotong University, China	RIL2

20:30-20:50 13:30-13:50	Composition Optimization Based on Cluster-plus-glue-atom Model for Bulk Metallic Glass $Zr_{55}Cu_{30}Al_{10}Ni_5$	Shuang Zhang Dalian Jiaotong University, China	RO3
20:50-21:10 13:50-14:10	Colorless and high refractive SnO - and Sb_2O_3 -containing borosilicate glasses	Kazuki Mitsui Ehime University, Japan	RO4
21:10-21:20 14:10-14:20	Coffee Break		
21:20-22:30 14:20-15:30	Session R4 Structure and Dynamics of Non-Crystalline Materials II	Chair: Yoichi Nakajima	
21:20-21:50 14:20-14:50	Invited Talk Understanding diffraction patterns of glassy, liquid and amorphous materials via topological analyses	Yohei Onodera Kyoto University, Japan	RIL3
21:50-22:10 14:50-15:10	Local structural investigation of non-crystalline materials at high pressure	Xinguo Hong Center for High Pressure Science and Technology Advanced Research, China	RO5
22:10-22:30 15:10-15:30	The structure of bismuth oxide glasses	Katsuki Hayashi Ehime University, Japan	RO6
22:30-22:40 15:30-15:40	Coffee Break		
22:40-23:40 15:40-16:10	Session R5 Structure and Dynamics of Non-Crystalline Materials III	Chair: Yohei Onodera	
22:40-23:00 15:40-16:00	Atomic structure of bulk metallic glasses studied by transmission electron microscopy, synchrotron-radiation X-ray diffraction, scanning tunneling microscopy and ab-initio molecular dynamics simulation	Dmitri V. Louzguine National Institute of Advanced Industrial Science and Technology (AIST), Japan	RO7
23:00-23:20 16:00-16:20	Short range order controlling the atomic dynamics in metallic glasses	Xiao-Dong Wang Zhejiang University, China	RO8
23:20-23:40 16:20-16:40	On the relationship between structural state, mechanical properties and wear resistance of a cu-based bulk metallic glass	Paul Laffont University Grenoble Alpes, SIMaP, France	RO9

Day 5 - Friday 9th, September 2022

JST
CEST

16:00-17:15 9:00-10:15	Plenary Session / Session R6 Phase Transitions and Thermophysical Behaviors I / State of the Art Manufacturing	Chair: Satoshi Ohmura	
16:00-16:40 9:00-9:40	Plenary Talk Behaviors of disordered alloys under high temperature and pressure	Jian-Zhong Jiang Zhejiang University, China	RPL1
16:40-16:55 9:40-9:55	Corporate Webinar Talk Heraeus AMLOY Technologies – The transition from scientific innovation to series production of high-performance application solutions	Hans-Jürgen Wachter Global Head of Heraeus AMLOY, Germany	RCW1
16:55-17:15 9:55-10:15	Large-scale density fluctuations during structural transition in metallic glass forming liquid beyond medium range order	Fan Yang Institute of Materials Physics in Space, Germany	RO10
17:15-17:25 10:15-10:25	Coffee Break		
17:25-18:20 10:25-11:20	Session R7 Poster Short Presentation	Chair: Shuji Munejiri	
18:20-19:00 11:20-12:00	Poster Session RPS1		
19:00-20:00 12:00-13:00	Meal Break		
20:00-21:00 13:00-14:00	Session R8 Phase Transitions and Thermophysical Behaviors II	Chair: Makina Saito	
20:00-20:20 13:00-13:20	Structure and dynamics in the no-man's land of phase-change materials	Shuai Wei Aarhus University, Denmark	RO11
20:20-20:40 13:20-13:40	Thermoplastic forming capacity of a ZrCoAl metallic glass for surface patterning	Loïcia Gaudilliere University Grenoble Alpes, SIMaP, France	RO12
20:40-21:00 13:40-14:00	Shape memory effect in metallic glasses	Tianding Xu Zhejiang University, China	RO13

21:00-21:10 Coffee Break

14:00-14:10

21:10-22:10 Session R9

Chair: Ayano Chiba

14:10-15:10

Phase Transitions and Thermophysical Behaviors III

 21:10-21:30 Role of Y content on glass-forming ability and soft
 14:10-14:30 magnetic properties of Co-Y-B metallic glasses

Shuang Ma
RO14

 Dalian University of Technology,
 China

 21:30-21:50 Formation of a local structural order in the aluminum
 14:30-14:50 melt before crystallization

Vadim B.Vorontsov
RO15

 Ural State University of Railway
 transport (USURT), Russia

 21:50-22:10 Development of metal-metalloid high-entropy bulk
 14:50-15:10 metallic glasses with ultrahigh thermal stability and
 strength

Yanhui Li
RO16

 Dalian University of Technology,
 China

22:10-22:20 Coffee Break

15:10-15:20

22:20-23:20 Session R10

Chair: Hironori Shimakura

15:20-16:20

Phase Transitions and Dynamic Properties

Cancelled

RO17

 22:20-22:40 Change of collective dynamics in supercooled glass-
 15:20-15:40 forming aluminium film

Dmitrii Fleita
RO18

HSE University, Russia

 22:40-23:00 Atomic transport properties of $\text{Bi}_{1-x}\text{Zn}_x$ segregating
 15:40-16:00 alloys

G. M. Bhuiyan
RO19

University of Dhaka, Bangladesh

Day 6 - Monday 12th, September 2022

JST
CEST

16:00-17:00 9:00-10:00	Session R11 Machine Learning I	Chair: Kohei Shimamura
16:00-16:30 9:00-9:30	Invited Talk High-Dimensional Neural Network Potentials for Simulations of Complex Systems	Jörg Behler RIL4 Universität Göttingen, Germany
16:30-17:00 9:30-10:00	Invited Talk Structural inheritance and machine learning for materials design: from study of liquid to prediction crystals	Nikolay Chtchelkatchev RIL5 Vereshchagin Institute for High Pressure Physics, Russia
17:00-17:10 10:00-10:10	Coffee Break	
17:10-18:00 10:10-11:00	Session R12 Poster Short Presentation	Chair: Shuta Tahara
18:00-18:40 11:00-11:40	Poster Session RPS2	
18:40-20:00 11:40-13:00	Meal Break	
20:00-20:50 13:00-13:50	Session R13 Machine Learning II	Chair: Akihide Koura
20:00-20:30 13:00-13:30	Invited Talk Finite-temperature modeling of materials with first-principles accuracy	Michele Ceriotti RIL6 École Polytechnique Fédérale de Lausanne, Switzerland
20:30-20:50 13:30-13:50	Composition Dependence of Melting Temperature of Rb-Na Alloy Using First-principles-based Thermodynamic Integration	Ayu Irie RO20 Kumamoto University, Japan
20:50-21:00 13:50-14:00	Coffee Break	

21:00-22:00 14:00-15:00	Session R14 Thermodynamics and Structure of Non-Crystalline Materials I	Chair: Osamu Yamamuro	
21:00-21:30 14:00-14:30	Invited Talk Response of the Free Energy Landscape to Temperature Modulation and Aging	Takashi Odagaki	RIL7
		Kyushu University and Research Institute for Science Education Inc., Japan	
21:30-22:00 14:30-15:00	Invited Talk New understanding of liquid thermodynamics, viscosity and its lower bounds	Kostya Trachenko	RIL8
		Queen Mary University of London, United Kingdom	
22:00-22:10 15:00-15:10	Coffee Break		
22:10-23:00 15:10-16:00	Session R15 Thermodynamics and Structure of Non-Crystalline Materials II	Chair: Yoshifumi Sakaguchi	
22:10-22:40 15:10-15:40	Invited Talk Thermodynamic and Structural Studies on Glass Transitions of Molecular Glasses	Osamu Yamamuro	RIL9
		The University of Tokyo, Japan	
22:40-23:00 15:40-16:00	On the thermodynamics and its connection to structure in the Pt-Pd-Cu-Ni-P bulk metallic glass forming system	Nico Neuber	RO21
		Saarland University, Germany	
23:00-23:10 16:00-16:10	Closing	Organizers	

LAM-18 Conference

Local Poster Programme

Day 1 - Monday 5th, September 2022

15:50-17:50 Poster Session PS1

Day 2 - Tuesday 6th, September 2022

16:40-18:40 Poster Session PS2

P1	Determination of cooperatively rearranging regions in binary glass former	Tomoko Mizuguchi Kyoto Institute of Technology, Japan
P2	Novel Experimental Scheme for Microscopic Study of Johari-Goldstein Process	Makina Saito Tohoku University, Japan
P3	Configurational entropy of an isotropic monatomic glass	A. Ueno Kyoto Institute of Technology, Japan
P4	Anomaly of Linear Thermal Expansion Coefficient induced by rejuvenation treatment	Tomoya Oshikiri Hokkaido University, Japan
P5	The structural analysis of low-density liquid phosphorus using reverse Monte Carlo simulation	Takuya Nishioka Ehime University, Japan
P6	Local Structure of $\text{Ga}_{85.8}\text{In}_{14.2}$ eutectic liquid alloy and its pressure temperature melting line	Andrea Di Cicco University of Camerino, Italy
P7	Development of an Analysis Method for Liquid Electrolyte at a Lithium Electrode Interface using X-ray Total Reflection	Koji Kimura Nagoya Institute of Technology, Japan
P8	Structure of amorphous $\text{Mg}_{85}\text{Zn}_6\text{Y}_9$ alloy as a seed of a long-period stacking ordered structure	Shinya Hosokawa Kumamoto University, Japan
P9	Collective dynamics of liquid sulfur across the polymerization transition temperature probed by inelastic x-ray scattering	Shinya Hosokawa Kumamoto University, Japan
P10	Phonon dynamics of liquid Hg probed by inelastic x-ray scattering	Shinya Hosokawa Kumamoto University, Japan

- P11** Inelastic x-ray scattering experiments for liquid GeCu_2Te_3 **Masanori Inui**
Hiroshima University, Japan
- P12** Q-gap behavior of low energy excitations in liquid Sb and liquid Bi observed by inelastic x-ray scattering measurements **Masanori Inui**
Hiroshima University, Japan
- P13** Phonon dispersion curves in the type-I crystalline and molten clathrate compound $\text{Eu}_8\text{Ga}_{16}\text{Ge}_{30}$ **Masanori Inui**
Hiroshima University, Japan
- P14** Density response function of valence electrons in liquid Li **Kazuhiro Matsuda**
Kumamoto University, Japan
- P15** Relationship Between Liquid Dynamics and Potential Energy Landscape **Noel Jakse**
Université Grenoble Alpes, CNRS, France
- P16** Selecting atomic fingerprints for high-dimensional neural network potentials: adaptive group lasso approach **Johannes Sandberg**
Université Grenoble Alpes, CNRS, France
- P17** GeO_2 glass structure from neural network potential molecular dynamics –dependence of intermediate-range order on density functional approximation **Kenta Matsutani**
Yamagata University, Japan
- P18** Optical properties of molten pure copper by density functional theory **Susumu Kato**
National Institute of Advanced Industrial Science and Technology (AIST), Japan

LAM-18 Conference

Online Poster Programme

JST
CEST

Day 5 - Friday 9th, September 2022

17:25-18:20 Session R7
10:25-11:20 Poster Short Presentation

18:20-19:00 Poster Session RPS1
11:20-12:00

Day 6 - Monday 12th, September 2022

17:10-18:00 Session R12
10:10-11:00 Poster Short Presentation

18:00-18:40 Poster Session RPS2
11:00-11:40

RP1	Development and optimization of sulfur-containing novel Ti-based Bulk Metallic Glasses and the correlation between primary crystalline phases, thermal stability and mechanical properties	Lucas Matthias Ruschel Saarland University, Germany	<div style="background-color: #f8d7da; padding: 2px; text-align: center;">R7</div> <div style="background-color: #d1ecf1; padding: 2px; text-align: center;">RPS1</div> <div style="background-color: #d4edda; padding: 2px; text-align: center;">RPS2</div>
RP2	Structural analysis of etidronate disodium	Hironori Shimakura Niigata University of Pharmacy and Applied Life Sciences, Japan	<div style="background-color: #f8d7da; padding: 2px; text-align: center;">R7</div> <div style="background-color: #d1ecf1; padding: 2px; text-align: center;">RPS1</div> <div style="background-color: #d4edda; padding: 2px; text-align: center;">RPS2</div>
RP3	Topological analysis for α -AgI	Shuta Tahara University of the Ryukyus, Japan	<div style="background-color: #f8d7da; padding: 2px; text-align: center;">R7</div> <div style="background-color: #d1ecf1; padding: 2px; text-align: center;">RPS1</div> <div style="background-color: #d4edda; padding: 2px; text-align: center;">RPS2</div>
RP4	Glass transition temperature of nickel based binary alloys and its interparticle dynamics features	Dmitrii Fleita Joint Institute for High Temperatures of the Russian Academy of Sciences, Russia	<div style="background-color: #f8d7da; padding: 2px; text-align: center;">R7</div> <div style="background-color: #d1ecf1; padding: 2px; text-align: center;">RPS1</div> <div style="background-color: #d4edda; padding: 2px; text-align: center;">RPS2</div>
RP5	Local density fluctuation realized in Nb-Ni amorphous alloys	Toru Kawamata Tohoku University, Japan	<div style="background-color: #f8d7da; padding: 2px; text-align: center;">R7</div> <div style="background-color: #d1ecf1; padding: 2px; text-align: center;">RPS1</div> <div style="background-color: #d4edda; padding: 2px; text-align: center;">RPS2</div>
RP6	Unsupervised topological learning of crystal nucleation in pure metals	Sébastien Becker Université Grenoble-Alpes, France	<div style="background-color: #d1ecf1; padding: 2px; text-align: center;">RPS1</div> <div style="background-color: #fff3cd; padding: 2px; text-align: center;">R12</div> <div style="background-color: #d4edda; padding: 2px; text-align: center;">RPS2</div>

P1	Determination of cooperatively rearranging regions in binary glass former	Tomoko Mizuguchi Kyoto Institute of Technology, Japan	R7 RPS1
P2	Novel Experimental Scheme for Microscopic Study of Johari-Goldstein Process	Makina Saito Tohoku University, Japan	R7 RPS1 RPS2
P5	The structural analysis of low-density liquid phosphorus using reverse Monte Carlo simulation	Takuya Nishioka Ehime University, Japan	RPS1 R12 RPS2
P7	Development of an Analysis Method for Liquid Electrolyte at a Lithium Electrode Interface using X-ray Total Reflection	Koji Kimura Nagoya Institute of Technology, Japan	R7 RPS1
P8	Structure of amorphous $Mg_{85}Zn_6Y_9$ alloy as a seed of a long-period stacking ordered structure	Shinya Hosokawa Kumamoto University, Japan	R7 RPS1
P9	Collective dynamics of liquid sulfur across the polymerization transition temperature probed by inelastic x-ray scattering	Shinya Hosokawa Kumamoto University, Japan	R7 RPS1
P10	Phonon dynamics of liquid Hg probed by inelastic x-ray scattering	Shinya Hosokawa Kumamoto University, Japan	R7 RPS1
P11	Inelastic x-ray scattering experiments for liquid $GeCu_2Te_3$	Masanori Inui Hiroshima University, Japan	RPS1 R12 RPS2
P12	Q-gap behavior of low energy excitations in liquid Sb and liquid Bi observed by inelastic x-ray scattering measurements	Masanori Inui Hiroshima University, Japan	RPS1 R12 RPS2
P13	Phonon dispersion curves in the type-I crystalline and molten clathrate compound $Eu_8Ga_{16}Ge_{30}$	Masanori Inui Hiroshima University, Japan	RPS1 R12 RPS2
P14	Density response function of valence electrons in liquid Li	Kazuhiro Matsuda Kumamoto University, Japan	RPS1 R12 RPS2

P15	Relationship Between Liquid Dynamics and Potential Energy Landscape	Noel Jakse Université Grenoble Alpes, CNRS, France	R12 RPS2
P16	Selecting atomic fingerprints for high-dimensional neural network potentials: adaptive group lasso approach	Johannes Sandberg Université Grenoble Alpes, CNRS, France	RPS1 R12 RPS2
P17	GeO ₂ glass structure from neural network potential molecular dynamics –dependence of intermediate-range order on density functional approximation	Kenta Matsutani Yamagata University, Japan	RPS1 R12 RPS2
P18	Optical properties of molten pure copper by density functional theory	Susumu Kato National Institute of Advanced Industrial Science and Technology (AIST), Japan	RPS1 R12 RPS2

LAM-18 Conference

Online Poster Short Presentation Programme

Day 5 - Friday 9th, September 2022

JST
CEST

17:25-18:20 Session R7			
10:25-11:20 Poster Short Presentation			
17:25-17:30 10:25-10:30	Development and optimization of sulfur-containing novel Ti-based Bulk Metallic Glasses and the correlation between primary crystalline phases, thermal stability and mechanical properties	Lucas Matthias Ruschel	RP1 Saarland University, Germany
17:30-17:35 10:30-10:35	Structural analysis of etidronate disodium	Hironori Shimakura	RP2 Niigata University of Pharmacy and Applied Life Sciences, Japan
17:35-17:40 10:35-10:40	Topological analysis for α -AgI	Shuta Tahara	RP3 University of the Ryukyus, Japan
17:40-17:45 10:40-10:45	Glass transition temperature of nickel based binary alloys and its interparticle dynamics features	Dmitrii Fleita	RP4 Joint Institute for High Temperatures of the Russian Academy of Sciences, Russia
17:45-17:50 10:45-10:50	Local density fluctuation realized in Nb-Ni amorphous alloys	Toru Kawamata	RP5 Tohoku University, Japan
17:50-17:55 10:50-10:55	Determination of cooperatively rearranging regions in binary glass former	Tomoko Mizuguchi	P1 Kyoto Institute of Technology, Japan
17:55-18:00 10:55-11:00	Novel Experimental Scheme for Microscopic Study of Johari-Goldstein Process	Makina Saito	P2 Tohoku University, Japan
18:00-18:05 11:00-11:05	Development of an Analysis Method for Liquid Electrolyte at a Lithium Electrode Interface using X-ray Total Reflection	Koji Kimura	P7 Nagoya Institute of Technology, Japan
18:05-18:10 11:05-11:10	Structure of amorphous $Mg_{85}Zn_6Y_9$ alloy as a seed of a long-period stacking ordered structure	Shinya Hosokawa	P8 Kumamoto University, Japan
18:10-18:15 11:10-11:15	Collective dynamics of liquid sulfur across the polymerization transition temperature probed by inelastic x-ray scattering	Shinya Hosokawa	P9 Kumamoto University, Japan

18:15-18:20 Phonon dynamics of liquid Hg probed by inelastic x-ray scattering **Shinya Hosokawa** **P10**
 11:15-11:20 Kumamoto University, Japan

Day 6 - Monday 12th, September 2022

JST
CEST

17:10-18:00 Session R12
 10:10-11:00 Poster Short Presentation

17:10-17:15 10:10-10:15	Unsupervised topological learning of crystal nucleation in pure metals	Sébastien Becker	RP6 Université Grenoble-Alpes, France
17:15-17:20 10:15-10:20	The structural analysis of low-density liquid phosphorus using reverse Monte Carlo simulation	Takuya Nishioka	P5 Ehime University, Japan
17:20-17:25 10:20-10:25	Inelastic x-ray scattering experiments for liquid GeCu ₂ Te ₃	Masanori Inui	P11 Hiroshima University, Japan
17:25-17:30 10:25-10:30	Q-gap behavior of low energy excitations in liquid Sb and liquid Bi observed by inelastic x-ray scattering measurements	Masanori Inui	P12 Hiroshima University, Japan
17:30-17:35 10:30-10:35	Phonon dispersion curves in the type-I crystalline and molten clathrate compound Eu ₈ Ga ₁₆ Ge ₃₀	Masanori Inui	P13 Hiroshima University, Japan
17:35-17:40 10:35-10:40	Density response function of valence electrons in liquid Li	Kazuhiro Matsuda	P14 Kumamoto University, Japan
17:40-17:45 10:40-10:45	Relationship Between Liquid Dynamics and Potential Energy Landscape	Noel Jakse	P15 Université Grenoble Alpes, CNRS, France
17:45-17:50 10:45-10:50	Selecting atomic fingerprints for high-dimensional neural network potentials: adaptive group lasso approach	Johannes Sandberg	P16 Université Grenoble Alpes, CNRS, France
17:50-17:55 10:50-10:55	GeO ₂ glass structure from neural network potential molecular dynamics –dependence of intermediate-range order on density functional approximation	Kenta Matsutani	P17 Yamagata University, Japan
17:55-18:00 10:55-11:00	Optical properties of molten pure copper by density functional theory	Susumu Kato	P18 National Institute of Advanced Industrial Science and Technology (AIST), Japan

Oral Presentations

Abstracts

Medium-range Order and Cluster Connectivity

Si Lan^{1,2}, Zhenduo Wu^{3,2}, Xiaoya Wei², *Xun-Li Wang^{2,4}

¹ Herbert Gleiter Institute of Nanoscience, School of Materials Science and Engineering, Nanjing University of Science and Technology, Nanjing 210094, China

² Department of Physics, City University of Hong Kong, City, 83 Tat Chee Ave., Kowloon, Hong Kong

³ Center for Neutron Scattering and Applied Physics, City University of Hong Kong Dongguan Research Institute, Dongguan 523000, China

⁴ City University of Hong Kong Shenzhen Research Institute, Shenzhen Hi-Tech Industrial Park, Shenzhen 518057, China

*xlwang@cityu.edu.hk

Keywords (Maximum: 6 keywords, Minimum: 3 keywords, 10 point): Synchrotron scattering, neutron scattering, short-range order, medium-range order, cluster, connectivity.

Amorphous materials have no long-range order, but there are ordered structures at short-range (2-5 Å), medium-range (5-20 Å), and even longer-length scales [1,2]. While regular and semiregular polyhedra are often identified as short-range ordering in amorphous materials, the nature of the medium-range order has remained elusive. In a recent study of a Pd-Ni-P amorphous alloy during crystallization, we captured an intermediate crystalline cubic phase and found a six-membered tricapped trigonal prism cluster (6M-TTP) existing in both phases [3]. The 6M-TTP clusters can periodically pack to several tens of nanometers to form the cubic phase. In this regard, our experimental observations established a structural link between the amorphous and crystalline phases and suggested that it is the connectivity of the 6M-TTP clusters that distinguish the crystalline and amorphous phases. Furthermore, we found the idea of cluster connectivity to be rather versatile, as it can explain the structure evolution during crystallization [3,4], mechanical deformation [5], and liquid-to-liquid phase transformation [6], where the short-range order structures or the clusters change only slightly. Rather, it is the connectivity between clusters at a medium-range scale that drives the dynamic response. In this talk, we discuss the meaning of cluster connectivity within the context of these in situ experimental results.

References.

1. D. B. Miracle, *Nature Materials* **3**, 697-702 (2004).
2. D. Ma, A. D. Stoica, and X.-L. Wang, *Nature Materials*, **8**, 30-34 (2009)
3. S. Lan et al., *Nature Materials*, **20**, 1347-1352 (2021)
4. X.-L. Wang et al., *Phys. Rev. Lett.*, **91**, 265501 (2003).
5. D. Ma et al., *Phys. Rev. Lett.*, **108**, 085501 (2012)
6. S. Lan et al., *Nature Comms.*, **8**, 14679 (2017)

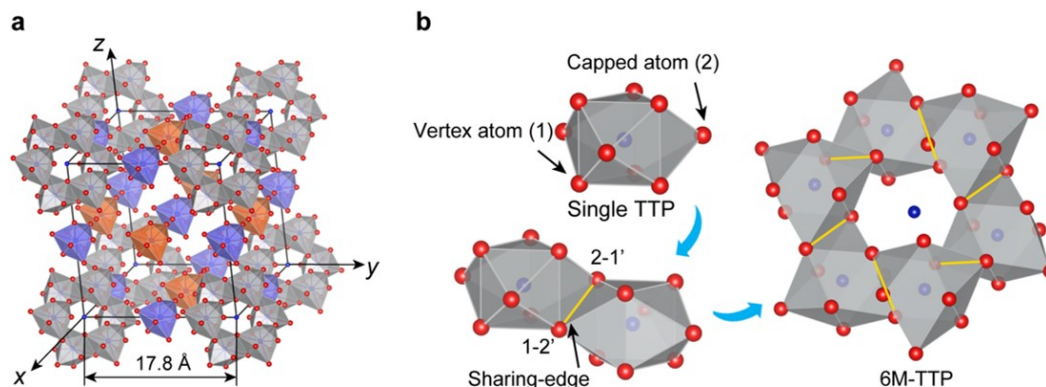


Fig. 1. A structure model illustrating the unit cell of the intermediate cubic crystalline phase in a Pd-Ni-P metallic glass during crystallization. (a) Red balls are Pd and Ni atoms, whereas the blue balls represent P atoms. The orange-colored polyhedron represents the Pd-enriched small cluster, and the blue-coloured polyhedron represents the Ni-enriched small cluster. Only part of the small clusters is displayed for clarification. (b). Schematic diagrams showing the construction of the 6M-TTP cluster by the edge-sharing scheme. The 6M-TTP cluster is the structural link between the cubic crystalline and the amorphous phases.

The Intermediate-Range Structure of Glasses as seen from their Magnetic Properties and Under an Optical Microscope

*Giancarlo Jug^{1,2,3}

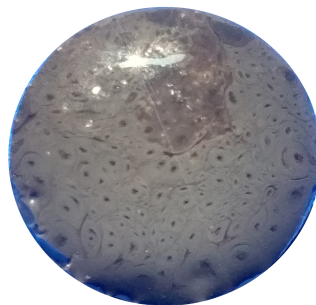
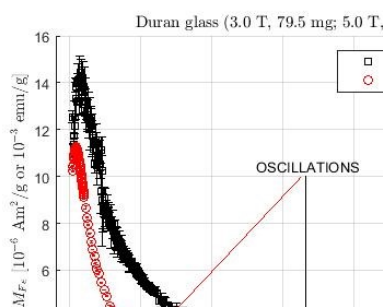
¹DiSAT, Università dell'Insubria, 22100 Como, 22100, Italy, ²INFN Sezione di Pavia, 27100 Pavia, Italy,

³To.Sca.Lab Università dell'Insubria, 22100 Como, Italy

*giancarlo.jug@uninsubria.it

Keywords: Glass structure, SQUID-Magnetometry, Nanometric structures, Optical microscopy.

While the atomic-range- and long-range-structure of glasses are basically agreed upon, the intermediate-range has witnessed controversy since the early 1930s. In this talk I shall argue that low-temperature experiments (particularly in a magnetic field) have recently contributed enormously to elucidate such intermediate structure as being characterized by frozen-in heterogeneities that issue from the super-cooled liquid state. When creating glass through avoided-crystallization, the liquid is characterized by solid-like fluctuations already in the proximity of T_x (the crystallization temperature). A highly correlated liquid ensues upon rapid cooling and the seeding with solid-like particles creates growing quasi-ordered clusters (Regions of Enhanced Regularity, RER) that jam-pack at the onset of glass formation. The RER become static and trap in their “voids” particles that remain liquid-like all the way down to the lowest temperatures ($T \ll T_g$, T_g the nominal “glass transition” temperature). These liquid-like regions are responsible for a plethora of new phenomena known as cryogenic anomalies: I will show that the magnetic (and other) effects arise from some collective yet localized modes and are responsible for new puzzling physical phenomena. I shall review the most-probable explanation for the magnetic and other anomalies, including a rationale for the so-called Two-Level Systems (TLS). The discovery of a new unexpected true magnetic effect will be reported and explained in its unusual details in the light of a new microscopic theory that relies on the existence of collective tunneling modes in the said “voids” between the RER. These collective modes have staggering new physics properties. At the same time, the creation in the laboratory of a glassy multi-silicate specimen provides the confirmation at milli-metric scale of the proposed cellular intermediate structure at the nano-metric scale characterizing all glasses. Including metallic glasses. Visible to the naked eye, and well-characterized in an optical and better in a scanning electron-microscope, the cells remain non-crystalline though seeded by dirt and nano-crystals and provide for the solidity of the whole specimen. Images taken with a simple smartphone camera and an optical microscope reveal a cellular, self-similar and fractal structure where the solid-like regions are jam-packed and yet present no crystallinity. The two investigations (SQUID-magnetometry and purpose-seeding of the hot liquid) corroborate each other and give full support to the cellular model of glasses.



Left: temperature dependence of the intrinsic magnetization of a borosilicate glass at 3.0 (red) and 5.0 (black) Tesla. Beside the unexpected peak at low temperatures, clear temperature oscillations arise at higher temperatures.
Right: smartphone camera image of the cellular structure (whitish regions) in a macroscopic BaO-Al₂O₃-SiO₂ glass specimen seen from above (meniscus of the vitrified liquid). Specimen diameter 16 mm.

Structural Origin of Temperature Memory Effect of Quenched Strain in Metallic Glasses

*Masato OHNUMA¹, Pawel KOZIKOWSKI¹, Giseller HERZER², Ryuichi HASHIMOTO¹, Tomoya OSHIKIRI¹, Merkus KUHNT², Christian POLAK²

¹ Hokkaido University, Sapporo, Postal code 060-8628, Japan, ² Vacuumschmelze GmbH & Co. KG, Hanau, D-63450, Germany

* ohnuma.masato@eng.hokudai.ac.jp

Keywords: Stress annealing, Linear Thermal Coefficient, Localized flow unit

Stress annealing (SA) induced magnetic anisotropy is known in iron, nickel and cobalt-based ferromagnetic metallic glass ribbons and it has already been used in commercial processes. Uniaxial elastic strain is introduced by SA and is quenched into the ribbons even after cooling and removing the external stress. The release of the uniaxial quenched strains is clearly observed as an anomaly in the linear thermal expansion coefficient, LTEC, when the ribbon is re-heated without stress as. The rate of strain release corresponding to the LTEC anomaly, reaches a maximum at the temperature at which the original SA was performed shown in Fig.1. We have observed this temperature memory effect for the first time over the whole temperature range from 280 to 400°C, which is below the crystallization temperature, T_x . As shown in Fig.2, the observed results are explained well by the existence of a localized “flow unit” embedded in an elastic matrix, which is accepted as the origin of the shear band formation and rejuvenation of metallic glasses with T_g (glass transition temperature) $< T_x$. Although T_g is hardly visible in calorimetry measurements in most of the ferromagnetic metallic glass ribbons ($T_g > T_x$), the results here indicate that the same important structural feature is common to metallic glasses with both $T_g < T_x$ and $T_g > T_x$. Because magnetization behavior is very sensitive to the existence of residual elastic strain which is difficult to evaluate in most of the metallic glasses, detailed studies, and a revival of interest in ferromagnetic ribbons will help us to understand more about the nature of the localized flow unit, as well as non-affine deformations.

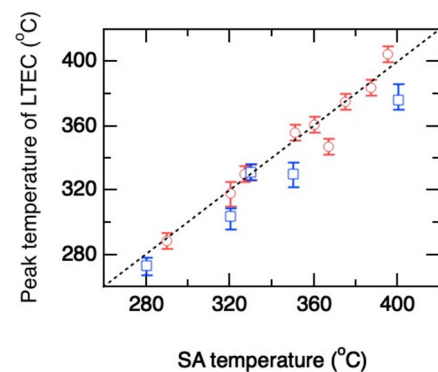
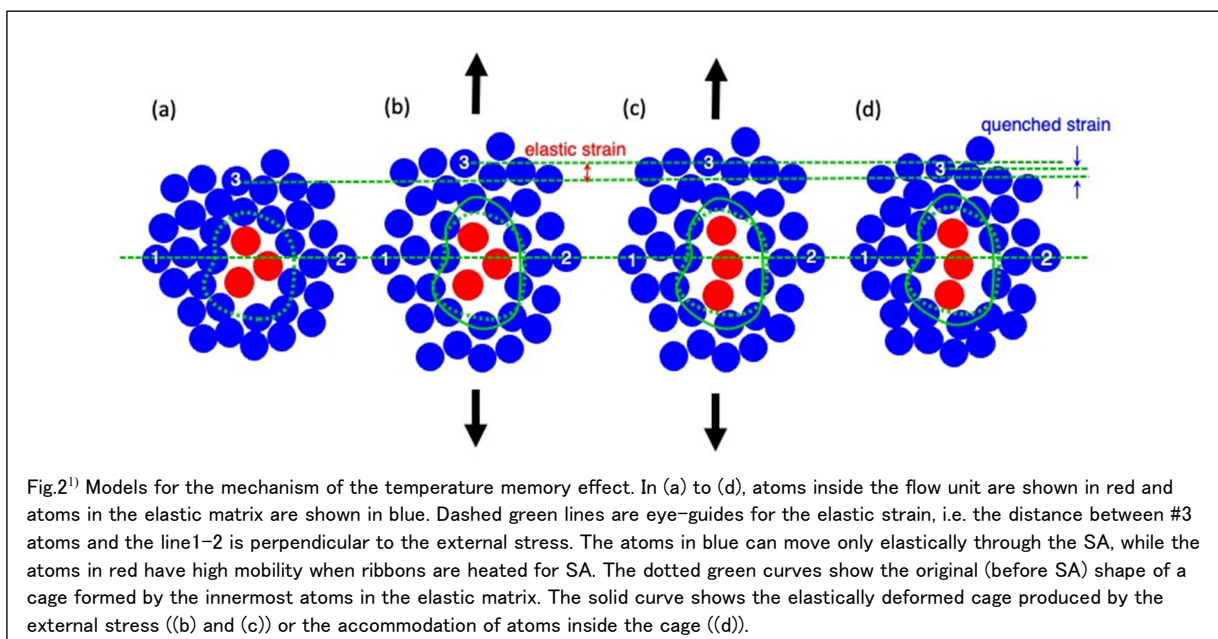


Fig.1¹⁾ Relation between SA temperatures and peak temperatures in LTEC. The difference in colors correspond to two experiments with different atmosphere (blue: in air, red: under N₂ flow). The dotted line corresponds to the case that peak temperature perfectly agree with the SA temperature.



References (Example: non-mandatory, 10 point):

1) P.Kozikowski, M.Ohnuma, R.Hashimoto, K.Takano, G.Herzer, M.Kuhnt, C.Polak, Phys.Rev. Mater., 4(2020), #095604

Synthesis and Mechanical Property of Highly Structure Controlled Metallic Glasses by Thermal Rejuvenation Technique

* J. Saida^{1,#}, W. Guo^{1,2}, R. Yamada^{1,3}, W.H. Ryu^{1,4}

¹ Frontier Research Institute for Interdisciplinary Sciences (FRIS), Tohoku University, 980-8578, Japan, ² State Key Lab of Materials Processing and Die & Mould Technology, Huazhong University of Science and Technology, 430074, China, ³ Institute for Materials Research, Tohoku University, 980-8577, Japan, ⁴ Department of Materials Science and Engineering, Research Institute of Advanced Materials & Institute of Engineering Research, Seoul National University, Seoul 08826, Republic of Korea

* jsaida@fris.tohoku.ac.jp

Keywords: Metallic glass, Thermal rejuvenation, Relaxation, Mechanical property, Local structure

Metallic glasses have random atomic configuration intrinsically and generally exhibit attractive mechanical behaviors such as high strength, elastic modulus, hardness and wide elastic limit¹. Recent progress of alloy development for highly stabilized glassy structure (high glass-forming ability) has enabled us to produce glassy alloys with a bulky shape. Such bulk metallic glasses (BMGs) are expected to apply for new industrial parts with a precision shape due to their attractive properties. Metallic glasses also cause a slight local atomic structure change, that is, “structural relaxation” by low temperature annealing and/or mechanical processing, which generally leads to serious embrittlement. However, since it has not been reported an effective way to get back the less relaxed state from the relaxed metallic glass, it has been necessary to avoid relaxation during a machining process until now.

The authors have studied the relaxation behavior in metallic glasses under the cooling process from the melt. Consequently, we have reported the strong dependence of relaxation state with the cooling rate just above the glass transition temperature, T_g in the supercooled liquid state². The results indicate a possibility of recovering the less relaxed metallic glass by a simple way using thermal process with heating above T_g for short duration followed by a rapid cooling. Actually, we succeeded in preparation of the recovered less relaxed metallic glass from the relaxed one by appropriate annealing and cooling conditions in Zr-Al-(Ni)-Cu and Mg-Cu-Ag-Gd BMGs³⁻⁸. This recovering process is so called as “rejuvenation”. These rejuvenated metallic glasses generally bring a mechanical softening with improved ductility. It is due to the re-introduction of free volume and local atomic structure change in the metallic glass^{4,5,9}.

In this presentation, detailed rejuvenation process and improved mechanical properties in metallic glasses will be reported. These studies provides beneficial information on the industrial application of metallic glasses.

References:

1. *for example*, A. Inoue, Acta Mater. 48, 279 (2000)
2. J. Saida *et al.*, Met. Mater. Trans. 42A, 1450 (2011)
3. J. Saida *et al.*, Appl. Phys. Lett. 103, 221910 (2013)
4. M. Wakeda *et al.*, Sci. Rep. 5, 10545 (2015)
5. J. Saida *et al.*, Sci. Tech. Adv. Mater. 18, 152 (2017)
6. W. Guo *et al.*, J. Non-Cryst. Solids 498, 8 (2018)
7. W. Guo *et al.*, Met. Mater. Trans. 50A, 1125 (2019)
8. W.H. Ryu *et al.*, NPG Asia Mater. 12, 52 (2020)
9. M. Wakeda *et al.*, Sci. Tech. Adv. Mater. 20, 632 (2019)

High-entropy design and its influence on glass-forming ability in Zr–Cu-based metallic glass

*Y. Ohashi¹, T. Wada², H. Kato²

¹ Department of Materials Science, Graduate School of Engineering, Tohoku University, Sendai 980-8577, Japan,

² Institute for Materials Research, Tohoku University, Sendai 980-8577, Japan

*yusuke.ohashi.q4@dc.tohoku.ac.jp

Keywords: Bulk metallic glass, High-entropy alloy, Glass-forming ability.

[Introduction] Bulk metallic glasses (BMGs) and high-entropy alloys (HEAs) are advanced materials that are attracting much attention in both the industrial and academic fields because of their various properties that differ from those of conventional alloys. BMGs have no long-range structural periodicity in their atomic arrangement and are generally obtained from freezing a disordered liquid structure below the glass transition temperature (T_g). HEAs are crystalline alloys with equimolar compositions of five or more elements, which form a single-phase solid solution with a simple lattice. Four core effects have been proposed [1] and several HEAs with novel properties that cannot be obtained with conventional materials have been reported. High-entropy metallic glasses, which combine the properties of BMGs and HEAs, have high mixing entropy in the liquid phase, and the confusion principle [2] is also applicable to them and excellent glass-forming ability is expected. BMGs have enhanced GFA in eutectic compositions, but most HEBMGs are set to equimolar compositions for entropy maximization, and alloys that combine both eutectic composition and high mixing entropy are currently extremely limited. In this work, we systematically increased the number of components up to a ternary system and fabricated new Zr–Cu-based multicomponent eutectic alloys. By doing so, we attempted to clarify the effect of component increase to the high-entropy region on the GFA from the thermodynamic and kinetic viewpoints.

[Experiments] The alloys were prepared by arc-melting high-purity elements of Zr, Hf, Al, Ag, Cu, and Ni under Ar gas. The fully melted alloy was poured into a cylindrical copper mold to produce rapidly quenched bulk samples. Heat treatment was performed by sealing specimens in a quartz tube under a vacuum of less than 5×10^{-3} Pa, and held at 1000 K, just below the melting point of the specimens, for 12 hours using an electric furnace. The phase of the cast specimens was identified using X-ray diffractometers. The microstructure and composition of the phase were analyzed by a scanning electron microscope equipped with an energy-dispersive spectrometer. Thermal analyses were performed using a differential scanning calorimeter (DSC8500, PerkinElmer) to evaluate the solidification behavior, phase transformation temperature and specific heat capacity.

[Results] Fig. 1 shows the slow-cooled solidification microstructure of the fabricated quaternary alloy, confirming its eutectic composition. Increasing the number of components in Zr–Cu-based eutectic alloys, e.g., $Zr_{48}Al_8Ag_8Cu_{36}$ ($n = 4$, $D_{max} = 25$ mm), and $Zr_{35}Hf_{13}Al_{11}Ag_8Ni_8Cu_{25}$ ($n = 6$, $D_{max} = 14$), does not result in increasing the GFA. A clear tendency exists where the GFA of the alloy decreases when the additive element is solidly dissolved into the original liquid competitive crystalline phase. This is because of the thermodynamical stabilization of the dissolved crystalline phase from the increased configurational entropy, which results in increasing the driving force of the eutectic reaction. In contrast, the GFA of the alloy increased when the additive element created a new crystalline phase. Ag and Ni have larger differences in atomic size and chemical interactions with other elements compared with the substitution source, Cu. The addition of Ag and Ni forms a new phase, and thus enhances the GFA in a Zr–Cu-based eutectic alloy. However, Hf has a smaller difference in atomic size from the substitution source, Zr, and a smaller heat of mixing difference from the constituent elements, so the Hf additive tends to replace Zr sites in the original crystalline phase, thus degrading the GFA. The GFA of the Zr–Cu-based multicomponent eutectic alloys can be understood using both thermodynamic and kinetic parameters, e.g., the $Zr_{48}Al_8Ag_8Cu_{36}$ quaternary alloy with the largest GFA bears both a smaller driving force for the eutectic reaction and the smallest fragility parameter ($m = 38$). In contrast, the $Zr_{31.6}Hf_{13.4}Al_{8.7}Ag_{8.4}Cu_{37.8}$ quinary alloy with the smallest GFA bears the largest driving force for the eutectic reaction and the largest fragility parameter ($m = 44$).

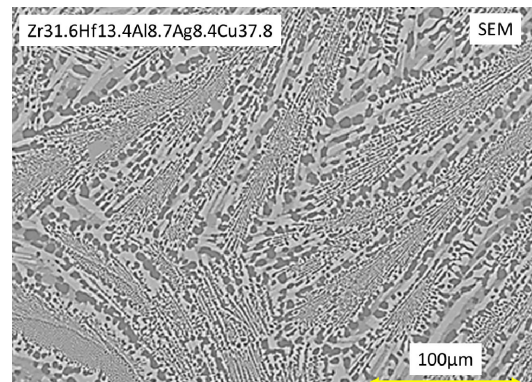


Fig 1. Slow-cooled eutectic microstructure of quaternary alloy

References:

- 1) M.H. Tsai et al., Mater. Res. Lett. 3 (2014) 107-123.
- 2) A.L. Greer, Nature. 366 (1993) 303.

Dynamic heterogeneities in undercooled metallic alloys

*Noel Jakse¹

¹ Université Grenoble-Alpes, CNRS, Grenoble INP, SIMaP, F-38000 Grenoble, France.

* noel.jakse@grenoble-inp.fr

Keywords: Dynamic Heterogeneities, Ab initio simulation, Molecular dynamics, alloys, undercooling, Machine learning.

Understanding evolution of dynamic properties in undercooled liquids and their interplay with their structural features represents an important issue for solidification processes of metallic alloys, such as crystallization and formation of quasi-crystalline or amorphous phases [1–4]. In the present work, we focus on various classes of Aluminum alloys such as Al-Ni [5], Al-Cu [6], Al-Cr [7] and Al-Zn-Cr [8] that we investigated using ab initio molecular dynamics. We simulate the undercooling process of these alloys during which we monitor the structural and atomic transport properties. We find that diffusion, viscosity and structural relaxation time undergo a crossover between an Arrhenius and non-Arrhenius behavior at a temperature T_X during the slowing down, which corresponds to an onset of developing dynamic heterogeneities (DHs). The structural features display characteristics compatible with the occurrence of the icosahedral short-range order (ISRO) as well as the development of a medium range order (MRO) upon cooling. The interplay between the ISRO, MRO and DHs is examined. New developments in detecting such heterogeneities using unsupervised topological learning will be discussed [9].

[1] C. P. Royall and S. R. Williams, Phys. Reports 56, 1 (2015).

[2] H. Tanaka, Eur. Phys. J. E 35, 113 (2012).

[3] Y. Q. Cheng and E. Ma, Prog. Mater. Sci. 56, 379 (2011).

[4] K. F. Kelton, G.W. Lee, A. K. Gangopadhyay, R.W. Hyers, T. J. Rathz, J. R. Rogers, M. B. Robinson, and D. S. Robinson, Phys. Rev. Lett. 90, 195504 (2003).

[5] N. Jakse and A. Pasturel, J. Chem. Phys. 143, 084508 (2015).

[6] N. Jakse and A. Pasturel, AIP Adv. 7, 105212 (2017).

[7] N. Jakse and A. Pasturel, Phys. Rev. B 95, 144210 (2017).

[8] A. Pasturel and N. Jakse, npj Computational Materials 3, 33 (2017).

[9] S. Becker, E. Devijver, R. Molinier, and N. Jakse, Sci. Rep. (Nature) 12, 3195 (2022).

Relaxation dynamics of glass forming metals: Study of aging, anelasticity and supercooled liquid behavior in a ZrTiCuNiBe alloy

*E. Pineda¹, M. Nabahat¹

¹Department of Physics, Institute of Energy Technologies, Universitat Politècnica de Catalunya – BarcelonaTech, Barcelona, 08019, Spain

*eloi.pineda@upc.edu

Keywords: Metallic glasses, physical aging, anelasticity, mechanical spectroscopy.

The structural relaxation of supercooled liquids (SCL) and glasses involves spatial and temporal heterogeneity, a high degree of cooperativity and long timescales. The complex relaxation spectrum of disordered materials, the effects of aging and the wide range of experimental timescales make difficult to relate the different observations in a whole picture of the liquid-glass dynamics. We will present here our recent work on a $\text{Zr}_{46.75}\text{Ti}_{18.25}\text{Cu}_{7.5}\text{Ni}_{10}\text{Be}_{27.5}$ alloy. This glass forming alloy is characterized by an outstanding stability against crystallization and decomposition. In addition, the mechanical spectrum shows a single α relaxation peak with no evidence of a secondary process. This makes this material a good model to get insight into the dynamics of metallic glasses discarding, as maximum as possible, the peculiarities of each particular composition.

Firstly, we will present the anelastic, or delayed elasticity, behavior. This phenomenon is particularly large in glasses due to a broad distribution of reversible deformation modes. Recovery experiments after different loading times show that the time distribution of modes is invariant over a large range of temperatures with a τ^{-n} dependence, that can be directly related to the high-frequency wing of the α relaxation. Fig. 1 shows the mechanical spectrum (a), the distribution of relaxation modes (b) and the corresponding anelastic recovery functions (c). Secondly, we will show the stress relaxation behavior obtained by strain step tests in both the SCL and glass states¹. In the SCL, the relaxation functions show an invariant shape, fulfilling the time-temperature superposition principle and in agreement with the viscosity behavior. In the glass state the relaxation becomes stretched, indicating an increase of dynamical heterogeneity. The study of the physical aging process, performed by means of step strain tests after different isothermal annealing times, shows that the atomic mobility decreases with an aging shift rate of $\mu \sim 0.5$ and, interestingly, the dynamical heterogeneity increases. This result implies that the dynamics becomes more heterogeneous in more stable glassy states, contrarily to the homogenization expected when the system evolves towards the equilibrated SCL configuration. Thirdly, we will compare the mechanical results with microscopic insights obtained by X-ray Photon Correlation Spectroscopy. At temperatures near and above T_g , the mechanical and microscopic results show a constant dynamical heterogeneity, fulfilling the time-temperature superposition principle. Below T_g , the microscopic and macroscopic dynamics disagree in both functional shape and timescale. The intermediate scattering function changes from a stretched shape in the SCL to a compressed and fast decay in the glass. Taking into account the aging and anelasticity behaviors, this effect may be explained by how the aging rate and the stress relaxation are observed in the microscopic scale. Finally, we will summarize the complete view of the metallic glass relaxation dynamics and we will compare with the results observed in other glass forming alloys.

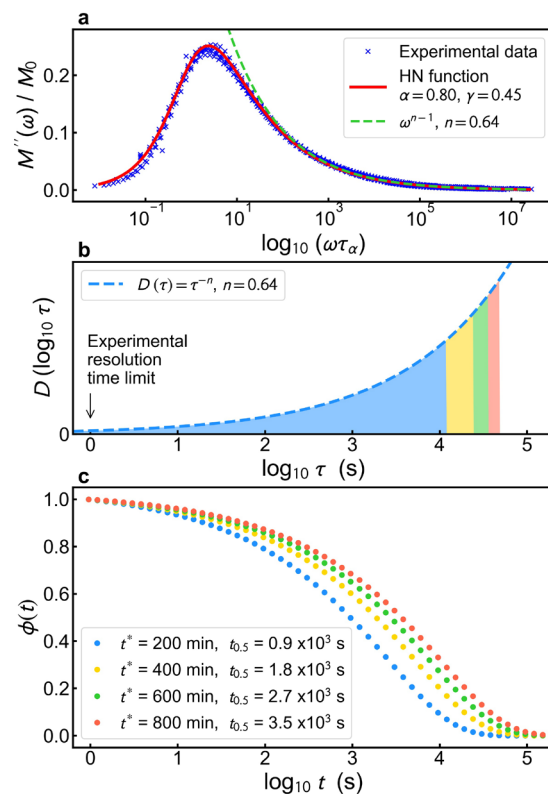


Fig. 1. a) Mechanical spectrum of the ZrTiCuNiBe glass. b) Distribution of reversible relaxation modes generating the transient creep and the recovery behaviors. The colored areas indicate the fraction of modes activated after different loading times c) Anelastic recovery functions after different loading times. The shape of the function remains invariant and the timescale evolves linearly with loading time.

References:

- 1) N. Amini, Phys. Rev. Mater. 5, 055601 (2021).

Emergent structural heterogeneity and its effect on viscosity and transport in a model binary metallic glass

*P. M. Derlet¹, H. Bocquet¹, R. Maass^{2,3}

¹Condensed Matter Theory Group, Paul Scherrer Institut, Forschungsstrasse 111, 5232 Villigen PSI, Switzerland

²Federal Institute of Materials Research and Testing (BAM), Unter den Eichen 87, Berlin 12205, Germany

³Department of Materials Science and Engineering, University of Illinois at Urbana Champaign, 1304 West Green Street, Urbana, IL 61801, USA

*peter.derlet@psi.ch

Keywords: Metallic glasses, Atomistic simulation, Structural heterogeneity, Structural evolution, Deformation

How thermally activated structural excitations quantitatively mediate transport and micro-plasticity in a model binary glass at the micro-second time-scale is revealed using atomistic simulation. It is found that such local excitations underlie the transport of free volume and bond geometry. Viscosity estimates are obtained giving a relaxation time-scale that is comparable to the strain recovery timescales seen in micro-plasticity simulations. The transport is found to correspond to the evolution of a disclination network describing the spatial connectivity of topologically distinct bonding environments, demonstrating the important role of geometrical frustration in both glass structure and its underlying thermally activated dynamics. The character of this disclination network, and how it emerges from quenching of the under-cooled liquid, is studied revealing a system-spanning micro-structure of icosahedral and Frank-Kasper structural motives which are essentially frozen at the time scale of molecular dynamics. Upon loading in the nominally elastic deformation regime, this leads to a dissipation-driven heterogeneous internal stress distribution, and upon unloading negative creep and complete residual-strain recovery.

References:

- 1) P. M. Derlet, H. Bocquet, and R. Maass, *Phys. Rev Mater* 5, 125601 (2021).
- 2) P. M. Derlet and R. Maass, *Acta. Mater.* 209, 116771 (2021).
- 3) P. M. Derlet, *Phys. Rev. Mater.* 4, 125601 (2020).

Creation of Three-Dimensional Relaxation State Gradient in $Zr_{50}Cu_{40}Al_{10}$ Metallic Glass Through a Thermal Process

*Rui Yamada^{1,3}, Wook Ha Ryu², Haruka Isano³, Tomohiro Yoshikawa³, Junji Saida³

¹Institute for Materials Research, Tohoku University, Sendai, 980-8577, Japan, ²Research Institute of Advanced Materials & Institute of Engineering Research, Seoul National University, Seoul, 08826, Republic of Korea, ³Frontier Research Institute for Interdisciplinary Sciences, Tohoku University, Sendai, 980-8578, Japan.

* rui.yamada.b6@tohoku.ac.jp

Keywords: metallic glass, relaxation state gradient, thermal process

Metallic glasses are attracted much attention in engineering materials owing to their superior mechanical properties and formability, which are originated from a unique random atomic configuration (amorphous structure). Previous studies revealed that the amorphous structure is not completely random but it would be rather heterogeneous¹). Recently, manipulation of heterogeneity through tailoring a relaxation state is intensively studied with the aim of extending the range of a glassy state²). One of the representative processes is mechanical way such as cold rolling, shot peening, high pressure torsion (HPT) etc.²). These processes are based on a heavy plastic deformation with introducing gigantic strain in the sample. Though such processes achieved a certain success in tailoring a glassy state, there still have some drawbacks. One is that these processes inevitably destruct an initial geometry shape of a sample. Another problem is that some of the process does affect only on a surface but it is difficult on a whole area. The third is that applicable sample size is limited, accordingly, most of them can apply only for a bulk sample. From these backgrounds, it has been highly desired a new process to solve these problems.

A thermal process is one of the strong candidates for meeting such demands. It is realized that, unlike the mechanical way, the process is non-destructive and there is no shape change. In addition, it is isotropic, homogeneous, and it can affect not just a part but an entire area of the sample. Moreover, it can apply to any shape of samples like ribbon, disk, bulk etc.. Because of these advantages, thermal process is currently getting attention regarding on tailoring the relaxation state heterogeneity.

In our previous study, it was revealed that a glassy state can be tuned by changing a cooling rate from a supercooled liquid region³). It was also found from a dynamic mechanical analysis that heterogeneities of the samples are different from each other with cooling rate³). These results confirmed that a relaxation state heterogeneity can be tailored through the thermal process. More recently, our research group revealed that relaxation state gradient can be created in a single monolithic metallic glass with creating a cooling rate difference within a rod sample⁴). Interestingly, the sample with relaxation state gradient showed an improved ductility during compression.

Though a creation of the gradient has already attained for a simple case (i.e. two-dimensional), more complex case (e.g. three-dimensional) has never been achieved yet. Moreover, key factors for creating such relaxation state gradient through the thermal process are still uncertain. Therefore, the objectives of the present study are to create a three-dimensional relaxation state gradient in a $Zr_{50}Cu_{40}Al_{10}$ metallic glass through the thermal process and to clarify what factors do affect a creation of the gradient.

In the present study, a sample holder with a tilt angle of 24 degree against a horizontal direction is newly developed aiming to create the relaxation state gradient in the diagonal direction of the rod sample. $Zr_{50}Cu_{40}Al_{10}$ rod sample was firstly heated to a supercooled liquid region and then one side of the holder was cooled down rapidly by attaching a Cu mesh which was indirectly cooled with liquid nitrogen in advance. After the heat treatment, a specific heat measurement and an indentation test were conducted to evaluate the creation of relaxation state gradient.

It was revealed that three-dimensional relaxation state gradient was successfully created in the rod sample through the thermal process. Thermal conductivity of the as-cast sample was calculated to be around 5-18 W/m · K which is far below the normal pure metal data. From the result, it was suggested that this low thermal conductivity of the sample plays an important role in a creation of relaxation state gradient during the heat treatment. Our present findings will give a beneficial information for creating a relaxation state heterogeneity in metallic glasses.

References:

- 1) H. B. Yu et al., National Science Review 1, 2014, 429-461.
- 2) Y. Sun et al., Nature Reviews Materials 1, 2016, 1-14.
- 3) J. Saida et al., Science and Technology of Advanced Materials 18, 2017, 152-162.
- 4) W.H. Ryu et al., NPG Asia Materials, 2020, 12:52.

Present address: Institute for Materials Research (IMR), Tohoku University, Sendai, 980-8577, Japan.

How the Liquid Structure is Formed; Bottom-up, Top-down, or Both?

*T. Egami^{1,2}

¹Shull-Wollan Center, University of Tennessee, Knoxville, TN 37996, USA, ²Oak Ridge National Laboratory, Oak Ridge, TN 37831, USA

*egami@utk.edu

Keywords: Liquid structure, Medium-range order, Pseudopotential, Density wave.

Liquid is a condensed matter of which physical density is similar to that of solid. Atoms form a random structure with short- and medium-range atomic correlations. To elucidate such local correlations has long been a major challenge. The conventional approach is to start with local structural units made of several atoms, and to use them as building blocks to form a global structure, the local *bottom-up* approach. However, this approach fails to explain the strong drive to form the medium-range order (MRO) which is different from the short-range order (SRO) in nature [1,2]. We propose to add an alternative global *top-down* approach to explain the driving force to form the MRO. In this approach we start with a high-temperature gas state and then apply interatomic potentials to all atoms at once. This causes collective density wave instability in all directions with the same wavelength. These two driving forces, local and global, are in competition and are mutually frustrated. The final structure is determined through the compromise of frustration between these two, which creates the MRO. This even-handed approach on global and local potential energy landscapes explains the distinct natures of SRO and MRO, and strong temperature dependence of various properties of liquid.

The key to the top-down approach is the use of the pseudopotential. To consider all atoms at once it is more convenient to use reciprocal space. However, the Fourier-transform of the interatomic potential, $\phi(r)$, is dominated by the strongly repulsive part of the potential and is meaningless. We consider the pseudopotential by truncating $\phi(r)$ at a cut-off distance, r_c , to remove the diverging repulsive part of the potential, and assume $\phi_{pp}(r) = \phi(r_c)$ for $r < r_c$ [1]. This is reasonable because at short distances no pair of atoms are found, so that the strongly repulsive part of the potential has no physical effect on the liquid. The Fourier-transform of $\phi_{pp}(r)$ has a strong minimum at q_1 which only weakly depends on r_c as shown in Fig. 1.

The minimum in $\phi_{pp}(r)$ at q_1 causes density waves with \mathbf{q} ($|\mathbf{q}| = q_1$) for all directions, forming a Bragg sphere. This state is the structurally coherent ideal glass state, conceived in extrapolation from the real liquid state [4]. The pair-distribution function (PDF), $g(r)$, of liquid and glass decays with distance as $|g(r)-1| \sim \exp(-r/\xi)/r$, as suggested by Ornstein and Zernike. Thus, the PDF of the ideal state is obtained as $g_0(r) = g(r)\exp(r/\xi)$. This state has long-range density correlations and is described by the density wave model. The local structure of this state is very diverse, with little icosahedral order [4]. Therefore, this state is not compatible with the driving force to form the SRO. This conflict between the SRO to minimize the local energy and the density wave to minimize the global energy is resolved by the compromise, resulting in the MRO. Thus, the structural coherence length of MRO, ξ , reflects the balance. When the density wave is strong ξ is long, whereas it is short when the SRO dominates. Therefore, it is short for systems with strong covalent bonds, and long for systems with metallic bonds. For this reason, the MRO coherence length is directly related to liquid fragility [5] through $\xi \sim m^3$, where m is the fragility coefficient [6]. Furthermore, the activation energy for viscosity is proportional to the coherence volume, ξ^3 , suggesting that the resistance by the density wave, not structural defects, determines the mechanical properties. Thus, the density wave theory explains a wide range of liquid properties.

References:

- 1) C. W. Ryu and T. Egami, *Phys. Rev. E* **104**, 064109 (2021).
- 2) T. Egami and C. W. Ryu, *Phys. Rev. E* **104**, 064110 (2021).
- 3) T. Egami and C. W. Ryu, *Frontier Mater.*, in press (2022).
- 4) C. W. Ryu, W. Dmowski, K. F. Kelton, G. W. Lee, E. S. Park, J. R. Morris and T. Egami, *Sci. Rep.* **9**, 18579 (2019).
- 5) C. A. Angell, *Science* **267**, 1924 (1995).
- 6) C. W. Ryu and T. Egami, *Phys. Rev. E* **102**, 042615 (2020).

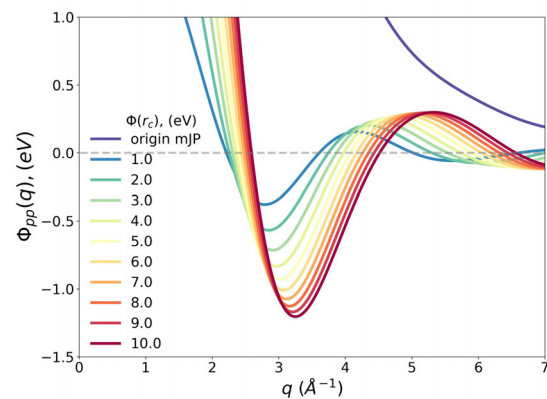


Fig. 1 The Fourier-transform of the pseudopotential for the Johnson potential for Fe, with various cutoff energies. The energy minimum causes the density waves.

Hydrodynamic Interaction Between Quasi-elastic and Acoustic Modes Observed by Inelastic X-Ray Scattering

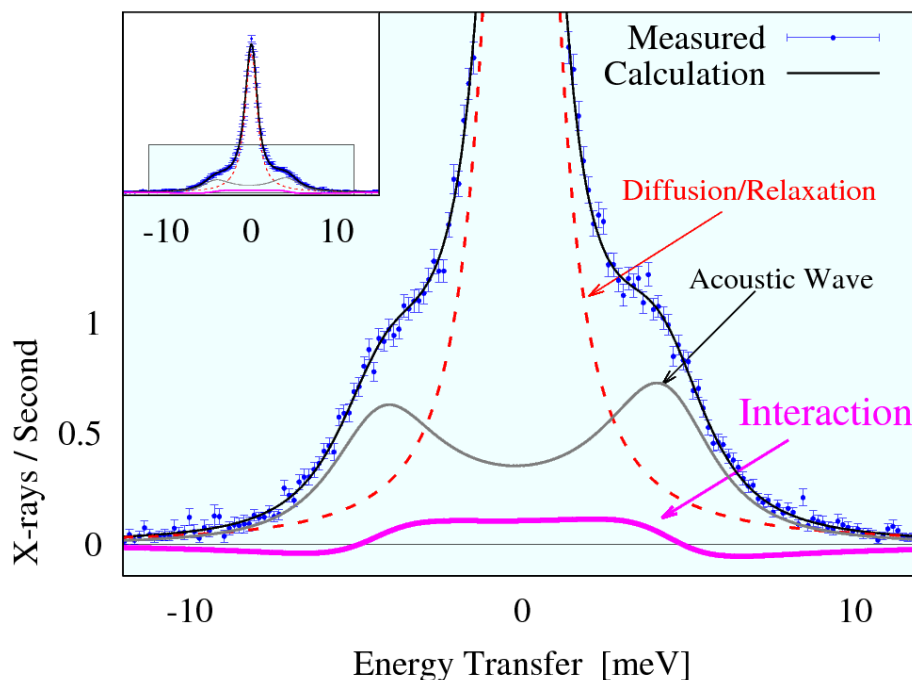
Alfred Q.R. Baron and Daisuke Ishikawa
baron@spring8.or.jp

Materials Dynamics Laboratory, RIKEN SPring-8 Center, Sayo, Hyogo 679-5148, JAPAN
Precision Spectroscopy Division, CSRR, SPring-8/JASRI, Sayo, Hyogo, 679-5198, JAPAN

Keywords: Mesoscale Liquid Dynamics, Dynamic Structure Factor, Water, Inelastic X-Ray Scattering

Improvements in methodology and instrumentation for meV-resolved inelastic x-ray scattering (IXS) [1–4], coupled with a fresh examination of older theory (e.g. [5]), allow identification of an **interaction between the quasi-elastic and acoustic phonon modes in liquids** [6]. This helps **explain a decades old controversy about the appearance of additional modes in water spectra**, and provides a strong base to discuss new phenomena in liquids on the mesoscale. Further, we find that the intensity of the quasi-elastic peak in water is in good quantitative agreement with an estimate from a simple viscoelastic model [7] using the magnitude of the positive dispersion, so the **huge increase in the quasi-elastic scattering** in water on the mesoscale (relative to the long wavelength Landau-Placzek ratio) **can robustly be interpreted as being due to the relaxation that causes fast sound** [6]. We also show that including the interaction changes the fit results, resulting in significant changes to the observed sound velocity relative to a model without interaction.

[1] A. Q. R. Baron, in *Synch. Light Srcs. & FELS*, edited by E. Jaeschke, et al. (Springer International Publishing, Cham, 2016), pp. 1643-1757. See also arXiv 1504.01098. [2] D. Ishikawa, D. S. Ellis, H. Uchiyama, and A. Q. R. Baron, *J. Synch. Rad.* **22**, 3 (2015). [3] A. Q. R. Baron, D. Ishikawa, H. Fukui, and Y. Nakajima, *AIP Conf. Proc.* **2054**, 20002 (2019). [4] D. Ishikawa and A. Q. R. Baron, *J. Synch. Rad.* **28**, 804 (2021). [5] J. P. Boon and S. Yip, *Molecular Hydrodynamics* (Dover Publications, Mineola, New York, 1980). [6] D. Ishikawa and A. Q. R. Baron, *J. Phys. Soc. Japan* **90**, 83602 (2021). [7] R. D. Mountain, *J. Res. Natl. Bur. Stand. -A. Phys. Chem.* **70A**, 207 (1966).



IXS from water at 301K at $Q=2.5 \text{ nm}^{-1}$. The various contributions are as indicated. A fit with the full interacting model (black line) gives small residuals (reduced chi-squared 0.92, probability >0.5) while a fit without interaction gives large and correlated residuals (reduced chi-squared 1.56, probability $<10^{-5}$). [6]

***Ab initio* Study of Collective Excitations in Liquid Sb**

Taras Bryk^{1,2}, *Ari Paavo Seitsonen³

¹ Institute for Condensed Matter Physics of NASU, UA-79011 Lviv, Ukraine, ² Lviv Polytechnic National University, UA-79013 Lviv, Ukraine, ³ Département de Chimie, École Normale Supérieure, F-75005 Paris, France

*Ari.P.Seitsonen@iki.fi

Keywords: collective excitations, speed of sound, generalized hydrodynamics, *ab initio* computer simulations

We report *ab initio* and machine learning study of dynamic properties of liquid Sb at temperature 973 K. The thermodynamic point corresponds to a recent experimental study of collective dynamics in liquid Sb by inelastic X-ray scattering [1]. In the *ab initio* simulation we used a system of 600 particles in order to reach small wave numbers k for the density-density and current-current time correlation functions. Additionally we used the trajectories, the forces on the ions and the total energies as input quantities in machine learning for fitting a potential for liquid Sb. We were able to perfectly recover structural properties of liquid Sb by machine learning as well as reasonable agreement for single-particle dynamic quantities.

The spectra of collective excitations in liquid Sb from *ab initio* simulations were derived by two methodologies: one was purely numerical via peak positions of longitudinal and transverse current spectral functions, while the second was based on an advanced approach of generalized eigenmode analysis of time correlation functions proposed for the case of *ab initio* simulations in Ref [2]. We discuss the comparison of simulation and experimental dynamic structure factor $S(k,\omega)$ and collective modes contributing to it in different regions of the (k,ω) -plane. Additionally we report an analysis of positive dispersion for longitudinal collective excitations outside the hydrodynamic region.

References:

- 1) M. INUI et al, J. Phys.: Condens. Matt. 33, p 475101 (2021)
- 2) T. BRYK and G. RUOCCO, Mol. Phys. 111, p 3457 (2013).

Interpretation of thermodynamic anomalies of liquid water in terms of critical fluctuations

*Yukio Kajihara¹, Kazuhiro Matsuda²

¹ Hiroshima University, Higashi-Hiroshima, Hiroshima 732-8651, Japan, ² Kumamoto University, Kumamoto 860-8555, Japan, *kajihara@hiroshima-u.ac.jp

Keywords: Liquid water, Thermodynamics, Liquid-liquid phase transition, Critical fluctuation

Liquid water near ambient conditions is known to exhibit various thermodynamic anomalies, and the relationship with the liquid-liquid phase transition (LLT), which is believed to exist in the supercooled region, has been discussed [1]. However, the actual first-order (discontinuous) phase transition is proposed to exist in the extremely supercooled and high-pressure region (no-man's land), and no conclusive experimental evidence has yet been obtained to complete the debate.

On the other hand, thermodynamic anomalies similar to those of liquid water have been known for liquid Te, and there is a long history of ongoing debate on the relationship with LLT separately from liquid water [2]. We aim to gain a comprehensive understanding of the thermodynamic anomalies commonly seen in liquid water and liquid Te, focusing on critical fluctuations. The important point here is to discuss the critical fluctuations of the LLT and liquid-gas phase transition (LGT), sorting out the similarities and differences. In LGT, density inhomogeneity, as measured by small-angle scattering, is a key parameter for critical fluctuation. On the other hand, in LLT, this density inhomogeneity = static critical fluctuation is overwhelmingly smaller than in LGT, a fact that is not a quantitatively important parameter [3]; dynamic critical fluctuation is considered important in LLT. As a physical quantity corresponding to this dynamic critical fluctuation, we have proposed the relaxation intensity [3], which is obtained by measuring the frequency dependence of the sound velocity [3].

The presentation will discuss the effect of static and dynamic critical fluctuations of LLT and LGT on the thermodynamic quantities of liquid water, showing the temperature and pressure dependence of some important thermodynamic quantities [4] (isochoric specific heat C_V is shown in the figure as an example).

References:

- 1) review: P. Gallo et al., Chem. Rev. 116, 7463 (2016)
- 2) Y. Kajihara et al., submitted; arXiv:2201.10065
- 3) Y. Kajihara et al., submitted; arXiv:2111.06589
- 4) W. Wagner et al., J. Chem. Ref. Data 31, 387 (2002)

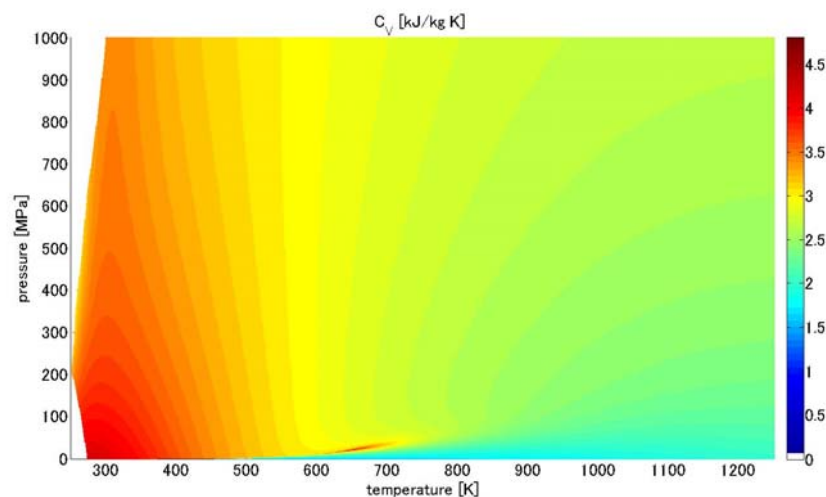


Fig. 1. Pressure and temperature dependence of isochoric specific heat capacity of liquid water [4]

Phase relation between supercooled liquid and amorphous Silicon

*Junpei T. Okada¹, Patrick H.-L. Sit², Takehiko Ishikawa^{3,4}, Jinfan Chen², Y. Watanabe⁵, P.-F. Paradis³, Kaoru Kimura⁶, and Satoshi Uda¹

¹Institute of Materials Research, Tohoku University, Sendai, Miyagi 980-8577, Japan, ²*School of Energy and Environment, City University of Hong Kong Kowloon, Hong Kong S. A. R.*, ³Institute of Space and Astronautical Science, Japan Aerospace Exploration Agency (JAXA), Tsukuba, Ibaraki 305-8505, Japan, ⁴The Graduate University for Advanced Studies (SOKENDAI), Sagamihara, Kanagawa 252-5210, Japan, ⁵Advanced Engineering Services Co., Ltd. Tsukuba, Ibaraki 305-0032, Japan, ⁶Department of Advanced Materials Science, The University of Tokyo, Kashiwa, Chiba 277-8561, Japan.

*junpei.okada.b6@tohoku.ac.jp

Keywords: first order phase transition, supercooled liquid Si, amorphous Si, electrostatic levitation technique

It is well known that liquid Si (*l*-Si) can be deeply supercooled by preventing heterogeneous nucleation. The phase relation between supercooled *l*-Si and amorphous Si (*a*-Si) has been widely investigated¹⁻⁴). It should be noticed that the electronic properties and the atomic structures are different in *l*-Si and *a*-Si; the former is metallic with the coordination number of 6 and the latter is semiconducting with the coordination number of 4. Therefore, it is difficult for the supercooled *l*-Si to directly transform into *a*-Si. In our experiments, electrostatically levitated *l*-Si samples were supercooled down to low temperatures, 300 K below the melting temperature (T_{cl} : 1683 K) and solidified accompanied with the release of latent heat. It was found that solidified Si samples melted again at 1480 K caused by the latent heat. Also, it was found that the Si samples rapidly quenched near the solidification temperature contained a large amount of *a*-Si with the tetrahedral coordination. These two findings indicate that the supercooled *l*-Si samples solidified into *a*-Si and *a*-Si melted, indicating a first-order phase transition between two metastable phases⁵).

References

- 1) Y. Shao, F. Spaepen, and D. Turnbull, *Metallurgical and Materials Transactions a-Physical Metallurgy and Materials Science* **29** (7), 1825 (1998).
- 2) A. Hedler, S. L. Klaumunzer, and W. Wesch, *Nat. Mater.* **3** (11), 804 (2004).
- 3) S. K. Deb, M. Wilding, M. Somayazulu, and P.-F. McMillan, *Nature* **414** (6863), 528 (2001)
- 4) T. Morishita, *Phys. Rev. Lett.* **93** (5), 055503 (2004).
- 5) J. T. Okada, P. H.-L. Sit, *et al.*, *Appl. Phys. Lett.* **116**, 093705 (2020).

Structure of amorphous Cu-Ge-Te and the implications for its functionality

*J. R. Stellhorn¹, S. Hosokawa², B. Paulus³, B. D. Klee³, W.-C. Pilgrim³, N. Boudet⁴, N. Blanc⁴, H. Ikemoto⁵, S. Kohara⁶ and Y. Sutou⁷

¹Hiroshima University, Higashi-Hiroshima 739-8527, Japan, ²Institute of Industrial Nanomaterials, Kumamoto University, Kumamoto 860-8555, Japan, ³Philipps University of Marburg, 35032 Marburg, Germany, ⁴Université Grenoble Alpes, CNRS, Institut Néel, 38000 Grenoble, France, ⁵University of Toyama, Toyama 930-8555, Japan, ⁶National Institute for Materials Science, Hyogo 679-5148, Japan, ⁷Tohoku University, Sendai 980-8579, Japan

*stellhoj@hiroshima-u.ac.jp

Keywords: phase-change material, amorphous local structure, anomalous X-ray scattering, EXAFS

We have investigated the structure of amorphous Cu-Ge-Te (CGT) by a combination of anomalous X-ray scattering (AXS) and extended X-ray absorption fine-structure (EXAFS) experiments [1,2]. In particular, Cu_2GeTe_3 is a novel phase-change material (PCM), i.e. it exhibits a reversible change from an amorphous phase to a crystalline phase, which can be utilized to encode binary data. CGT is expected to be used for a next generation of (nonvolatile) data storage devices due to its favorable properties [3,4]. For example, the CGT crystalline film was found to be amorphized by laser irradiation with a lower power and shorter pulse width than currently employed and widely studied Ge-Sb-Te alloys, which are essential properties to achieve rapid data recording and low power consumption in PCMs [3-5]. Further differences between these PCM systems are a reverse density change, i.e. amorphous CGT is actually denser than the crystal, and a negative optical contrast, i.e. the reflectivity of the crystalline phase is lower than that of the amorphous phase, contrary to Ge-Sb-Te [6].

The experimental AXS and EXAFS data are analyzed with reverse Monte Carlo (RMC) modeling, and they are interpreted in terms of short-range-order parameters as well as by using ring statistics and persistent homology to study the intermediate-range order. Based on this information, the structural relationship of the amorphous phase to the corresponding crystal can be discussed. It is found that the amorphous network can be rationalized by small atomic displacements of the crystal structure, directed toward the intrinsic void regions. This structural similarity establishes the possibility of a fast phase-change process. On the other hand, the atomic rearrangements also lead to the formation of new chemical bonds and to distortions on the intermediate-range-order level. These are realized by a collapse and contraction of the strict hexagonal ring arrangements of the crystal and by the formation of small, triangular rings as well as Cu cluster configurations. These structural features allow for a new understanding of the phase-change property contrast of this material, especially concerning the density change and the optical contrast.

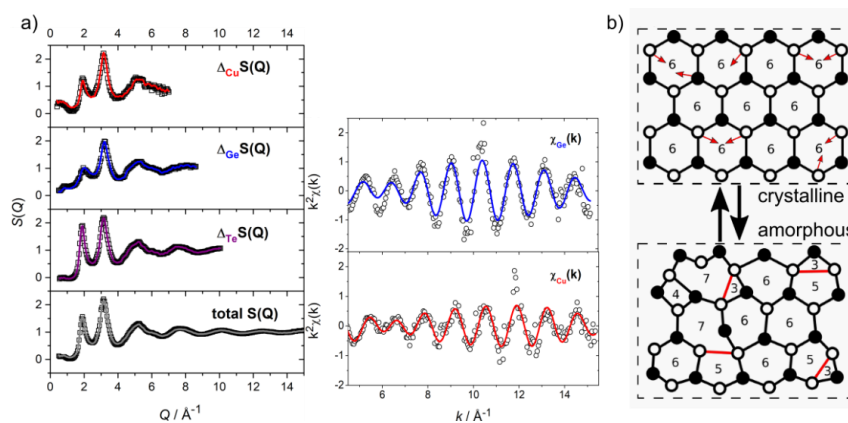


Fig. 1. a) experimental AXS and EXAFS datasets (symbols) and results of the RMC modelling (colored lines). b) model of the phase change-process regarding the ring structure.

References

- [1] J. R. Stellhorn et al, Phys. Rev. B. 101, 214110 (2020)
- [2] B. Paulus, J. R. Stellhorn, B. D. Klee, S. Hosokawa, W.-C. Pilgrim, Phys. Status Solidi B 2100619 (2022).
- [3] Y. Sutou, T. Kamada, M. Sumiya, Y. Saito, and J. Koike, Acta Mater. 60, 872 (2012).
- [4] Y. Saito, Y. Sutou, and J. Koike, Appl. Phys. Lett. 102, 051910 (2013).
- [5] M. Wuttig and N. Yamada, Nat. Mater. 6, 824 (2007).
- [6] N. Yamada, E. Ohno, K. Nishiuchi, N. Akahira, and M. Takao, J. Appl. Phys. 69, 2849 (1991).

X-ray and neutron diffraction of semi-crystalline isotactic poly (4-methyl-1-pentene) with alkane absorption

*Ayano Chiba¹, Hiromi Murashige¹, Yusuke Sanada², Yusuke Hiejima³

¹ Department of Physics, Keio University, Yokohama 223-8522, Japan, ² Department of Chemistry, Faculty of Science, Fukuoka University, Fukuoka, 814-0180, Japan, ³ Department of Chemical and Materials Science, Kanazawa University, Kanazawa 920-1192, Japan

*ayano@phys.keio.ac.jp

Keywords: X-ray diffraction, X-ray small-angle diffraction, Infrared absorption spectroscopy, Semi-crystalline polymers, Polymer host-guest structures, Small-angle neutron scattering

We are studying the possibility that confined space is useful for liquid separation. Syndiotactic polystyrene (SPS) is known to form host-guest co-crystals with various small molecules, and it may be useful for liquid separation because some small molecules are preferentially absorbed when an SPS film is immersed in a mixed liquid [1,2]. Although there are many studies on SPS, there had been no study on isotactic poly (4-methyl-1-pentene) (P4MP1) from such a point of view.

We used to study the structure of high temperature and high pressure liquids such as arsenic and antimony, and noticed that some similarities between the pressure-temperature (P-T) phase diagram of SPS and that of P4MP1. Based on the similarity, it was conceived that the phenomena found in SPS might also occur in P4MP1.

With this idea, it was found that P4MP1 as-cast film absorbs various organic solvents [3]. Not only that, but we also found the preferential absorption of long alkanes from a liquid mixture of long and short alkanes by using this polymer film and it may be useful for liquid separation [3]. However, not even whether the solvent is absorbed in the crystalline region or in the amorphous region is clear. We thus aimed to clarify the host-guest structure when this polymer (host) absorbs small molecules such as alkanes (guests).

Generally, polymer semi-crystals have both crystalline and amorphous regions. The solvent is likely to be absorbed in the amorphous region, which usually have lower density than crystalline regions. However, the density of the crystalline region of P4MP1 is slightly smaller than the density of the amorphous region, and there was a possibility that it was absorbed in the crystalline region. In order to clarify whether the absorption was mainly in the crystalline region or the amorphous region, samples with different crystallinities were prepared and the solvent absorption was investigated by infrared absorption spectroscopy. As a result, it was found that more solvent was absorbed in the amorphous region. Specifically, P4MP1 films of crystallinity of 38% and 26% absorbed decane for 0.5 mmol/cm³ and 1.6 mmol/cm³, respectively.

We also measured small-angle X-ray scattering (SAXS) accompanying absorption of the solvent, and found that a peak occurred at 0.15 nm⁻¹ accompanying absorption. This peak is assigned to the lamellar long period, and is usually not observed in this polymer because the crystal and amorphous densities are too close. It seems that the scattering contrast became non-negligible as the solvent is preferentially absorbed in the amorphous region, and the peak appears as the solvent is absorbed (Fig. 1). In the presentation, we will discuss the results of wide angle x-ray diffraction and small-angle neutron scattering as well.

References:

- 1) G. Guerra, C. Daniel, P. Rizzo, O. Tarallo, J. Polym. Sci. Part B: Polym. Phys. **50**, 305 (2012).
- 2) Y. Uda, F. Kaneko, T. Kawaguchi, Macromol. Rapid Commun. **25**, 1900 (2004).
- 3) A. Chiba, A. Oshima, R. Akiyama, Langmuir **35**, 17177 (2019).

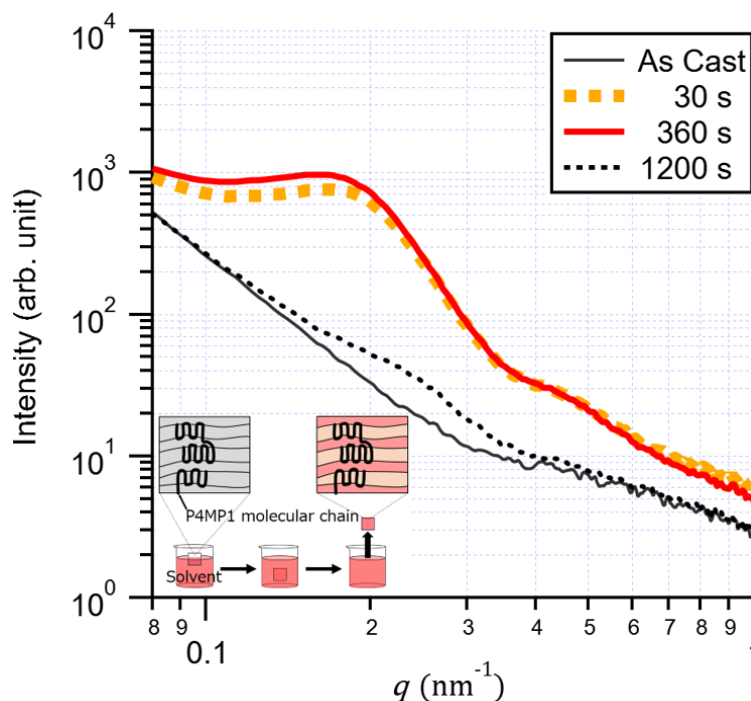


Fig. 1. SAXS profile of the As-cast film (black thin line) and the time dependence of the profile of the film after hexane is added. Orange dashed line, red thick line, and black dotted line show the SAXS profile of the as-cast film at 30, 360 and 1200 s after hexane is added.

Direct observation of concentration fluctuations in Au-Si eutectic liquid by small-angle neutron scattering

*Yoshifumi Sakaguchi¹, Shin'ichi Takata², Yukinobu Kawakita²

¹ Neutron Science and Technology Center, Comprehensive Research Organization for Science and Society (CROSS), Tokai, 319-1106, Japan, ² J-PARC Center, Japan Atomic Energy Agency, Tokai, 319-1195, Japan

*y_sakaguchi@cross.or.jp (Corresponding author)

Keywords: Eutectic alloys, melting point depression, small-angle neutron scattering.

Eutectic alloys have attracted much attention because of their low melting temperatures from both application and scientific points of view. Especially, gold-silicon (Au-Si) alloy exhibits anomalous melting point depression, which is more than 1000 °C from the melting point of pure Si (1414 °C). It is noted that the eutectic alloy is not a compound with lower melting point, but a mixture with two phases, Au and Si phases which have higher melting points. According to the thermodynamics theory, the mixture melts at lower temperature than the melting points of individual elements when the free energy of the homogeneous liquid (completely mixed liquid) is lower than the sum of the free energies of the two elemental solids. For Au-Si eutectic alloys, this mixing state was proved by the detection of the Au-Si pair correlations from the diffraction measurements [1, 2] and the molecular-dynamics simulations [3-5]. However, it is not fully explained yet why the mixing occurs at such lower temperatures at the specific eutectic composition (Au_{81.4}Si_{18.6}).

To date, an anomalous behavior in the deep eutectic liquids was pointed out from the electrical resistivity measurements by Itami *et al.* [6]. They observed a deviation from a linear temperature dependence of the electrical resistivity in liquid Ag-Si and Au-Si alloys and proposed that there were concentration fluctuations in the liquids. A presence of concentration fluctuations contradicts the theoretical understanding of the eutectic liquids where atoms are homogeneously mixed. However, such micro-heterogeneity in eutectic melts was also pointed out by other research group [7] in the same period (2004), when the 12th International Conference on Liquid and Amorphous Metals was held at Metz in France. Concentration fluctuations are often referred while fluids above a critical point of two liquid phase separation are concerned. However, there may exist small fluctuations of mixing state, where a clear liquid phase separation is not related. Assuming such concentration fluctuations, they can disturb the solidification where each kind of atoms is perfectly aligned, resulting in the anomalous melting point depression.

To directly observe such concentration fluctuations in the Au-Si eutectic liquid, we performed small-angle neutron scattering (SANS) measurement of Au_{81.4}Si_{18.6} (room temperature ~ 800 °C) and Au₇₅Si₂₅ (room temperature ~ 900 °C) on BL15 (TAIKAN) at the Materials and Life Science Experimental Facility, Japan Proton Accelerator Research Complex (J-PARC). To observe small SANS signals as clear as possible, we developed a furnace for SANS measurement with a low background [8]. At room temperature, a large small-angle scattering resulted from a sharp interface between Au and Si phases was observed in both samples. In both liquids, there still remains a small-angle scattering although its intensity is weaker than that at room temperature. This small-angle scattering in the liquid state could indicate a presence of concentration fluctuations in the liquid which Itami *et al.* suggested. The relationship between the small-angle scattering and the anomalous melting point depression is discussed in terms of the concentration fluctuations.

References:

- 1) H. Fujii, S. Tahara, Y. Kato, S. Kohara, M. Itou, Y. Kawakita, S. Takeda, J. Non-Cryst. Solids 353, 2094 (2007).
- 2) P. Chirawatkul, A. Zeidler, P. S. Salmon, S. Takeda, Y. Kawakita, T. Usuki, H. E. Fischer, Phys. Rev. B 83, 014203 (2011).
- 3) A. Pasturel, E. S. Tasci, M. H. F. Sluiter, N. Jakse, Phys. Rev. B 81, 140202(R) (2010).
- 4) N. Jakse, T. L. T. Nguyen, A. Pasturel, J. Phys.: Condens. Matter 23, 404205 (2011).
- 5) N. Jakse, T. L. T. Nguyen, A. Pasturel, J. Chem. Phys. 137, 204504 (2012).
- 6) T. Itami, H. Aoki, T. Shibata, M. Ikeda, K. Hotozuka, J. Non-Cryst. Solids 353, 3011 (2007).
- 7) P. S. Popel, M. Calvo-Dahlborg, U. Dahlborg, J. Non-Cryst. Solids 353, 3243 (2007).
- 8) Y. Sakaguchi, S. Takata, H. Arima, R. Takahashi, J. Neutron Res. 21, 29 (2019).

Structural Relaxation in Complex Liquid Metals, Antimony and Bismuth, by Means of Coherent Quasi-Elastic Neutron Scattering and Time -Space Correlation Function

*Y. Kawakita¹, T. Kikuchi^{1,2,3}, Y. Sakaguchi⁴, T. Hanashima⁴, R. Takahashi¹, D. Wakai⁵, K. Nakajima¹

¹ J-PARC Center, Japan Atomic Energy Agency, Tokai, Naka, Ibaraki, 319-1195, Japan, ² Sumitomo Rubber industries, Ltd., 3-6-9 Wakinohama-cho, Chuo-ku, Kobe, Hyogo, 651-0072, Japan, ³ Institute of Materials Structure Science, High Energy Accelerator Research Organization, Tokai, Naka, Ibaraki, 319-1106, Japan, ⁴ Neutron Science and Technology Center, Comprehensive Research Organization for Science and Society, Tokai, Naka, Ibaraki, 319-1106, Japan, ⁵ NAT Corporation, Tokai, Naka, Ibaraki, 319-1112, Japan, Affiliation, City, Postal code, Country (10 point)

*yukinobu.kawakita@j-parc.jp

Keywords Neutron scattering, Liquid metal, QENS, Time space correlation function, Antimony, Bismuth

Antimony (Sb) and bismuth (Bi) have A7 crystal structure which a simple cubic lattice is deformed to by Peierls distortion and is characterized as three short bonds and three long bonds¹⁾. The complex local structures in their liquid state are considered to be originated from the Peierls distortion and inferred to have a layered structure²⁾. We performed quasi-elastic neutron scattering (QENS) by utilizing AMATERAS spectrometer³⁾ which is cold neutron disk chopper instrument installed at Materials and Life Science Experiment Facility (MLF) in Japan Proton Accelerator Research Complex (J-PARC) aiming at extraction of a direct evidence for layered structure by difference in structural relaxation time between intra- and inter-layers. From QENS experiments for Bi and Sb, their coherent dynamics structure factor is obtained directly because of small incoherency of their neutron scattering lengths, which is useful to deduce a time-space correlation function (tscf), so-called van Hove function⁴⁾.

Figure shows the tscf obtained for liquid Sb at 650°C. The top line exhibits the tscf at $t = 0.01$ ps which is almost similar to pair correlation function. It has a main peak about at 3 Å accompanying shoulder and small peaks in a longer side up to about 4.6 Å. A time-evolution shows different relaxation time among characteristic peaks. The main peak has a relaxation time of around 0.3 ps which is contrast with much longer relaxation of the main peak (the shortest bond) in liquid Bi. In the presentation, we will discuss on structural anomaly in complex liquid metals from the viewpoint of structural relaxation dynamics with comparing liquid Bi and Sb.

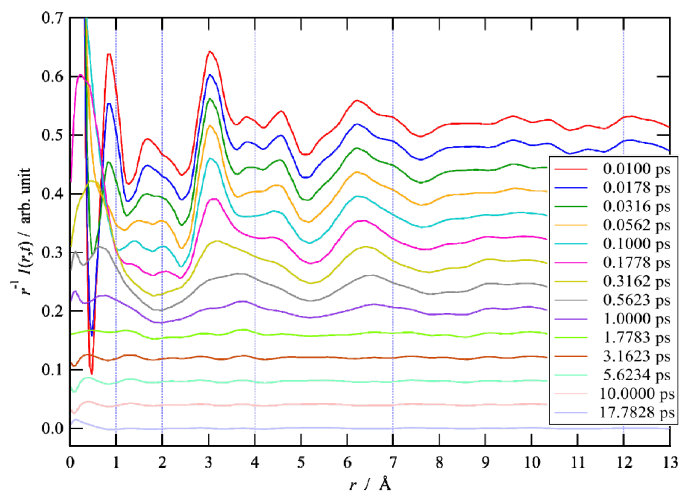


Fig. 1. Time evolution of time-space correlation functions of liquid Sb at 650°C. 14 functions with equi-interval in a logarithmic scale of time from 0.01 to 17.8 ps are shown with gradual shift from the top to the bottom..

References:

- 1) R.W.G. Wyckoff, Crystal Structures, Wiley, New York, 1963.
- 2) M. Mayo, E. Yahel, Y. Greenberg, G. Makov, J. Phys. Condens. Matter 25 (2013) 505102 and so on.
- 3) K. Nakajima et al., J. Phys. Soc. Jpn. 80 (2011), SB028.
- 4) T. Kikuchi and Y. Kawakita; Physica B 567 (2019) 51.

Estimating Thermal Conductivity of Silver Chalcogenides Using Machine-Learning Interatomic Potentials

*K. Shimamura¹, A. Koura¹, F. Shimojo¹

¹Department of Physics of Kumamoto University, Kumamoto, 860-8555, Japan

*shimamura@kumamoto-u.ac.jp

Keywords: Green-Kubo method, Machine learning, Thermal conductivity, Silver chalcogenides.

The Green-Kubo (GK) method, which is the combination of Molecular dynamics (MD) simulations and the GK formula for estimating thermal conductivity (TC), have the powerful advantage of being applicable to even irregular systems such as liquid systems. The combination of machine-learning interatomic potentials (MLIPs) with the GK method further improves the accuracy of TC and broadens the scope of application. MLIPs, which are trained with data from first-principles molecular dynamics (FPMD) simulations, successfully reproduce the high accuracy of FPMD while maintaining the low computational cost of conventional empirical interatomic potentials (EIPs). The MD simulations using MLIPs can yield sufficient statistics concerning fundamental physical quantities such as TC and free energy, or to investigate atomic dynamics in large-scale systems. However, even though heat flux is a major factor in the accuracy of TC in the GK method, the definitions of heat flux formulas for MLIPs employed in the previous studies were inconsistent with each other. MLIPs is a many-body potential that includes not only two-body functions but also three-body functions, and heat fluxes that did not account for the many-body effect have been used in previous studies. The heat flux formulas correspond to analogues of the rigorous one for two-body interatomic potentials, which would fail to estimate TC. This meant that the methodology for the combination of MLIPs and the GK method had not yet been established.

Therefore, we aimed to establish a methodology that can calculate TC with high accuracy [1-3]. Here, artificial neural networks were used for MLIPs (hereinafter referred to as ANN potential). The derivation of the heat flux formula (referred to as \mathbf{J}_Q^1) considering the many-body effect of ANN potentials was based on the previous work for Tersoff-potential by Fan *et al* [4]. We also found that this \mathbf{J}_Q^1 was closely related to the pressure formula of the virial theorem. Current standard training of MLIPs does not guarantee pressure accuracy, which could interfere with accurate estimates of TC. It became necessary to train MLIPs with pressure. To investigate the effect of heat flux formula \mathbf{J}_Q^1 and pressure training on TC, we set a superionic conductor, α -Ag₂Se, as the test system. The EIP of Ag₂Se [5] was used to generate training data for ANN potentials. With EIPs, which have a low computational cost, a reference TC value can be obtained in advance and compared with the TCs obtained from ANN potentials. Figure 1 shows the absolute differences between the TC (κ^{EP} , 0.274 Wm⁻¹K⁻¹) obtained by the EIP of Ag₂Se and those obtained by ANN potentials (κ^{ANN}) as function of pressure training errors (ΔP). Model 1 and Model 2 denote the ANN potentials without/with pressure training, respectively. For comparison, the TCs calculated by the heat flux formulas without considering the many-body effect (\mathbf{J}_Q^2 and \mathbf{J}_Q^3) which were used in previous studies. In addition, to clarify the dependence of the initial weight values of ANNs, we constructed five ANN potentials for each Model and calculated κ^{ANN} . Only when \mathbf{J}_Q^1 and Model 2 were used, the absolute differences showed almost zero, indicating that κ^{EP} was reproduced correctly. In contrast, Model 1, not only with \mathbf{J}_Q^2 and \mathbf{J}_Q^3 but also even with \mathbf{J}_Q^1 did not show the correct TC, and there were some ANN potentials that showed significant deviation from κ^{EP} . This is due to the fact that Model 1 does not guarantee pressure accuracy, and the deviation was positively correlated with ΔP . Therefore, the use of pressure training and the heat flux formula considering many-body effect of MLIPs would be essential for TC calculations.

In the presentation, we will report the results using the above method to compare the TCs obtained for not only the superionic conducting phase but also liquid and low-temperature (β) phases of silver chalcogenides including Ag₂Se.

References:

- [1] K. Shimamura *et al.*, J. Chem. Phys. **153**, 234301 (2021).
- [2] K. Shimamura *et al.*, Chem. Phys. Lett. **778**, 138748 (2021).
- [3] Y. Takeshita *et al.*, J. Phys. Chem. Solids **163**, 110580 (2022).
- [4] Z. Fan *et al.*, Phys. Rev. B **92**, 094301 (2015).
- [5] J. P. Rino *et al.*, J. Chem. Phys. **89**, 7542 (1988).

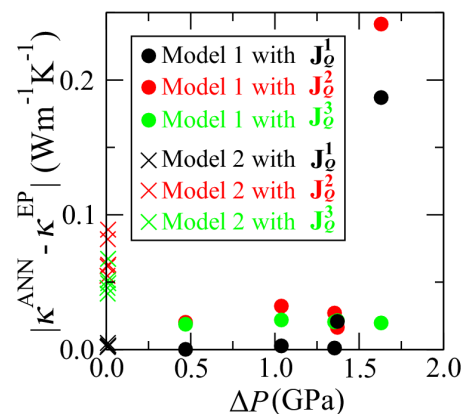


Figure 1: The absolute differences between κ^{EP} obtained from the EIP for α -Ag₂Se at 500 K and the respective κ^{ANN} calculated from ANN potentials with five different initial weight values belonging to Model 1 or Model 2 as a function of the training error (root mean square error, ΔP) [2]. κ^{ANN} was calculated for each Model using \mathbf{J}_Q^1 , \mathbf{J}_Q^2 , and \mathbf{J}_Q^3 , respectively.

Supercritical Elasticity and Structural Entanglement of Multicomponent alloys

Haiyang Chen¹, Yan-Dong Wang^{1,*}, Yang Ren^{2,*}¹ Beijing Advanced Innovation Center for Materials Genome Engineering, State Key Laboratory for Advanced Metals and Materials, University of Science and Technology Beijing, Beijing, China; ² Department of Physics, City University of Hong Kong, Kowloon, Hong Kong, China* ydwang@mail.neu.edu.cn; yangren@cityu.edu.hk

Keywords: Supercritical elasticity, order and disorder entanglement, multicomponent alloys, X-ray/Neutron scattering, Phase transformation.

Elasticity is an important property of solids. The elastic strain limit of metals rarely exceeds 1%. Shape memory alloys exhibit a large recoverable pseudo-elastic strain of up to 10% resulted from the stress-induced martensitic transformation (SIMT). However, the intrinsic hysteresis and temperature sensitivity of the first-order phase transformation significantly hinder the usage of smart metallic components in many critical areas, such as in deep-space and deep-sea exploration and intelligent robotics etc. We have prepared a series of metallic fibers of multicomponent alloys, $\text{Ni}_{55-x}\text{Co}_x\text{Fe}_{18}\text{Ga}_{27}$, by the Taylor liquid drawing technique. We found that at low Co concentration, $x=6$, the fiber shows a stress-strain behavior with typical SIMT characteristics, exhibiting a large hysteresis between the loading and unloading plateaus. With increasing Co concentration, the flat and hysteretic region diminishes, and trilinear non-hysteretic stress-strain responses occur. This peculiar elastic behavior closely resembles the characteristic feature of the isothermal pressure-volume (P-V) curves of a gas-liquid system, where the discontinuous P-V curve gradually becomes continuous above a critical temperature/pressure. Both pressure-volume and stress-strain curves present energy variation of the system, reflecting compressibility and elasticity, respectively. A modified Landau model was proposed to describe the supercritical feature of observed stress-strain curves, which indicate that an endpoint exist for the SIMT at a critical Co content. We found that fibers with high Co content exhibit over 15% non-hysteretic elasticity, a small temperature dependence, high-energy-storage capacity and ultra-stable cyclability. In-situ synchrotron X-ray diffraction measurements show that the supercritical elasticity is correlated with a stress-induced continuous variation of lattice parameters accompanied by structural fluctuation. Neutron diffraction and electron microscopy observations reveals an unprecedented microstructure consisting of atomic-level entanglement of ordered and disordered crystal structures, which can be manipulated to tune the supercritical elasticity. The discovery of the large elasticity related to the entangled structure paves the way for exploiting elastic strain engineering and development of related functional materials.

References (Example: non-mandatory, 10 point):

1) H.Y. Chen, H., Wang, YD., Nie, Z. et al. Unprecedented non-hysteretic superelasticity of [001]-oriented NiCoFeGa single crystals. *Nat. Mater.* 19, 712–718 (2020).

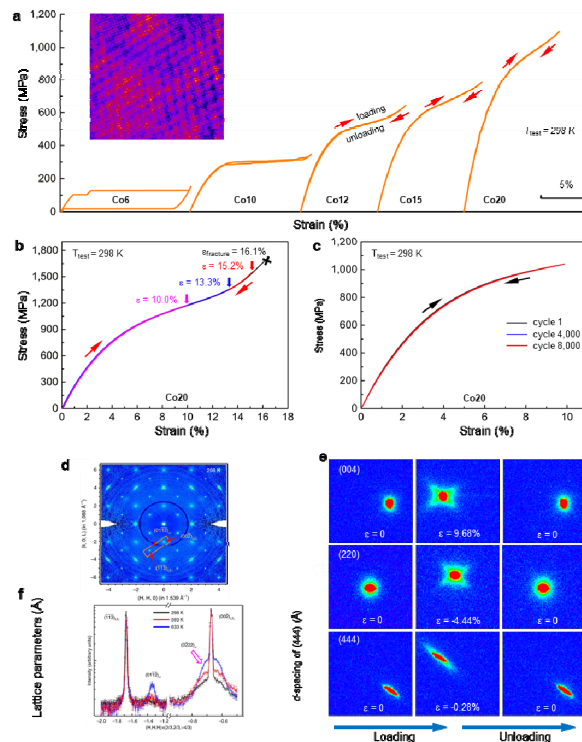


Fig. 1. Super-elastic behavior and *in situ* synchrotron x-ray diffraction of $\text{Ni}_{55-x}\text{Co}_x\text{Fe}_{18}\text{Ga}_{27}$ single crystal fibers. (a) Stress-strain curves for different Co-concentration alloys on loading and unloading. Inset: high resolution transmission electron microscope image of a Co20 alloy, showing an atomic-level entanglement of ordered/disordered structures. (b) Ultimate mechanical tests for the Co20 alloy. (c) Cyclic stress-strain curves of the Co20 alloy performed up to 8,000 cycles, without any degradation of the functional properties. (d) 2D neutron diffraction pattern collected at 298 K. (e) 1D neutron diffraction profiles of the characteristic region delineated by the frame in d. (f) Lattice parameters a , b and c and d -spacing of (444) reflection as a function of engineering strain, showing continuous changes.

Investigation of local structural changes in GeSe₂ glass under ultra-high pressure

Yimin Mijiti¹, Joao Elias Rodrigues², Aangela Trapananti¹, Javad Rezvani¹, Toru Shinmei³, Tetsuo Irifune³, Angelika dorothea Rosa², Andrea Di Cicco^{1,*}

¹ School of Science and Technology, University of Camerino, Via Madonna delle Carceri 9, Camerino, MC 62032, Italy

² European Synchrotron Radiation Facility - 71, avenue des Martyrs, CS 40220, 38043 Grenoble Cedex 9, France

³ Geodynamics Research Center Ehime University Matsuyama 790-8577, Japan

[*andrea.dicicco@unicam.it](mailto:andrea.dicicco@unicam.it)

Keywords : EXAFS, Local structure, ultra-high pressure, chalcogenide glasses.

Experimental studies of ultra-high pressure ($P > 1$ Mbar) polyamorphism in the covalently bonded network forming amorphous systems has long been a challenging topic. There is not yet enough experimental data for convincingly describe the densification and evolution of local structures in the common simple amorphous materials including SiO₂ and other geophysically relevant disordered systems under ultra-high pressures (e.g. conditions in the deep Earth), because of the experimental challenges related with the studies of tiny amorphous samples (typically in diamond anvil cells) using diffraction techniques. Here, using extended x-ray absorption fine structure (EXAFS, an ideal probe of local structures in the amorphous systems) technique, we investigated the pressure induced local structural changes in the network forming GeSe₂ glass under ultra-high pressures exceeding 150 GPa. For each pressure point, EXAFS data have been measured scanning through both Ge and Se K-edges along the same compression run, allowing us to perform more reliable data analysis using the double-edge EXAFS refinements.

Bonding and structure of liquid iron-light-element-oxygen ternary alloys under high pressure: molecular dynamics simulations

*Satoshi Ohmura^{1, #}, Fuyuki Shimojo², Taku Tsuchiya³

¹ Faculty of Engineering, Hiroshima Institute of Technology, Hiroshima, 731-5193, Japan,

² Department of Physics, Kumamoto University, Kumamoto, 860-8555, Japan,

³ Geodynamics Research Center, Ehime University, Matsuyama, 790-8577, Japan.

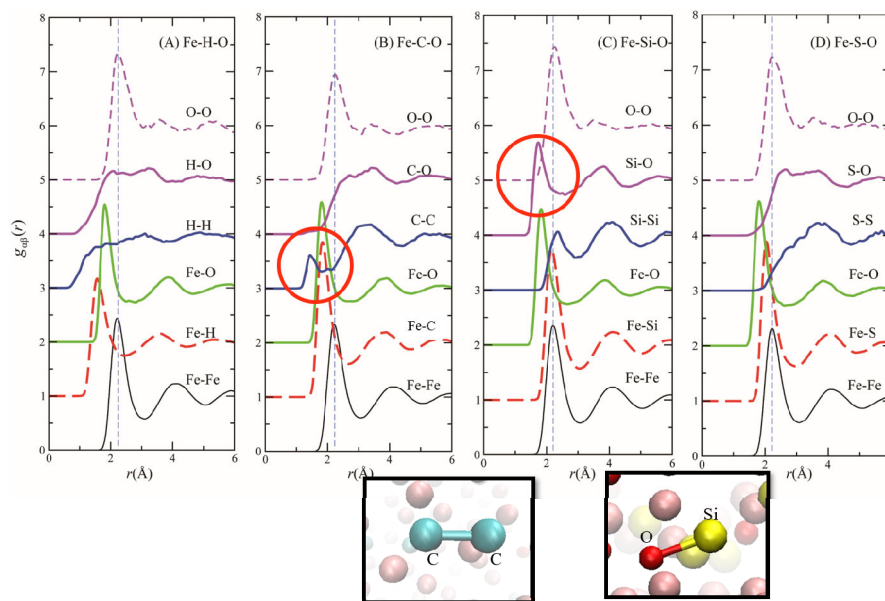
*s.ohmura.m4@cc.it-hiroshima.ac.jp

Keywords: Liquid Fe ternary mixture, High-pressure, bonding property, Ab initio simulation.

Liquid iron-light-element (LE) mixture is a constituent of Earth's outer core [1,2]. LE have a strong influence on the structural and transport properties of liquid iron under high pressure. However, there are still many uncertainties regarding the influence of LE. Recently, a systematic theoretical investigation based on ab initio MD simulations for the LE-effect on the structural properties of liquid Fe-LE binary systems under high pressure was reported [3]. The simulation clarified that H, C, and O are incorporated into liquid Fe interstitially, while Si and S are "substitutional" type impurities.

For the liquid Fe-LE-O ternary systems, several experimental and theoretical studies on the properties of liquid Fe-LE-O, including immiscibility of liquid Fe-Si-O [4,5], have been reported. However, the detailed local structures and bonding properties in liquid Fe-LE-O ternary systems, which are the origins of various properties of liquid, remain unclear. For this reason, in this study, we have investigated the structural and bonding properties of liquid Fe-LE-O ternary systems such as Fe-H-O, Fe-C-O, Fe-Si-O and Fe-S-O under high pressure using ab initio molecular-dynamics simulations.

From our simulations, it is found that H, C and O show "interstitial-type" behavior while Si and S show "substitutional" type properties in the liquid iron-light-element-O ternary systems, similar to liquid Fe-LE binary systems. For the interactions between light elements, C-C, Si-Si and Si-O shows covalent-like interactions while H-H, S-S, C-O and S-O have no strong interactions. We will also discuss the effects of the covalent-like interactions on the atomic charges in the liquids.



Partial pair distribution functions of liquids Fe-H-O, Fe-C-O, Fe-Si-O and Fe-S-O at 140 GPa and 5000 K. (Bottom panel) Snapshots of C-C bond in liquid Fe-C-O and Si-O bond in liquid Fe-Si-O

References (Example: non-mandatory, 10 point):

- 1) F. Birch, J. Geophys. Res. 69, 4377-4388 (1964)
- 2) J.-P. Poirier, Phys. Earth and Planet. Inter. 85, 319 (1994).
- 3) S. Ohmura, T. Tsuchiya and F. Shimojo, *physica status solidi (b)* 257, 2000098 (2020).
- 4) S.M. Arveson, et. al., Proc. Nat. Acad. Sci. 116, 10238 (2019).
- 5) D. Huang, et al., Geophys. Res. Lett. 46, 6397-6405 (2019)..

Inelastic X-ray scattering measurements of liquid Fe-S at high pressure

*Yoichi Nakajima^{1,2}, Asaki Iwamoto¹, Yuki UENO¹, Yasuhiro KUWAYAMA³,
Kei HIROSE^{3,4}, Guillaume MORARD⁵, Daisuke ISHIKAWA^{2,6}, Alfred Q.R. BARON^{2,6}

¹Department of Physics, Kumamoto University, Kumamoto-shi, Kumamoto 860-8555, Japan, ²Material Dynamics Laboratory, RIKEN Spring-8 Center, Sayo-cho, Hyogo 679-5148, Japan, ³Department of Earth and Planetary Science, The University of Tokyo, Bunkyo-ku, Tokyo 113-0033, Japan, ⁴Earth-Life Science Institute, Tokyo Institute of Technology, Meguro-ku, Tokyo 152-8550, Japan, ⁵ Université Grenoble Alpes, Université Savoie Mont Blanc, CNRS, IRD, Université Gustave-Eiffel, ISTerre, 38000 Grenoble, France, ⁶JASRI, Sayo-cho, Hyogo 679-5198, Japan

*yoichi@kumaoto-u.ac.jp

Keywords: Geoscience, Liquid alloys, Sound velocity, High-pressure, Inelastic X-ray scattering.

The physical properties of liquid Fe alloys are crucial to understanding planetary metallic cores. Terrestrial planets such as Earth, Mercury, and Mars have molten cores. Because these cores are located inside deep planets, the pressure (P) and temperature (T) conditions are extremely high, e.g., the P-T conditions of Earth's core are 136-364 GPa and 4000-6000 K. Iron is the dominant component of planetary cores. The cores also contain lighter elements such as H, C, O, S, and Si [1]. Longitudinal sound velocity (P-wave velocity) and density are the primary observables of Earth's liquid core. Therefore, these properties of liquid Fe alloys under relevant extreme conditions are important to investigate the core. Sulfur (S) is one of the candidates for the core light elements. Iron sulfides are commonly found in variety of meteorites, and the S concentrations are relatively high in chondrites [2]. However, sulfur is depleted in Earth's silicate mantle [3]. A recent study on the element partitioning between magma ocean and core-forming metal proposed that a large amount of S could have been trapped in the core-forming metals during planetary formation processes [4]. To examine the possibility of S in the core, we have determined the P-wave velocity of liquid Fe-S alloy based on inelastic X-ray scattering (IXS) measurements.

We carried out IXS measurements at the RIKEN Quantum NanoDynamics beamline BL43LXU of SPring-8 [5,6]. High P-T conditions were generated using a laser-heated diamond anvil cell. A foil of Fe₈₃S₁₇ was loaded in LH-DAC together with single-crystal Al₂O₃ discs that act as thermal and chemical insulators. The sample melting was confirmed based on X-ray diffraction measurements. IXS spectra of the liquids were collected in an energy range of ± 40 meV and a momentum transfer range of 3-5.7 nm⁻¹ with an energy resolution of ~ 2.8 meV at 17.79 keV. Then we obtained the dispersion relation of the longitudinal acoustic phonon mode of the liquid sample. We determined the P-wave velocity of liquid Fe₈₃S₁₇ at 32-98 GPa and 2100-2950 K from the dispersion relations obtained at each P-T condition.

The P-wave velocity of liquid Fe₈₃S₁₇ is slightly higher than that of liquid Fe [7]. Using the present P-wave data-set, we constructed an equation of state (EoS) for liquid Fe₈₃S₁₇ and estimated the P-wave velocity and density under the core P-T conditions. Comparing with seismological observations of the outer core, we found liquid Fe alloying with 6-7 wt% S to satisfy both P-wave velocity and density of the outer core simultaneously, which is similar to the S content based on previous element-partitioning experiments [4]. The present results imply that S can be the dominant light element in the Earth's outer core.

References:

- 1) Stevenson, *Science* **214**, 611-619 (1981).
- 2) Wasson and Kallemeyn, *Phil. Trans. R. Soc. Lond. A* **325**, 535-544 (1988).
- 3) McDonough. *Treatise on Geochemistry (Second Edition)*, 3, 559-577 (2014).
- 4) Mahan et al. *Geohim. Cosmochim. Acta* **196**, 252-270 (2017).
- 5) Baron, *SPring-8 Inf. Newsl.* **15**, 14-19 (2010).
- 6) Baron, in *Synchrotron Light Sources and Free-Electron Lasers: Accelerator Physics, Instrumentation and Science Applications*, edited by E. J. Jaeschke, S. Khan, J. R. Schneider, and J. B. Hastings (Springer, New York, 2016), pp. 1643-1757.
- 7) Kuwayama et al. *Phys. Rev. Lett.* **124**(16), 165701 (2020).

Simulation study of the collective excitations in liquid sodium under high pressure

*J.-F. Wax¹, E. Mocchetti^{1,2}

¹LCP-A2MC, Université de Lorraine, Metz, 57000, France,

²CRM2, Université de Lorraine, Nancy, 54000, France.

*jean-francois.wax@univ-lorraine.fr

Keywords: Molecular dynamics, dynamic structure, High pressure, sodium

The dynamic structure of liquid sodium is investigated using classical molecular dynamics simulations over a wide range of densities (from 951 to 4177 kg/m³) (see figure 1). The interactions are described using screened pseudopotential formalism with Fiolhais model of electron-ion interaction. The effective pair potentials obtained are validated by comparing the predicted static structure and self-diffusion coefficients with ab-initio simulations at the same state point.

Both longitudinal and transverse collective excitations are computed from the corresponding current correlation functions and their evolution with density is investigated. The frequency of the longitudinal excitations increases with density (see figure 2), as well as the sound speed, which is extracted from their dispersion curves. The frequency of the transverse excitations also increases with density, but they cannot propagate over macroscopic distances and the propagation gap clearly appears (see figure 3). The value of the viscosity, which is extracted from these transverse functions is in good agreement with available results computed from stress autocorrelation functions.

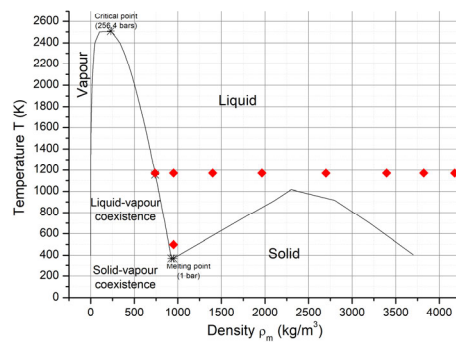


Fig. 1. Phase diagram of sodium and investigated state points.

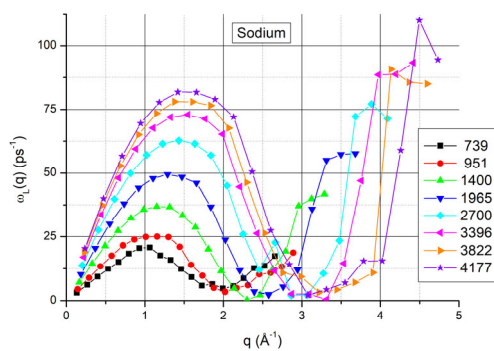


Fig. 2. Longitudinal excitations dispersion curves.

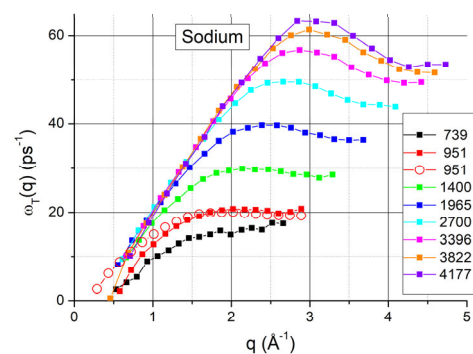


Fig. 3. Transverse excitations dispersion curves.

Structure of liquid Cd under high-pressure condition

F. Iesari^{1,*}, T. Okajima¹, M. Minicucci², A. Trapananti², A. Di Cicco²

¹Aichi Synchrotron Radiation Center, Seto, Aichi, 489-0965, Japan, ²Physics Division, School of Science and Technology, Camerino University, Camerino, 62032, Italy

*fabio.iesari@aichisr.jp

Keywords: X-ray absorption, Reverse Monte Carlo, High-pressure, Ab-initio simulation

The structure of liquid metals lacks the long-range order typical of crystals, but still maintains a short-range ordering. In particular, in previous studies the presence of local icosahedral configuration has been identified in liquid Cu and Ni [1,2], possibly explaining the deep undercooling properties of small metal particles. Under high-pressure condition, molecular dynamics (MD) simulations have shown that the fraction of icosahedral ordering increases in liquid Cu [3], at the expenses of crystal-like configurations (fcc, hcp).

In this work, we present a study on the structure of liquid cadmium under pressure probed both by experimental X-ray absorption spectroscopy (XAFS) data [4] and computer simulations. Cd, like other group 12 elements, possesses particular physical properties respect to other transition metals, like lower melting point, due to the completely filled *d*-orbital in the outer shell. At ambient condition, Cd crystallizes in an hexagonal structure, but with an axial ratio *c/a* of ~ 1.886 , far from the ideal value for hexagonal close-packed configuration, indicating complex interactions that could also affect the liquid structure.

XAFS experiments have been carried out at different temperatures and pressures above the melting line: data have been analyzed using the Reverse Monte Carlo (RMC) method to obtain compatible three-dimensional models, which can be directly compared with ab-initio MD simulations. The evolution of the local structure at different thermodynamic conditions is presented.

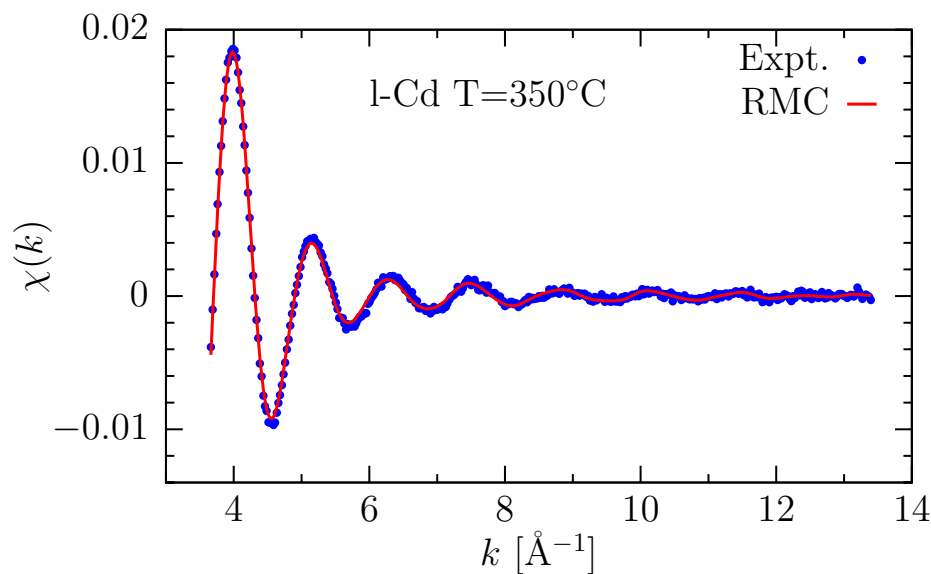


Fig. 1. EXAFS signal for liquid Cd at 350°C and ambient pressure and corresponding RMC fit.

References:

- 1) A. Di Cicco, A. Trapananti, S. Faggioni, and A. Filipponi, Phys. Rev. Lett. 91, 135505 (2003).
- 2) A. Di Cicco, F. Iesari, S. De Panfilis, M. Celino, S. Giusepponi and A. Filipponi, Phys. Rev. B 89, 060102 (2014).
- 3) M. Celino, F. Coppati and A. Di Cicco, Solid State Sciences 12, 179-182 (2010).
- 4) M. Minicucci, A. Trapananti, A. Di Cicco, S. De Panfilis and G. Aquilanti, Physica Scripta T115, 1056-1058 (2005).

Ab initio simulation for the ductility mechanism of silver chalcogenides

*H. Hokyō¹, M. Misawa², K. Shimamura¹, A. Koura¹, F. Shimojo¹

¹Kumamoto University, Kumamoto City, 860-8555, Japan, ²Okayama University, Okayama City, 700-8530, Japan,

*hokyohinata@gmail.com

Keywords : Silver chalcogenides, Ductility, *Ab initio* simulation

Silver chalcogenides are candidate for thermoelectric materials and attracting attention as new device materials. Among them, Ag_2S is an important inorganic semiconductor that has metal-like ductility despite being a semiconductor [1]. On the other hand, Ag_2Se , which has a similar chemical composition, is non-flexible but has high electrical conductivity suitable for thermoelectric materials. Experimental studies have reported that the ductility is confirmed in the compositions $\text{Ag}_2\text{S}_{1-x}\text{Se}_x$ ($x \leq 0.6$) with Ag_2S -type (monoclinic) crystal structure [2]. In this study, we performed simple shear deformation simulations as shown in Fig. 1 for (100)[010], (100)[001], (010)[100], (010)[001], (001)[100], (001)[010] shear systems of $\text{Ag}_2\text{S}_{1-x}\text{Se}_x$ ($x = 0.0, 0.2, 0.4, 0.6, 1.0$) based on *Ab initio* molecular dynamics (AIMD), where the (KLM)[klm] shear system means that the (KLM) plane is slipped toward [klm] direction during the shear deformation. As a result, disappearance and restoration of the peak of the radial distribution function between chalcogens during the deformation process were observed for almost all shear deformations. This implies that the chalcogen sublattice is structurally recovered under shear stress. By analyzing the movement of chalcogen atoms, we confirmed that structural recovery of the chalcogen sublattice occurs. As an example, Figure 2 shows the structural recovery of chalcogen atoms during the shear deformation process of (100)[010]. It can be seen that chalcogen atoms, which were initially aligned vertically, tilt in response to deformation and move collectively in the plane parallel to the deformation direction, reorganizing the vertical lines and recovering their structure. In doing so, the atomic arrangement is rearranged, as indicated by the color of atoms above and below the red dotted line. Analysis of the mechanism of structural recovery of the chalcogen sublattice revealed that chalcogen atoms move collectively into three planes: 1) a plane that slides during shear deformation, 2) a plane that is tilted by shear deformation, and 3) a plane that forms a parallelepiped with the above two planes. In general, atoms can move to the direction in which the distance between atoms is the shortest, e.g., the [111] direction in the bcc structure. At room temperature, the Ag_2S -type crystal structure is characterized by the fact that chalcogen atoms are almost equally spaced in all directions. This feature allows the chalcogen sublattice of Ag_2S to select the plane and direction of atom transfer for each of the six types of shear deformation, and to recover the structure. In addition to the above structural recovery of chalcogen ions, silver ions have high mobility. This high mobility allows silver ions to flexibly recombine their bonds with surrounding chalcogen ions and follow the structural recovery of the chalcogen ion sublattice without destroying the crystal structure. This can be interpreted as the silver ions functioning like free electrons in the metal. Thus, the high mobility of silver ions enables the structural recovery of the chalcogen ion sublattice, which is thought to be responsible for the ductility of the inorganic semiconductor $\text{Ag}_2\text{S}_{1-x}\text{Se}_x$.

Based on these considerations of ductility due to chalcogen sublattice structure and high mobility silver ions, it can be predicted that Ag_2Se , which is not ductile at room temperature, is also ductile at high temperature because the Se sublattice in the superionic conducting phase has a cubic bcc structure and is more isotropic than the S sublattice in Ag_2S . To verify this, we performed simple shear deformation simulations for Ag_2Se based on classical molecular dynamics rather than AIMD, using a model potentials that that reproduce the nonsuperionic-superionic phase transition [3]. In this simulation, the peak of the radial distribution function between seleniums, which once disappeared during the deformation process, reappeared, confirming that the structure is recovered as predicted.

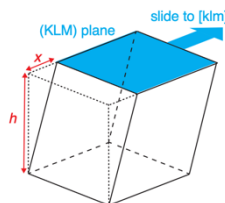


Fig. 1. Simple shear deformation that slides the (KLM) plane in the [klm] direction while keeping the height constant.

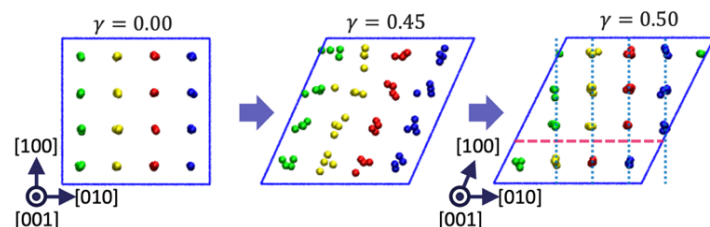


Fig. 2. Chalcogen atoms recovering structure during (100)[010] deformation process. γ represents the degree of deformation.

References:

- [1] X. Shi, H. Chen, F. Hao, R. Liu, T. Wang, P. Qiu, U. Burkhardt, Y. Grin, and L. Chen. *Nat. Mater.* **17**, 421-426 (2018).
- [2] K. Hirata, T. Matsunaga, S. Singh, M. Matsunami, and T. Takeuchi, *J. Electron. Mater.* **49**, 2895-2901 (2020).
- [3] J. P. Rino, Y. M. Hornos, G. A. Antonio, I. Ebbsjö, R. K. Kalia, and P. Vashishta, *Chem. Phys.* **89**, 7542-7555 (1988).

Reverse Monte Carlo modeling: state of affairs and applications to metallic glasses

*PUSZTAI, László^{1,2}

¹ Wigner Research Centre for Physics, Konkoly Thege út 29-33., Budapest H-1121, Hungary, ² IROAST, Kumamoto University, 2-39-1 Kurokami, Chuo-ku, Kumamoto 860-8555, Japan

*pusztai.laszlo@wigner.hu

Keywords: Reverse Monte Carlo modeling, X-ray/Neutron scattering, microscopic structure, metallic glasses

Reverse Monte Carlo (RMC) [1] is a computer modeling tool that enables us to create large scale, three dimensional structural models, containing (tens, or even hundreds of) thousands of atomic coordinates. These structural models are consistent, within errors, with experimental data from neutron and X-ray diffraction, EXAFS and anomalous X-ray scattering (AXS). The later versions of the RMC computer code [2,3] make it possible to also include various constraints on, e.g., coordination numbers and angular distributions.

In this contribution, I will briefly introduce the RMC algorithm, then focus on a conundrum very much relevant to metallic glasses: that of information deficiency. The easiest to understand reason behind this phenomenon is that for a multicomponent material, such as bulk metallic glass, the number of independent (diffraction, EXAFS, AXS) measurements is practically always lower than the number of partial pair correlations in the system. In addition, available experimental techniques can provide information only on two-particle correlations: the validity of structural models must therefore be addressed.

Metallic glasses were among the very first targets of Reverse Monte Carlo modeling [4,5], so it is rather apt to finish the presentation with showing and analyzing old [5] and new [6,7] results on Pd-based metallic glasses.

References:

- 1) R.L. McGreevy, L. Pusztai, *Molec. Simul.* 1, 359 (1988)
- 2) O. Gereben, P. Jónvári, L. Temleitner, L. Pusztai, *J. Optoelect. Adv. Mater.* 9, 3021 (2007)
- 3) O. Gereben, L. Pusztai, *J. Comput. Chem.* 33, 2285 (2012)
- 4) L. Pusztai, *Z. Naturf.* 46a, 69 (1991)
- 5) P.A. Duine, J. Sietsma, B.J. Thijsse, L. Pusztai, *Phys. Rev. B*, 50, 13240 (1994)
- 6) Hosokawa, S., Berar, J.-F., Boudet, N., Pilgrim, W.-C., Pusztai, L., Hiroi, S., Maruyama, K., Kohara, S., Kato, H., Fischer, H. E. & Zeidler, A., *Phys. Rev. B* 100, 054204 (2019)
- 7) Hosokawa, S., Berar, J.-F., Boudet, N., Pilgrim, W.-C., Pusztai, L., Hiroi, K., Kohara, S., Kato, H., Fischer, H. E. & Zeidler, A., *Journal of Non-Crystalline Solids* 555, 120536-1-10 (2021)

Long-time and intermittent structural evolution of metallic glasses

*R. Maass^{1,2}, B. Riechers¹, A. Das³, Z. Wang¹, E. M. Dufresne⁴, P. M. Derlet⁵

¹ Federal Institute for Materials Research and Testing (BAM), Unter den Eichen 87, 12205 Berlin, Germany

² Department of Materials Science and Engineering, University of Illinois at Urbana-Champaign, Urbana, Illinois, 61801, USA

³ Cornell High Energy Synchrotron Source, Cornell University, Ithaca, NY 14853, USA

⁴ Advanced Photon Source, Argonne National Laboratory, Lemont, IL, 60439, USA

⁵ Condensed Matter Theory Group, Paul Scherrer Institut, Forschungsstrasse 111, 5232 Villigen PSI, Switzerland

* robert.maass@bam.de

Keywords: metallic glasses, aging, relaxation, structural dynamics, x-ray photon correlation spectroscopy

The advent of x-ray photon correlation spectroscopy (XPCS) allows now for a detailed in-situ exploration of the structural evolution of metallic glasses. Based on intensity-intensity cross-correlations of coherent speckle patterns, it is possible to extract time scales that are characteristic of the atomic-scale structural dynamics. Such data generates a fundamental understanding of glass dynamics both for the undercooled liquid regime and for glassy solids well below the glass transition temperature, T_g . The increasing body of literature relying on XPCS presents a consistent picture of stationary structural dynamics well above T_g , but a variety of monotonous and non-monotonous signatures have been reported in the glassy solid regime at or below T_g . Observed during step-wise cooling, first evidence of non-monotonous aging, also called intermittent aging, was reported for a Pd-based metallic glass [1]. Our own work focusing on stress-driven structural dynamics far below T_g also revealed various signatures of intermittent aging [2, 3]. Surprisingly, this was also the case for a completely unbiased state along an isotherm at ambient conditions. What could the underlying structural mechanisms for such temporal fluctuations of the characteristic momentary time scales be?

In this talk, we shed light onto such intermittent aging signatures via both long-time XPCS experiments and molecular dynamics simulations. Specifically, we track the temporal fluctuations of aging at $0.98T_g$ of a Zr-based bulk metallic glass. Probed over the duration of eight individual experiments of ca. 35000 s each, we reveal temporal fluctuations of all extracted quantities, including the short-time plateau, the first moment in time, the relaxation time, and the shape parameter. Whilst strong fluctuations of any investigated parameter may appear as a rare event in an individual two-time correlation function, variations over larger timescales emerge as the norm, which emphasizes the time-scale interplay between an experimental time and a broad distribution of material timescales. This suggests that aging close to or below T_g is generally a temporal heterogeneous process, if sufficiently sampled in time. We further observe changes in correlations between the quantified parameters upon the occurrence of an intermittent aging event, which indicates disruptive collective structural activity. MD simulations of isothermal annealing and simulated XPCS data complete our effort in understanding temporal fluctuations in the intensity-intensity cross-correlations, implying that much of the seen effects originate from atomic activity associated with the emergence of structural heterogeneity within the glassy solid.

References:

- [1] Z. Evenson, B. Ruta, S. Hechler, M. Stolpe, E. Pineda, I. Gallino, R. Busch, *Physical Review Letters* 115 (2015) 175701.
- [2] A. Das, P.M. Derlet, C. Liu, E.M. Dufresne, R. Maass, *Nature Communications* 10 (2019) 5006.
- [3] A. Das, E.M. Dufresne, R. Maass, *Acta Materialia* 196 (2020) 723-732.

Decoupling between thermodynamic and dynamical glass transitions in high-entropy metallic glasses

Jing Jiang, Takeshi Wada*, Hidemi Kato

Institute for Materials Research, Tohoku University, Sendai, 980-8577, Japan

*takeshi.wada.d7@tohoku.ac.jp

Keywords: High entropy metallic glasses, glass transition, α -relaxation

[Introduction]

Glass transition is one of the critical unresolved issues in glassy physics and materials science, at which a viscous liquid is frozen into the solid state or structurally arrested state. On account of the uniform arrested mechanism, calorimetric glass transition temperature (T_g) always presents a same tendency with dynamical glass transition (or α -relaxation) temperature (T_α). Here, we explored the correlations between the calorimetric and dynamic glass transitions of three prototypical high-entropy metallic glasses (HEMGs) systems. We found that HEMGs present a depressed dynamical glass transition phenomenon, i.e. HEMGs with moderate T_g represent the highest T_α and the maximum corresponding activation energy. This decoupled glass transitions are associated with the high mixing entropy effect and the induced nanoscale spatial homogeneity. The results have implications for understanding the high mixing entropy effect on dynamics of metallic glasses for designing new metallic glasses with plentiful physical and mechanical performances.

[Experimental]

Master alloys were prepared by arc-melting mixtures of raw metals (purity: >99.9 mass %) in an Ar atmosphere purified with a Ti getter. Ribbon specimens were obtained via a melt spinning technique. Three systems were designed, La (Ce)-based, Pd (Pt)-based and Zr (Hf)-based, to compare the behaviors of high entropy and low entropy metallic glasses. The microstructure was observed by X-ray Diffraction, Scanning Electron Microscopy combined with energy dispersive X-ray spectroscopy and Transmission Electron Microscopy. The thermal characters were detected by the Differential Scanning Calorimetry (DSC). The dynamic processing was performed by the Dynamic Mechanical Analyzer (DMA).

[Results]

Differential scanning calorimeter (DSC) traces shows obvious glass transition and crystallization signals confirm the glassy state of the three samples. LaCe-HEMG with the highest ΔS_{mix} yields an intermediate value of T_g . MGs exhibit multi-complex relaxation dynamics, α -relaxation as the main relaxation mode is directly related to the viscous flow and the glass transition. With Ce half replacing La, LaCe-HEMG exhibits the highest α -relaxation temperature T_α , which is not synchronous with the calorimetric T_g . According to the conventional wisdom, a glass with a higher T_g always poses higher difficulty in activation of α -relaxation and thus has a larger value of T_α . Nevertheless, LaCe-HEMG, with the modest thermodynamic devitrification behavior, performs the uppermost dynamic glass transition process.

Structure Determination in a new Type of Amorphous Molecular Solids with Extreme Nonlinear Optical Properties

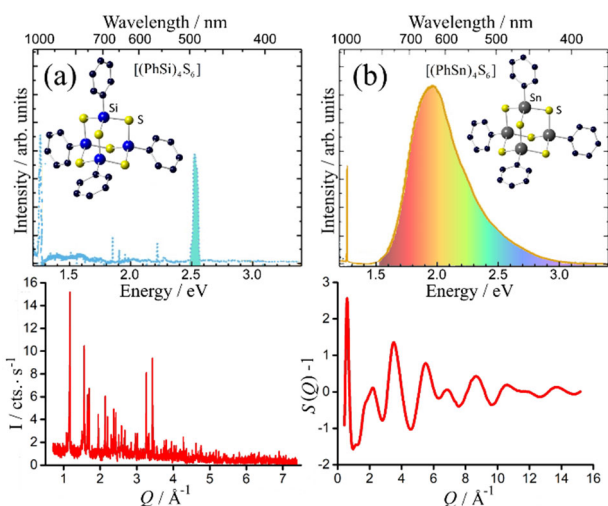
*W.-C. Pilgrim¹, B. D. Klee^{1,2}, J. R. Stellhorn^{1,3}, J. Link Vasco¹, K. Volz¹, A. Zeidler⁵, S. Hosokawa⁴, B. Paulus¹ and S. Dehnen¹

¹Philipps-University, Marburg, 35032, Germany, ²Wigner Research Centre for Physics, Budapest, H-1121, Hungary, ³Hiroshima University, Hiroshima, 739-8527, Japan, ⁴Kumamoto University, Kumamoto, 860-8555, Japan, ⁵University of Bath, Bath, BA2 7AY, UK

*pilgrim@staff.uni-marburg.de

Keywords: molecular amorphous solids, molecular RMC-simulation, White-Light-Generator, X-ray and neutron scattering.

A new class of molecular cluster material has recently been synthesized exhibiting extreme nonlinear optical behavior when irradiated just by an inexpensive continuous wave infrared laser diode.¹⁾ The molecular building blocks consist of adamantane-like cluster units of general formula $[(RX)_4Y_6]$, where X is a group-14 element, Y is a chalcogen and R is an organic ligand attached to a group 14 atom. The shape of these materials is displayed in the insets of the Figure, where the organotin and the organosilicon sulfide clusters $[(PhSn)_4S_6]$ and $[(PhSi)_4S_6]$ are respectively shown, with phenyl (Ph) ligands ($-C_6H_5$) attached to the Sn and Si atoms. The materials can be synthesized comparatively easily and variation of the ligands and/or the chalcogens or of the group 14 element allows great chemical variability of the cluster composition. A large number of derivatives has now been synthesized as easy-to-handle powders. All of them either act as second harmonics generators (SHG) or as White-



NLO-responses from (a) the crystalline $[(PhSi)_4S_6]$ and (b) the amorphous $[(PhSn)_4S_6]$, respectively (top). The driving excitation is visible at 1.265 eV. The 2nd-harmonic of (a) is seen at 2.53 eV, while (b) depicts a broad white spectrum. The X-ray patterns are also shown below indicating that the SHG-material is crystalline (left) while the WLGMaterial is crystalline (left) while the WLGMaterial (right) shows the typical $S(Q)$ of an amorphous solid

Light-Generators (WLG), the latter providing a bright white optical emission.²⁾ The visible part of such spectra resembles the color of a tungsten-halogen lamp at about 2900 Kelvin and the emitted beam retains the excellent beam divergence of the driving laser. However, the morphology of the substance has a significant impact on the type of response. While crystalline compounds clearly react as SHGs, only amorphous materials respond as WLGs. This is exemplarily demonstrated for two of these systems in the Figure. The two compounds differ only by the exchange of Sn by Si in the cluster core, but they show completely different optical and morphological properties. The Figure shows the optical answers if being irradiated by a 980 nm laser-line (1.265 eV). While the Si-based compound replies with a distinct 2nd order harmonics at 2.53 eV (a), the Sn-containing material emits a broad white spectrum ranging from about 1.5 to 3 eV (b). Also shown are the respective diffraction-patterns of the two substances. The $[(PhSi)_4S_6]$ material is clearly crystalline, indicated by the Bragg peak dominated diffractogram, while $[(PhSn)_4S_6]$ is fully amorphous and the scattered X-rays yield a structure factor $S(Q)$, typical of a fully disordered system. Hence, disorder seems to be a

mandatory requirement for the WLGs. The fact that WLG is never observed from crystalline cluster materials indicates that the effect is enabled by microscopic structural correlations or degrees of freedom which are only accessible in a sufficiently disordered state. To understand this, we have developed a new code to perform molecular Reverse Monte Carlo simulations and we have started a comprehensive exploration on the structural properties of the WLG materials using scattering and EXAFS experiments. We will report on the current state of research on the amorphous WLG materials and we will present our findings regarding structural differences between SHG and WLG materials.

1) N. W. Rosemann, J. P. Eußner, A. Beyer, S. W. Koch, K. Volz, S. Dehnen, and S. Chatterjee, Science 352, 1301 (2016).

2) S. Dehnen, P. Schreiner, S. Chatterjee, K. Volz, N. W. Rosemann, W.-C. Pilgrim, D. Mollenhauer, and S. Sanna, ChemPhotoChem 5, 1 (2021).

Static Structure of Liquid Ag_2Se Based on Molecular Dynamics Simulations Using Artificial Neural Network Potential

*Akihide Koura¹, Kohei Shimamura¹, Fuyuki Shimojo¹

¹Department of Physics, Kumamoto University, Kumamoto, 860-8555, Japan

*koura@tech.kumamoto-u.ac.jp

Keywords: Liquids, Ab initio simulation, Machine learning, Molecular dynamics, Ag_2Se .

Silver chalcogenides (Ag_2Se , Ag_2S , and Ag_2Te) are important materials for thermoelectric devices, which contribute to capture/reuse waste heat. They have high Seebeck coefficient and low thermal conductivity [1,2]. These features are suitable for the devices. It is reported that the thermal conductivity has a peak at around phase transition temperature between non-superionic and superionic phases [1,2]. In the superionic phase, Ag atoms migrate in the chalcogen sublattice even in the crystalline state. In order to clarify the mechanism of such interesting properties, many experimental and theoretical studies have been reported so far. On the other hand, the number of structural studies on liquid silver chalcogenides are not reported so much. For example, details of the static structure of liquid Ag_2Se was reported with the neutron scattering measurements [3] and the molecular dynamics (MD) using empirical potential and the *ab initio* molecular dynamics (AIMD) simulations [4]. The theoretical result [4] is in good agreement with the experimental result [3], however, it is necessary to be careful to discuss based on these studies due to the system size of theoretical study consisting of only 69 atoms [4].

To study the static and dynamic properties Ag_2Se with computer simulations, it is necessary to solve the calculation cost problem. Using AIMD simulations, the precise calculation can be performed in principle, however, the calculation cost is extremely high. Although MD simulations with empirical potentials are quite faster than AIMD simulations, making potential functions is difficult. In recent years, the machine learning based on the result of AIMD simulations to construct an interatomic potential is developed with the artificial neural network (ANN) [5]. MD simulations with ANN potential (ANN-MD) is actually slower than typical empirical MD simulations, however, it enables us to perform the fast calculation with the high precision as same as AIMD simulations.

In this study, we focused on the static and dynamic properties of liquid Ag_2Se based on the ANN-MD simulations. We used a 384-atom system (256 Ag + 128 Se). Training data, i.e., AIMD simulations were performed at 1200 K with our previous condition of the Hubbard correction for Ag atoms [6]. The total simulation time of training data was 9.4 ps with the time step of 2.4 fs. ANN-MD simulations were executed at least 240 ps with the canonical ensembles. Figure 1 shows the partial radial distribution functions (PRDFs) $g_{\alpha\beta}(r)$ of liquid Ag_2Se obtained by ANN-MD and AIMD simulations drawn with black solid and red dashed lines, respectively. The blue circle shows the experimental result [3]. Peak positions of PRDFs $g_{\text{AgSe}}(r)$ and $g_{\text{SeSe}}(r)$ obtained by AIMD and ANN-MD are in reasonable agreement with those by experimental result. $g_{\text{AgAg}}(r)$ obtained by simulations are different from the experimental result. ANN-MD simulations well reproduced AIMD except for the Se-Se correlation. In the presentation, we will discuss details of static structure, bonding and dynamic properties obtained by AIMD and ANN-MD simulations.

References:

- [1] K. Hirata, T. Matsunaga, S. Singh, M. Matsunami, and T. Takeuchi, *J. Elec. Mater.* **49**, 2895 (2020).
- [2] K. Hirata, T. Matsunaga, S. Singh, M. Matsunami, and T. Takeuchi, *Mater. Trans.* **61**, 2402 (2020).
- [3] A. C. Barnes, S. B. Lague, P. S. Salmon, and H. E. Fischer, *J. Phys.: Condens. Matter* **9**, 6159 (1997).
- [4] F. Kirchoff, J. M. Holender, and M. J. Gillan, *Phys. Rev. B* **54**, 190 (1996).
- [5] N. Arthith, A. Urban, *Comput. Mater. Sci.* **114** (2016) 135.
- [6] S. Fukushima, M. Misawa, A. Koura, and F. Shimojo, *J. Phys. Soc. Jpn.* **88**, 115002 (2019).

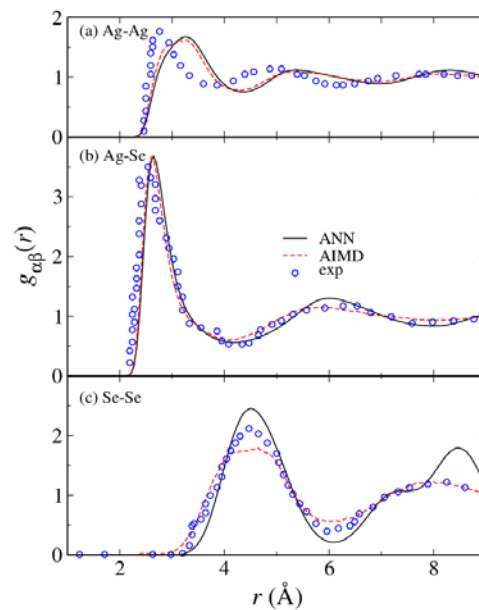


Figure 1 Partial radial distribution functions $g_{\alpha\beta}(r)$ of liquid Ag_2Se . Black and red lines correspond to the result of ANN-MD and AIMD simulations, respectively. The blue circle shows the experimental result [3].

Semianalytic Formula for Multiphonon Thermal Diffuse Scattering in Solids

Hikaru Kitamura

Department of Physics, Kyoto University, Sakyo-ku, Kyoto 606-8502, Japan

kitamura@scphys.kyoto-u.ac.jp

Keywords: Static structure factor, Thermal diffuse scattering, Phonon, Debye-Waller factor, Powder diffraction

A new semianalytic formula for the static structure factor $S(k)$ of polycrystalline and amorphous solids at elevated temperatures, applicable to the entire wavenumber (k) range, is presented. Particular attention is paid to the contribution from thermal diffuse scattering (TDS) due to phonons, $S_{\text{TDS}}(k)$, where multiphonon processes beyond the one-phonon term are taken into account up to infinite order within the Debye model. It is thereby proven that the one-phonon TDS accounts for the compressibility relation in the $k = 0$ limit as well as the logarithmic singularity at the Bragg points, whereas the multiphonon TDS ensures the convergence of $S(k)$ towards unity at large k . The present formula is computationally efficient, requiring only a one-dimensional radial integration of the elastic scattering part of the structure factor $S_{\text{el}}(k)$ and the kernel function (see Fig. 1); the latter is expressed analytically in terms of the atomic density n , average sound velocity, and the Debye-Waller exponent $W(k)$. A numerical example for a face-centred-cubic polycrystal near the melting point is exhibited in Fig. 2; significance of the multiphonon contribution is clearly indicated. Comparison with the previous formula by Meisel and Cote¹⁾ will be discussed.

References:

- 1) L.V. Meisel and P.J. Cote, Phys. Rev. B **16**, 2978 (1977).

$$S(k) = e^{-2W(k)} S_{\text{el}}(k) + S_{\text{TDS}}(k)$$

$$S_{\text{TDS}}(k) = \bar{y}(k, 0) + \frac{1}{2\pi^2 n} \int_0^\infty dq q^2 \underbrace{\bar{y}(k, q)}_{\text{kernel function}} S_{\text{el}}(q)$$

Fig. 1. Structure of the semianalytic formula for $S(k)$.

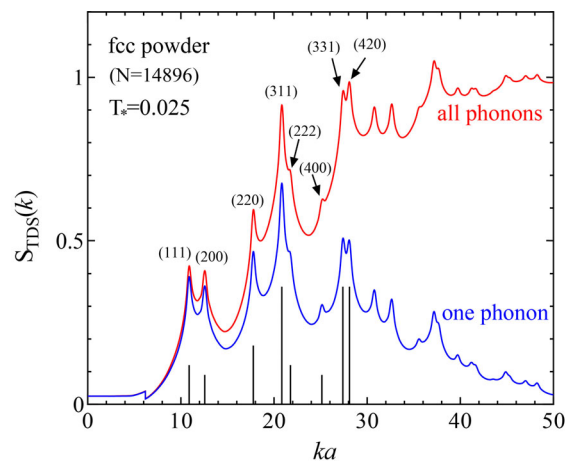


Fig. 2. TDS structure factor for *fcc* polycrystal near the melting point, with a denoting the lattice constant. Full result is indicated by the red curve ('all phonons'), whereas the blue curve represents the one-phonon contribution. The first eight Bragg peaks are indicated by vertical bars and Miller indices (hkl).

Dynamic properties of liquids of interest in nuclear energy production: liquid Li-Pb alloys and molten UO_2 .

*L. E. González, B. G. del Rio, D. J. González

Dept. Física Teórica, Universidad de Valladolid, Valladolid, 47011, Spain

*luisen@metodos.fam.cie.uva.es

Keywords: Ab initio simulation, liquid structure, dynamics.

Li-Pb alloys and UO_2 are systems of technological interest in the field of energy production through nuclear reactions. The liquid alloy at the Pb-rich eutectic composition is a strong candidate to be used as breeding blanket in tokamak fusion reactors, while the study of the properties of molten uranium dioxide is important in terms of risk assessment in fission reactors.

From the physical point of view, Li-Pb alloys and uranium dioxide share some common characteristics, such as a large mass disparity between their components. We have also recently observed [1] that, at the stoichiometric composition Li_4Pb , the liquid structure (like the solid one at a nearby composition) can be described in terms of interconnected polyhedra, which is a structural feature typical of molten (and solid) oxides. But they also show some large discrepancies, with a melting temperature lower than 1000 K for Li-Pb alloys and larger than 3000 K for UO_2 , due to a strong difference between the bonding type in both systems (metallic in Li-Pb alloys, ionic/semiconducting in UO_2). It is therefore interesting to compare also the dynamic properties of both systems, in particular the effect that such different bonding characteristics may have on features like the particular type of “fast sound” phenomenon that was observed for the first time in Li_4Pb several decades ago.

The accurate description of the forces involved in the dynamics, obtained from first principles, enables us to study with confidence the atomic trajectories so as to compute the longitudinal and transverse collective dynamic properties, which are analyzed and compared with some theoretical approaches. We also present some results for other less commonly studied magnitudes such as the cage correlation functions. We finally discuss the limitations inherent to the method employed and possible alternatives that preserve the accuracy of the forces.

References

[1] M.M.G. Alemany, J. Souto-Casares, L.E. González and D.J. González, *J. Molec. Liq.* 344, 117775 (2021).

Origin of Positive Sound Dispersion in Simple Liquids and Liquid Alloys

*Taras Bryk^{1,2}

¹Institute for Condensed Matter Physics of NASU, Lviv, 79011, Ukraine, ²Lviv Polytechnic National University, Lviv, 79013, Ukraine

*bryk@icmp.lviv.ua

Keywords: collective excitations, positive sound dispersion, generalized hydrodynamics, eigenmode analysis, computer simulations

I will review recent theoretical approaches for explanation of positive sound dispersion (PSD – a bending of the dispersion curve of collective excitations beyond the hydrodynamic regime towards higher frequencies) in liquids and will present results of a very recent eigenmode analysis for density-density time correlation functions in simple fluids, liquid metals and binary liquid alloys.

The eigenmode analysis enables an estimation of mechanisms of sound propagation on different spatial scales: k -dependent contributions from different types of fluctuations to eigenvectors corresponding to sound excitations provide very clear picture of dynamic processes responsible for sound propagation in and outside the hydrodynamic regime. Two dynamic models were used for the eigenmode analysis: viscoelastic and thermo-viscoelastic ones [1,2]. The k -dependent eigenvectors of sound eigenmodes make evidence that the change from hydrodynamic mechanism (due to conservation laws) to the elastic one is taking place via a gradual replacement of contribution from density fluctuations by a contribution from stress fluctuations. For large wave numbers the longitudinal and transverse (shear) collective excitations propagate solely due to coupled mass-current and stress fluctuations. Namely this gradual replacement of the contribution from conserving density fluctuations by the one coming from stress fluctuations is responsible for emergence of the positive sound dispersion. Another very important consequence of this eigenmode analysis is a prediction when the slowest relaxation mode shows a crossover from thermal relaxation (hydrodynamic regime) to non-hydrodynamic structural relaxation [3] with increasing wave number, that should be observed in behavior of the central peak of experimental dynamic structure factors $S(k,\omega)$.

For the case of liquid binary alloys additional crossover takes place because of interaction of sound modes with concentration fluctuations and overdamped optic-like modes.

References:

- 1) I.M. de SCHEPPER, E.G.D. COHEN, C. BRUIN, J.C. van RIJS, W.MONTFROOIJ and L.A. de GRAAF, Phys. Rev. A 38, p 271 (1988).
- 2) T. BRYK, I. MRYGLOD, T. SCOPIGNO, G. RUOCCO, F. GORELLI and M. SANTORO, J. Chem. Phys. 133, p 024502 (2010).
- 3) T. BRYK, Eur. Phys. J. Special Topics 196, p 65 (2011)

Chemical short-range order in undercooled Cu-Ni melts

*Dirk Holland-Moritz¹, Fan Yang¹, Thomas Hansen², Florian Kargl¹

¹ Deutsches Zentrum für Luft- und Raumfahrt (DLR), Institut für Materialphysik im Weltraum, 51170 Köln, Germany, ² Institut Laue-Langevin (ILL), 38042 Grenoble, France

* dirk.holland-moritz@dlr.de

Keywords: Short-range order, Demixing, Neutron scattering

For liquid Cu-Co, which shows a rich phase diagram, it has been shown that Cu and Co demix, if the liquid is undercooled below its binodal line. In contrast Ni-Cu shows a comparatively simple phase diagram of a solid solution and no phase separation in liquid state has been reported so far. On the other hand, measurements of the electrical resistivity show a non-linear temperature dependence for melts of the Cu-rich alloys Ni₄₀Cu₆₀ and Ni₂₀Cu₈₀ [1]. A possible explanation for this non-linear temperature dependence might be concentration fluctuations that increase with increasing undercooling of the liquid, hence indicating a tendency for demixing. Also the slightly positive enthalpy of mixing of Ni-Cu points towards a demixing nature of this system.

While these are indirect arguments, in this work we present direct investigations on the short-range order in Ni_{42.5}Cu_{57.5} alloy melts by elastic neutron diffraction that have been performed on the D20 diffractometer at the Institute Laue-Langevin. An electromagnetic levitation furnace was used as sample environment allowing to undercool the melts below the melting temperature [2]. Partial structure factors have been determined by application of an isotopic substitution technique using samples of the four different isotopic compositions ⁵⁸Ni_{42.5}^{nat}Cu_{57.5}, ⁶⁰Ni_{42.5}^{nat}Cu_{57.5}, ^{nat}Ni_{42.5}^{nat}Cu_{57.5} and ⁶²Ni_{42.5}⁶³Cu_{57.5}.

The Bhatia-Thornton partial structure factor S_{NN} that describes the topological short-range order of the melt closely resembles the structure factors observed for melts of the pure elements Ni [3] and Cu, indicating a similar topological structure. For the Bhatia-Thornton partial structure factor S_{CC} that describes the chemical short-range order of the melt a rise in intensity is observed at low momentum transfer, q , on top of a relatively large flat background with some smaller oscillations towards larger q . The rise of S_{CC} at low q increases with decreasing temperature. It directly points to the demixing nature of the system with concentration fluctuations on large length scales that become more pronounced with increasing undercooling.

Interestingly, the generic behavior of phase separation has recently been studied by means of molecular dynamics simulations on binary symmetric Lennard-Jones mixtures [4,5]. A demixing behavior has been found for attractive Lennard-Jones liquids, if the interaction parameters of the unlike atomic pairs are smaller than those of the like atomic pairs. The shape of S_{CC} and its temperature dependence calculated by the molecular dynamics simulations closely resemble those we observed experimentally for liquid in Ni_{42.5}Cu_{57.5} showing that main predictions on the dependence of the chemical short-range order on the atomic interactions inferred from this simple generic model are found in real metallic systems like Cu-Ni.

References

- 1) T. Richardsen, G. Lohöfer, Int. J. Thermophys. 23, 1207 (2002).
- 2) D. Holland-Moritz *et al.*, Meas. Sci. Techn. 16, 372 (2005).
- 3) T. Schenk *et al.*, Phys. Rev. Lett. 89, 075507 (2002).
- 4) S.K. Das *et al.*, J. Chem. Phys. 125, 024506 (2006).
- 5) S. Amore *et al.*, J. Chem. Phys. 134, 044515 (2011).

The Short-Range Order in Liquid Water

*Neta Ellert¹, Guy Makov¹¹ Materials Engineering Department, Ben-Gurion University of the Negev, 84105 Beer-Sheva, Israel

* netani@post.bgu.ac.il

Keywords: short range order, liquids, water, Quasi Crystalline Model.

The short-range order in water was determined from experimentally measured partial radial distribution functions by applying the Quasi Crystalline Model (QCM), an approach to analyzing the short-range order in liquids and amorphous systems, which employs a structural model to determine the short-range order of a liquid directly from the radial distribution function. This model uses a reference lattice structure to generate a hypothetical amorphous radial distribution function that is compared with the radial distribution function obtained from experiments or simulations. The short-range order of the amorphous system is identified with the specific reference lattice producing the best fit for the data.

Three partial radial distribution functions were analyzed for water at several pressures and temperatures. It was found that at low temperatures and pressures, the short-range order of water is similar to that of the hexagonal ice (Ih) structure. At higher pressures and low temperatures, the short-range order of water becomes similar to that of tetragonal ice III structures with c/a ratio of 0.8. At higher temperatures of 573K, the short-range order obtained was similar to that of rhombohedral ice II.

An example for a successful fit of the partial O-O radial distribution function at ambient conditions is shown below:

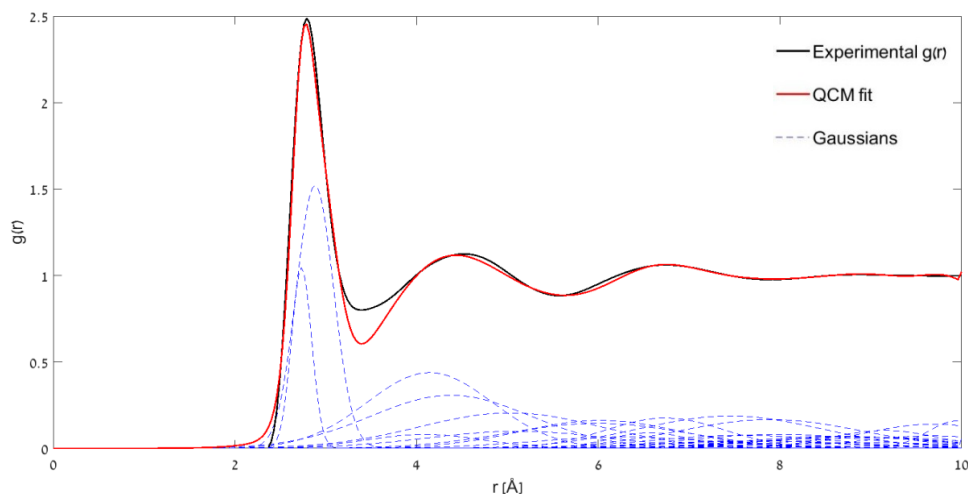


Figure 1 The QCM of water at ambient conditions., RDF of partial O-O modeled by the QCM using the ice Ih structure with $c/a=1.5$

Impact of sulfur addition on the structure and dynamics of Ni-Nb alloys

N. Grund¹, *F. Yang¹, D. Holland-Moritz¹, L. Ruschel², B. Adams², T. Buslaps³, S. Banerjee⁴, R. Busch², A. Meyer¹

¹ Institut für Materialphysik im Weltraum, Deutsches Zentrum für Luft- und Raumfahrt, Cologne, 51170, Germany,

² Lehrstuhl für metallische Werkstoffe, Universität des Saarlandes, Saarbrücken 66123, Germany,

³ European Synchrotron Radiation Facility (ESRF), Grenoble 38043, France,

⁴ Deutsches Elektronen-Synchrotron (DESY, Hamburg 22607, Germany

*fan.yang@dlr.de

Keywords: sulfur bearing alloys, electrostatic levitation, synchrotron X-ray diffraction.

Bulk metallic glasses feature an amorphous structure, which results in exceptional properties as engineering materials. Typically alloying additional components improves the glass forming ability (GFA). Beside adding non-metallic elements like P, B, C, recently sulfur has been found to facilitate bulk metallic glasses formation at different concentration levels [1]. This makes them promising candidates for commercialization, where the alloy composition can be tuned according to applications. In the case of the binary Ni₆₂Nb₃₈ glass forming alloy, it has been found that an optimal enhancement of the GFA can be achieved by alloying only 3 at% S. Such kind of “minor alloying” effects cannot be understood by applying the common empirical rules like a denser packing of the melt, or the formation of deep eutectic compositions.

Employing electrostatic levitation combined with in-situ synchrotron diffraction, we studied impacts of sulfur on the structure and dynamics of Ni-Nb based alloys, as well as on the solidification behavior from undercooled melt. First results show that small, but notable changes can be observed in the measured liquid structure factor upon an addition of 3 at% S. In particular, in the obtained X-ray total structure factor the position of the first structure factor maximum appears to shift towards lower q values. The structure changes are analyzed with the help of the partial structure factors of the binary Ni-Nb alloy [2]. It has been also observed that the initial phases solidified from the undercooled melt seem to be different with and without S. The implication of these changes on the glass forming behavior is discussed together with the melt viscosity measured using the oscillating drop technique.

References:

[1] A. Kuball, O. Gross, B. Bochtler, R. Busch, *Scr. Mater.* **146**, 73-76 (2018).

[2] D. Holland-Moritz, F. Yang, J. Gegner, T. Hansen, M. D. Ruiz-Martín, and A. Meyer, *J. Appl. Phys.* **115**, 203509 (2014).

Cluster-plus-glue-atom Model and the Thus-obtained Composition Genes for Metallic Glasses

*Chuang Dong^{1,2}, Shuang Zhang¹, Cunlei Zou¹, Chenxi Dong¹, and Yajun Zhao¹

¹School of Materials Science and Engineering, Dalian Jiaotong University, Dalian 116028, China;

²Key Laboratory of Materials Modification by Laser, Ion and Electron Beams (Dalian University of Technology), Ministry of Education, Dalian 116024, China.

*dong@djtu.edu.cn

Keywords: Metallic glasses, Cluster-plus-glue-atom model, Molecule-like structural units, Composition genes, Composition design.

Composition interpretation of metallic glasses with high glass-forming abilities is an important issue, which relies on insights into their complex atomic structures. Metallic glasses, especially bulk metallic glasses, do have specific compositions, which strongly suggest the possible existence of some molecule-like structural units, in which the versatile but specific compositions are rooted. These structural units mimic the molecules in chemical substances but generally differ from the crystallographic unit cells. The possibility of having these fundamental units has been apparently overlooked because of the lack of structural models to properly address the short-range order in metallic glasses. A simplified atomic picture for short-range order is therefore required to identify the molecule-like composition units, in combination with an electronic factor for the concern of the structural stability.

Our research group has already proposed the cluster-plus-glue-atom model in 2007, which is a short-range-order structural model that renders any structure with a structural unit containing the essential structural information of the whole system. From the nomination of this model, one immediately determines a molecule-like structural unit consisting of a nearest-neighbor cluster plus a few outer-shell glue atoms. Actually, such structural unit, serving as the composition carrier, can be seen as the composition gene of the material. The proposition of composition genes facilitates the understanding of prevailing metallic glasses and can be a useful tool to guide the exploration of new composition space. With aides of the cluster-plus-glue-atom model and the thus-obtained molecule-like structural units (or said composition genes), fairly accurate composition interpretation and eventually design of metallic glasses with large glass-forming abilities could be envisaged.

Composition Optimization Based on Cluster-plus-glue-atom Model for Bulk Metallic Glass $Zr_{55}Cu_{30}Al_{10}Ni_5$

*Shuang Zhang¹, Cunlei Zou¹, Yajun Zhao¹, Chenxi Dong¹, and Chuang Dong^{1,2}

¹School of Materials Science and Engineering, Dalian Jiaotong University, Dalian 116028, China;

²Key Laboratory of Materials Modification by Laser, Ion and Electron Beams (Dalian University of Technology), Ministry of Education, Dalian 116024, China.

*zhangshuang@djtu.edu.cn

Keywords: Bulk metallic glass $Zr_{55}Cu_{30}Al_{10}Ni_5$, Composition origin, Composition optimization, Cluster-plus-glue-atom model, Dual-cluster formalism.

Previously we have proposed the cluster-plus-glue-atom model, by introducing a new description method based on the short-range-order structural units. In this model, good glass formers satisfy the general formula [cluster](glue atom)_{1 or 3}, where the cluster is the nearest-neighbor coordination polyhedron with a central atom and the glue atoms are situated between the clusters. Thereof, the dual-cluster formalism is developed, which assumes that a complex material may consist of two subunits, each being expressed by a cluster formula. Thus, the structural unit of a multi-element metallic glass can be deciphered to be composed of two clusters from basic binary crystalline phases plus 2, 4, or 6 glue atoms.

In the present work, the bulk metallic glass $Zr_{55}Cu_{30}Al_{10}Ni_5$ is taken as a typical example of quaternary complex systems, and the cluster-plus-glue-atom model is extended to the dual-cluster case to conduct the composition interpretation. Combing the cluster-based composition analysis method and the 24-electron rule for ideal metallic glasses, the composition origin of the bulk metallic glass $Zr_{55}Cu_{30}Al_{10}Ni_5$ is revealed and a series of possible new compositions are designed. Finally, higher glass forming ability is exhibited experimentally, indicating the achievement of composition optimization. This work provides a quantifiable composition design method for multi-element metallic glasses.

Colorless and high refractive SnO- and Sb₂O₃-containing borosilicate glassesKazuki Mitsui¹, *Akira Saitoh¹¹Graduate School of Science and Engineering, Ehime University, Matsuyama, Ehime 790-8577, Japan

*asaito@ehime-u.ac.jp

Keywords : Oxide glasses, Structure, Transparency, Refractive index.

We studied a relationship between the structure and optical properties in SnO- and Sb₂O₃-containing borosilicate glasses. Recently, PbO containing oxide glass has been excluded from optical devices such as lenses and optical fibers, caused by its toxicity. Instead, Bi₂O₃ containing oxide glasses show the high refractive and small photoelastic properties that meet an optical criterion about lenses and filters ¹). However, one of the drawbacks is a coloration in the visible range attributed to the mid-gap absorption ²). A notion is to choose Sb₂O₃ oxide as a co-dopant since no absorption derived from 5s²-5s¹p¹ bands exists.

Fig. 1 shows transmission spectra of SnO and Sb₂O₃-containing borosilicate glasses. Meanwhile, these glasses exhibit a high refractive index (~1.8) and very small photoelastic constant ($\pm 0.05 \times 10^{-12} \text{ Pa}^{-1}$). The optical absorption edge is blue-shifted with increasing of B₂O₃. The optical bandgap of the 55SnO–45B₂O₃ glass is about 3.6 eV. The micro-Raman scattering spectra elucidates that a four-coordinated borate unit (BO₄) exists in the SnO and Sb₂O₃-containing glass systems. Then, a blue-shift occurs by substitution of B₂O₃ by SiO₂ in SnO-containing borosilicate glasses. This may corroborate that the tetrahedral BO₄ units with non-bridging oxygens are selectively coordinated to a Sn²⁺ ion, resulting in a weak ligand.

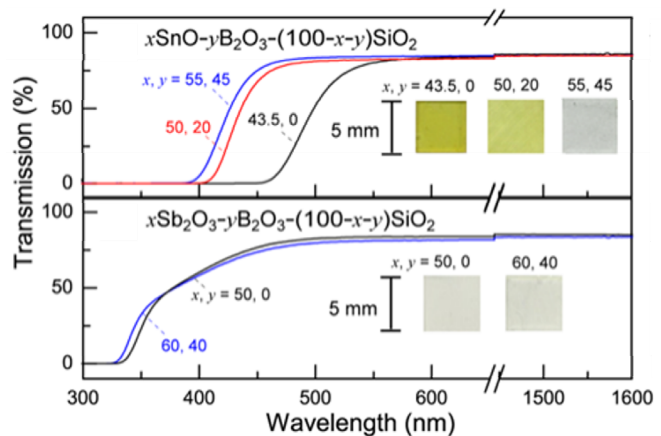


Fig. 1. Transmission spectra of $x\text{SnO}-y\text{B}_2\text{O}_3-(100-x-y)\text{SiO}_2$ (upper), and $x\text{Sb}_2\text{O}_3-y\text{B}_2\text{O}_3-(100-x-y)\text{SiO}_2$ (lower) glasses with 1-mm thickness show very small PEC values.

References

1) R. Morena, J. Non-Cryst. Solids 263, 382 (2000).

2) A. Saitoh, K. Hayashi, K. Hanzawa, S. Ueda, S. Kawachi, J. Yamaura, K. Ide, J. Kim, G. Tricot, S. Matsuishi, K. Mitsui, T. Shimizu, M. Mori, H. Hosono, and H. Hiramatsu, J. Non-Cryst. Solids 560, 120720 (2021).

Present address: Graduate School of Science and Engineering, Ehime University, Matsuyama, Ehime 790-8577, Japan

Understanding diffraction patterns of glassy, liquid and amorphous materials via topological analyses

*Yohei Onodera^{1,2}, Shinji Kohara²

¹ Institute for Integrated Radiation and Nuclear Science, Kyoto University, 2-1010 Asashiro-nishi, Kumatori-cho, Sennan-gun, Osaka 590-0494, Japan, ² Research Center for Advanced Measurement and Characterization, National Institute for Material Science, 1-2-1 Sengen, Tsukuba, Ibaraki, Tsukuba 305-0047, Japan

*y-onodera@rri.kyoto-ac.jp

Keywords: structure, X-ray/Neutron diffraction, reverse Monte Carlo simulation, classical molecular dynamics simulation, topological analyses.

The structure of glassy, liquid and amorphous materials is still not well understood, due to the insufficient structural information from diffraction data. Here, attempts are made to understand the origin of diffraction peaks in disordered materials. Furthermore, we applied topological analyses to reveal the relationship between diffraction pattern and topology of disordered materials¹⁾.

Figure 1 shows total structure factors, $S(Q)$, for disordered materials whose structure contains tetrahedral motifs obtained by neutron diffraction (ND) and X-ray diffraction (XRD). All amorphous and glassy materials form a tetrahedral network whereas two liquids are molecular liquids in which CCl_4 and P_4 tetrahedra are isolated. As can be seen in the figure, a three-peak structure, the first sharp diffraction peak (FSDP, Q_1), the principal peak (PP, Q_2), and the third peak (Q_3), can be observed in the $S(Q)$ except α -Si. It is confirmed that the FSDP is not a signature of the formation of a network, because an FSDP is observed in molecular liquids. The FSDP appears as the result of a sparse distribution of planes in polyhedra by analyzing the atomic configuration for g - SiO_2 generated by a combination of reverse Monte Carlo (RMC)¹⁰⁾ and molecular dynamics (MD) simulations. It is found that the PP reflects orientational correlation of polyhedra. Q_3 , that can be observed in all disordered materials, stems from simple pair correlations. Moreover, information of the topology of disordered materials was revealed by utilizing persistent homology¹¹⁾ analyses. The persistence diagram of silica (SiO_2) glass suggests that the shape of rings in the glass is similar not only to those in the crystalline phase with comparable density (α -cristobalite), but also to rings present in crystalline phases with higher density (α -quartz and coesite); that is thought to be a signature of good glass-forming ability in SiO_2 glass. Our series of analyses demonstrated that a combination of diffraction, computer simulation and topological analyses is a useful tool to uncover structural features hidden in halo pattern of disordered materials.

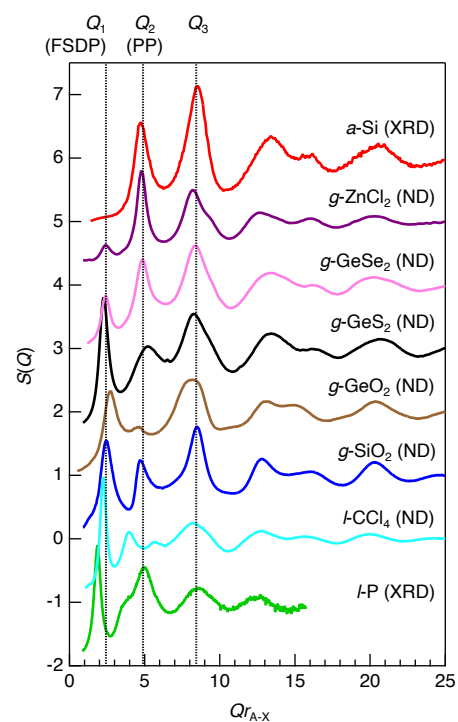


Fig. 1. Total structure factors, $S(Q)$, for amorphous (α)- Si ²⁾, glassy (g)- ZnCl_2 ³⁾, g - GeSe_2 ⁴⁾, g - GeS_2 ⁵⁾, g - GeO_2 ⁶⁾, g - SiO_2 ⁷⁾, l - CCl_4 ⁸⁾, and l - P ⁹⁾. The scattering vector Q is scaled by multiplying by r_{A-X} (distance between center and corner of tetrahedra). In the case of l - P , r_{A-X} is estimated from the side length of P_4 tetrahedron).

References:

- 1) Y. Onodera et al., J. Ceram. Soc. Jpn. 127, 853 (2019).
- 2) K. Laaziri et al., Phys. Rev. Lett. 82, 3460 (1999).
- 3) A. Zeidler et al., Phys. Rev. B 82, 104208 (2010).
- 4) E. Bychkov et al., Phys. Rev. B 72, 172107 (2005).
- 5) A. Bychkov et al., Phys. Chem. Chem. Phys. 15, 8487 (2013).
- 6) A. C. Hannon et al., J. Phys. Chem. B 111, 3342 (2007).
- 7) A. C. Hannon, Encyclopedia of glass science, technology, history and culture, John Wiley & Sons Inc, 129 (2021).
- 8) H. Morita et al., J. Mol. Liq. 147, 182 (2009).
- 9) Y. Katayama et al., Nature 403, 170 (2000).
- 10) R. L. McGreevy and L. Pusztai, Mol. Simul. 1, 359 (1988).
- 11) Y. Hiraoka et al., Proc. Natl. Acad. Sci. USA 113, 7035 (2016).

Local structural investigation of non-crystalline materials at high pressure

Xinguo Hong

Center for High Pressure Science and Technology Advanced Research, Beijing 100094, P.R. China

*xinguo.hong@hpstar.ac.cn and xinguo.hong@gmail.com

ABSTRACT

Local structure plays a dominant role in the structural polyamorphism and novel electronic properties under extreme conditions[1-4]. Liquids and disordered solids under extreme conditions in the Earth interior is important for Earth and planetary science. However, measurement of the local structure of non-crystalline materials at high pressure remains a challenge. Recently we have succeeded in obtaining high-quality atomic pair distribution function (PDF) using high-energy X-ray microbeam[5] and X-ray absorption fine structure at high pressure[1,6].

PDF is a powerful local-structural tool for studying crystalline, disordered and nano materials [7-13]. The total scattering, including Bragg peaks as well as diffuse scattering, contributes to the PDF, and is particularly useful for characterizing the local structure of amorphous materials, e.g. ref. [14] and the aperiodic distortions in crystals as well [10]. XAFS is a well-known local structural tool, which can provide an upper level resolution in the short order of local structure, being able to probe the subtle structural and electronic polymorphs[3,4,15]. In this conference, we will report our recent progress in the high-energy X-ray focusing, HP-PDF and HP-XAFS, and the related first-principles calculations.

References:

- [1] X. Hong, M. Newville, T. S. Duffy, S. R. Sutton, and M. L. Rivers, *Journal of Physics: Condensed Matter* **26**, 035104 (2014).
- [2] X. Hong, L. Ehm, and T. S. Duffy, *Applied Physics Letters* **105**, 081904 (2014).
- [3] X. Hong, M. Newville, Y. Ding, D. Zhang, T. Irifune, G. Gu, and H.-K. Mao, *Physical Review B* **102**, 134110 (2020).
- [4] X. Hong, M. Newville, Y. Ding, T. Irifune, G. Gu, and H.-K. Mao, *Physical Review B* **101**, 214107 (2020).
- [5] X. Hong, L. Ehm, Z. Zhong, S. Ghose, T. S. Duffy, and D. J. Weidner, *Scientific Reports* **6**, 21434 (2016).
- [6] X. Hong, M. Newville, V. B. Prakapenka, M. L. Rivers, and S. R. Sutton, *Review of Scientific Instruments* **80**, 073908 (2009).
- [7] T. Egami and S. J. L. Billinge, Pergamon, Oxford (1994).
- [8] J. L. Billinge Simon, in *Zeitschrift für Kristallographie/International journal for structural, physical, and chemical aspects of crystalline materials* 2004, p. 117.
- [9] T. Proffen, R. G. DiFrancesco, S. J. L. Billinge, E. L. Brosha, and G. H. Kwei, *Physical Review B* **60**, 9973 (1999).
- [10] S. J. L. Billinge and M. G. Kanatzidis, *Chemical Communications*, 749 (2004).
- [11] S. J. L. Billinge and I. Levin, *Science* **316**, 561 (2007).
- [12] B. Gilbert, F. Huang, H. Zhang, G. A. Waychunas, and J. F. Banfield, *Science* **305**, 651 (2004).
- [13] C. D. Martin, S. M. Antao, P. J. Chupas, P. L. Lee, S. D. Shastri, and J. B. Parise, *Applied Physics Letters* **86** (2005).
- [14] M. Inui, X. Hong, and K. Tamura, *Physical Review B* **68**, 094108 (2003).
- [15] X. Hong and M. Newville, *physica status solidi (b)*, 2000052 (2020).

The structure of bismuth oxide glasses

Katsuki Hayashi¹, Tatsuki Shimizu¹, * Akira Saitoh¹¹Graduate School of Science and Engineering, Ehime University, Matsuyama, Ehime 790-8577, Japan

* asaito@ehime-u.ac.jp

Keywords: Oxide glasses, Structure, Optical properties.

Functional oxide glasses are one of the key materials in our life. For example, lead oxide glasses providing high refractive index have been applied to optical glass devices¹⁾. But the toxicity elements including PbO are restricted in the optical devices, nevertheless the ns²-type ions (Sn²⁺, Sb³⁺, Pb²⁺, and Bi³⁺) with high electron polarizability being effective. We have reported a non-toxic oxide glass being high refractive index over 2.0 and very small photoelastic constant less than $0.05 \times 10^{-12} \text{ Pa}^{-1}$ by choosing Bi³⁺ ion^{2,3)}.

The sesquioxide Bi₂O₃ in oxide glasses lead large ion-filling structure constituted by octahedral BiO₆ units by micro-Raman spectroscopy. However, no direct evidence regarding the valence of bismuth ions and the short- and medium-range structures had not been elucidated. Thus, we report the valence state of bismuth ions elucidated by HAXPES and XANES (Bi L_{III}-edge) and anionic structure about silicate, borate, and phosphate glasses network by ²⁹Si, ¹¹B, and ³¹P MAS-NMR spectra and EXAFS.

Fig. 1 shows EXAFS spectra of the (a) NaBiO₃, (b) Bi₂O₃, (c) 57Bi₂O₃-43SiO₂, (d) 55Bi₂O₃-45B₂O₃, and (e) 40Bi₂O₃-60P₂O₅ glasses. The first coordination manners of a Bi³⁺ ion in (c) and (d) are almost the same of the crystalline Bi₂O₃. On the other hand, the second-nearest coordination in phosphate glass (e) is slightly shorted compared with that of crystalline Bi₂O₃. In short, there are four oxygens that position at ~0.28 nm from a Bi³⁺ ion. These structures relate to optical properties such as light absorption and photoelasticity.

References

- 1) K. Kurosawa, Photonic Sensors 4, 12 (2014).
- 2) A. Saitoh, K. Hayashi, K. Hanzawa, S. Ueda, S. Kawachi, J. Yamaura, K. Ide, J. Kim, G. Tricot, S. Matsuishi, K. Mitsui, T. Shimizu, M. Mori, H. Hosono, and H. Hiramatsu, J. Non-Cryst. Solids 560, 120720 (2021).
- 3) K. Hayashi, T. Shimizu, S. Matsuishi, H. Hiramatsu, and A. Saitoh, J. Mater. Sci.: Mater. Electron. 33, 2242 (2022).

Present address: Graduate School of Science and Engineering, Ehime University, Matsuyama, Ehime 790-8577, Japan.

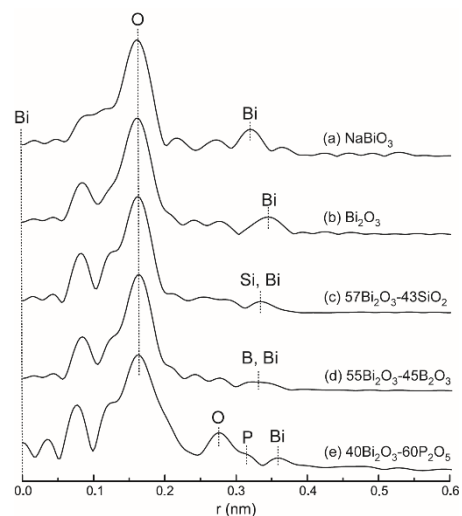


Fig. 1. EXAFS spectra of (a) NaBiO₃, (b) Bi₂O₃, (c) 57Bi₂O₃-43SiO₂, (d) 55Bi₂O₃-45B₂O₃, and (e) 40Bi₂O₃-60P₂O₅ glasses.

Atomic structure of bulk metallic glasses studied by transmission electron microscopy, synchrotron-radiation X-ray diffraction, scanning tunneling microscopy and ab-initio molecular dynamics simulation

*D. V. Louzguine^{1,2}

¹ MathAM-OIL, National Institute of Advanced Industrial Science and Technology (AIST), Sendai 980-8577, Japan

² Advanced Institute for Materials Research (WPI-AIMR), Tohoku University, Aoba-Ku, Sendai 980-8577, Japan,

* dml@wpi-aimr.tohoku.ac.jp

Keywords (Maximum: 6 keywords, Minimum: 3 keywords, 10 point): X-ray scattering, Scanning tunneling microscopy, Ab initio simulation.

Structural changes in a relatively *strong* Zr-Cu-Ni-Al bulk glass-forming liquid alloy on cooling from above the equilibrium liquidus temperature were studied in-situ by synchrotron radiation X-ray diffraction and supported by the results of first-principles molecular dynamics (MD) simulation. The results are also compared with those of a relatively *fragile* Pd-Cu-Ni-P liquid alloy, studied earlier. According to the pair distribution functions (PDF(R)) obtained chemical ordering forming extra Zr-Cu,Ni, Zr-Al and Zr-Zr atomic pairs takes place in the Zr-Cu-Ni-Al supercooled liquid alloy on cooling towards the glass-transition temperature (T_g) [1]. However, here the change in the ratio of Zr-Cu,Ni atomic peak area to other peaks area in the first coordination shell (Fig. 1a) is smaller than that found in case of the Pd-Cu-Ni-P alloy (Cu,Ni-P to other peaks ratio) in accordance with a lower *fragility* index $m = d \log(\eta) / d(T_g/T)$ (where η is the viscosity) of the Zr-Cu-Ni-Al melt. Atomic redistribution between the first and second coordination shells is also observed. These findings indicate that *fragility* is a sign of instability of short and medium range order in *fragile* liquids. These results will be compared with those of other research groups.

Also, the atomic structure of a Ni-Nb bulk metallic glass was directly resolved (Fig. 1b) by means of ultra high vacuum scanning tunneling microscopy (STM). Owing to the complicated electronic structure of the Ni-Nb glassy alloy it also acts as a spectroscopy giving a chance to resolve local chemistry. STM allows detection of Ni and Nb atomic positions separately depending on the applied potential. Direct atomic structure observation was supported by MD simulation [2].

The structure of these and other bulk metallic glasses was also studied by high-resolution transmission electron microscopy. New results will be presented.

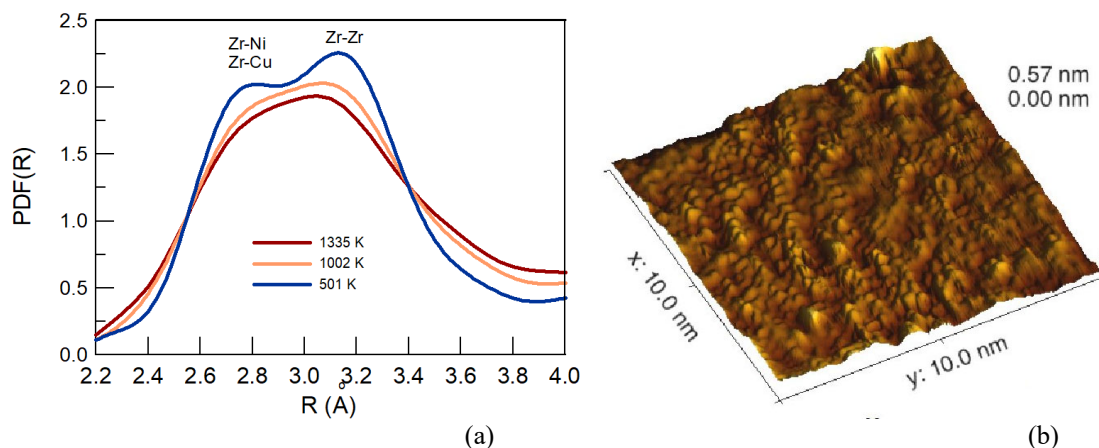


Figure 1. (a) Three typical PDF(R) ($g(R)$) functions of the $Zr_{55}Cu_{30}Ni_5Al_{10}$ glass-forming alloy upon in-situ vitrification experiment on cooling. (b) An atomic structure of the $Ni_{63.5}Nb_{36.5}$ glassy alloy (STM).

References:

- 1) D.V. LOUZGUINE-LUZGIN, K. GEORGARAKIS, J. ANDRIEUX, L. HENNET, T. MORISHITA, K. NISHIO, R.V. BELOSLUDOV, *Intermetallics*, 122, 106795, (2020).
- 2) R.V. BELOSLUDOV, A.I. ORESHKIN, S.I. ORESHKIN, D.A. MUZYCHENKO, H. KATO, D.V. LOUZGUINE-LUZGIN, *Journal of Alloys and Compounds*, 816, 152680, (2020).

Short range order controlling the atomic dynamics in metallic glasses

*X.D.Wang¹, T.D. Xu¹, K.K. Qiu¹, S.F. Wei¹, Q.P. Cao¹, D. X. Zhang², J.Z. Jiang¹

¹ International Center for New-Structured Materials (ICNSM), Laboratory of New-Structured Materials, State Key Laboratory of Silicon Materials, and School of Materials Science and Engineering, Zhejiang University, Hangzhou, 310027, People's Republic of China

² State Key Laboratory of Modern Optical Instrumentation, Zhejiang University, Hangzhou, 310027, People's Republic of China

* wangxd@zju.edu.cn

Keywords (Maximum: Metallic glasses, X-ray absorption fine structure, Short range order, Atomic dynamics, Ab initio simulation.

The secondary β -relaxation is an intrinsic feature in glassy materials. However, its structural origin is still not well understood. Here we report that the β -relaxations in metallic glasses (MGs) mainly depend on the vibration of small atoms, not only related to their surrounding local geometry but also chemical constitutions, i.e., the short-range order. For examples, by using advanced synchrotron x-ray techniques and theoretical calculations, we find that the tricapped-trigonal-prism-like polyhedra with more large La atoms in shells favor the local vibration of center Ni atoms, leading to the pronounced β -relaxation event in $\text{La}_{50}\text{Al}_{15}\text{Ni}_{35}$ MG [1]. In contrast, Cu atoms are relatively close-packed with some Cu in the nearest neighbors while they could easily diffuse out of the cages compared to Ni, somehow triggering the onset of α -relaxation in $\text{La}_{50}\text{Al}_{15}\text{Cu}_{35}$ MG. When focusing on the as-cast and annealed $\text{La}_{50}\text{Al}_{15}\text{Ni}_{35}$ MGs[2], we demonstrate that the chemical constitution around mobile Ni atoms in Ni-centered polyhedra tends to transform from Al-free to Al/Ni-containing with decreasing the free after annealing, suppressing the local vibration of central Ni atoms and thus leading to the unpronounced β -relaxation event. Moreover, the atomic mobility of Ni atoms more depends on their local polyhedral geometry and chemical constitution than the content of surrounding free volume. Despite the same composition and similar atomic sizes of Ni and Fe atoms, the β -relaxation in $\text{Y}_{60}\text{Ni}_{16}\text{Al}_{24}$ and $\text{Y}_{60}\text{Fe}_{16}\text{Al}_{24}$ MGs mainly depends on the vibration of small Ni and Fe atoms, respectively [3]. From the x-ray absorption fine structure and Voronoi tessellation statistics, it is found that the dominant local structure of mobile atoms changes from $\langle 0, 3, 6, 0 \rangle$ centered by Ni atoms into $\langle 0, 2, 8, 0 \rangle$ centered by Fe atoms. More large Y atoms in shells promote the local vibration of center Ni atoms. In contrast, with more Y atoms replaced by Fe atoms, the vibration of center Fe atoms gets significantly slow down, thus leading to an unpronounced β relaxation. Our results provide an idea for understanding the structural origin of β -relaxation behaviors in MGs and other glassy materials from their local atomic environments and dynamics point of view.

References

- [1] X.D. Wang, J. Zhang, T.D. Xu, Q. Yu, Q.P. Cao, D.X. Zhang, J.Z. Jiang, J. Phys. Chem. Lett. **9**, 4308(2018).
- [2] K.K. Qiu, X.D. Wang, T.D. Xu, J. Liu, Q.P. Cao, D.X. Zhang, J.Z. Jiang, Mater. Today Phys. **21**, 100515 (2021).
- [3] S.F. Wei, X.D. Wang, K.K. Qiu, T.D. Xu, Q.P. Cao, S.Q. Ding, D.X. Zhang, J.Z. Jiang, Phys. Rev. B **105**, 054313 (2022).

ON THE RELATIONSHIP BETWEEN STRUCTURAL STATE, MECHANICAL PROPERTIES AND WEAR RESISTANCE OF A CU- BASED BULK METALLIC GLASS.

*P. Laffont¹, R. Daudin¹, JJ. Blandin¹, A. Lenain², S. Gravier², S. Stoens³, G. Colas³, P.H. Cornuault³

¹Univ. Grenoble Alpes, SIMaP, Grenoble, F-38000, France, ²Vulkam Inc. Amorphous metal micro casting / www.vulkam.com / Gières, 38610, France, ³Univ. Bourgogne Franche-Comté FEMTO-ST Institute CNRS/UFC/ENSMM/UTBM, Département de Mécanique Appliquée, Besançon, 25000, France

*paul.laffont@grenoble-inp.fr

Keywords: Metallic glasses, alloying, relaxation, mechanical properties, wear resistance,

By quenching a liquid metallic alloy, the crystallization process can be bypassed to obtain an amorphous metal called metallic glass. This class of metallic materials exhibits very high mechanical properties (high yield stress, high hardness, large elastic strain) perfectly suitable for applications in micro-mechanics (such as micro-gears for example) [1]. However, in this kind of application, the life time of the metallic glass object is directly related to its wear resistance which is not clearly understood up to date depending on the contact conditions as well as the mechanical properties of both the metallic glasses and the counterpart. For most of the crystalline metallic alloys, the Archard's law directly correlates the wear resistance with the hardness of the material: the harder the better. This law does not always apply for metallic glasses [2] suggesting that the difference in the local deformation mechanisms (shear bands VS dislocations) can play an important role in predicting the tribological behaviour of amorphous metals.

In the case of metallic glasses, the nucleation of shear bands is related to the hardness but their propagation is related to the plasticity. This work aims to propose a correlation between the wear resistance and the hardness as well as plasticity. To do so, three strategies are performed to modify the hardness and/or plasticity of a Cu-based BMG ($\text{Cu}_{47}\text{Zr}_{46}\text{Al}_7$, at%): the addition of Nb, the relaxation of the excess free volume and the partial crystallization of the alloy (see Figure). Each strategy is evaluated by micro-indentation as well as three points bending. Moreover, using the results of numerous micro-scratch tests analysed by optical interferometric profilometry, we will show the impact of these different strategies on the wear resistance, both on the wear rate and the friction coefficient. Specific structural analyses along the wear tracks also show the development of different shear bands patterns depending on the chosen strategy revealing the importance of the hardness and/or plasticity.

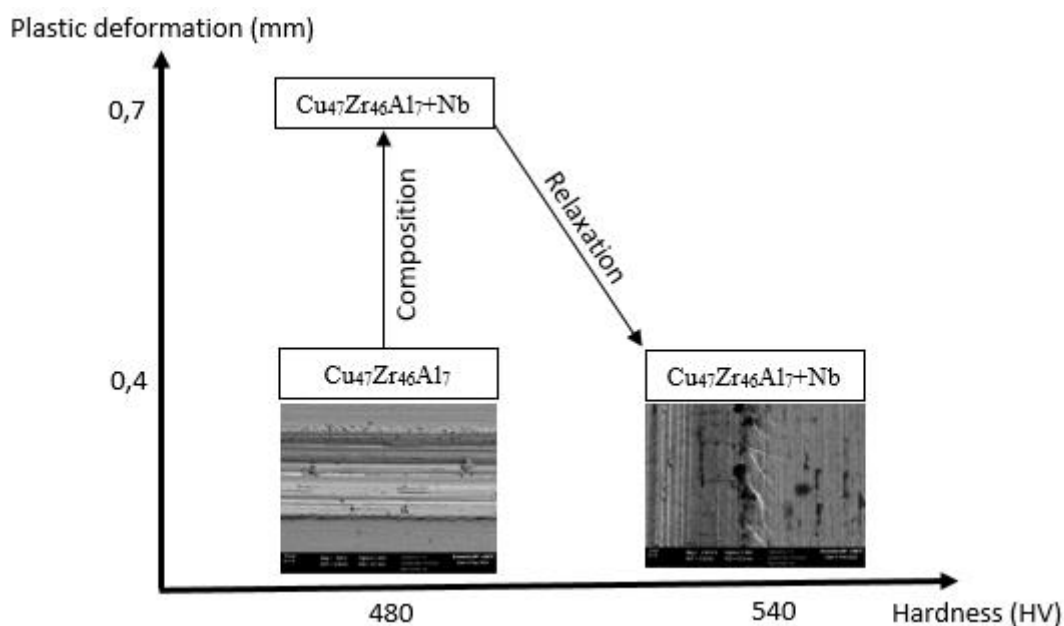


Fig. 1. Hardness and plastic deformation in function of the different treatments

Behaviors of disordered alloys under high temperature and pressure

* Jian-Zhong Jiang¹, X.D. Wang¹, Q.P. Cao¹ and D.Z. Zhang¹

¹ International Center for New-Structured Materials (ICNSM), School of Materials Science & Engineering, Zhejiang University, Hangzhou, P.R. China

jiangjz@zju.edu.cn

Keywords: Amorphous alloys, Metallic liquids, Temperature and pressure, X-ray scattering, MDs.

Phase transitions in materials are the subject of great interest. The polyamorphic transition induced by temperature and/or pressure, defined as a transition between two different disordered phases (without long range translation and orientation symmetries and with the same composition) in disordered materials, e.g., liquids and amorphous materials, is often more complex as compared to the polymorphic transition in crystalline materials. In this talk, we will survey behaviors of disordered alloys (metallic liquids and metallic glasses) under various temperatures and pressures. Firstly, temperature-dependent atomic structure evolutions in various metallic liquids (from pure element to multi-component systems) will be mentioned, esp. challenges and potential for liquid-to-liquid transition in metallic liquids will be critically discussed. Secondly, pressure-induced phase transformation in various metallic glasses will be further discussed. Finally, simultaneously temperature- and pressure-induced polyamorphic transitions in disordered materials will be presented.

Heraeus AMLOY Technologies –
The transition from scientific innovation to series production of high-performance application solutions

Dr. Hans-Jürgen Wachter¹, *Mrs. Valeska Melde²

¹Global Head of Heraeus AMLOY, Karlstein am Main, 63791, Germany, ²Head of Marketing & Sales, Karlstein am Main, 63791, Germany

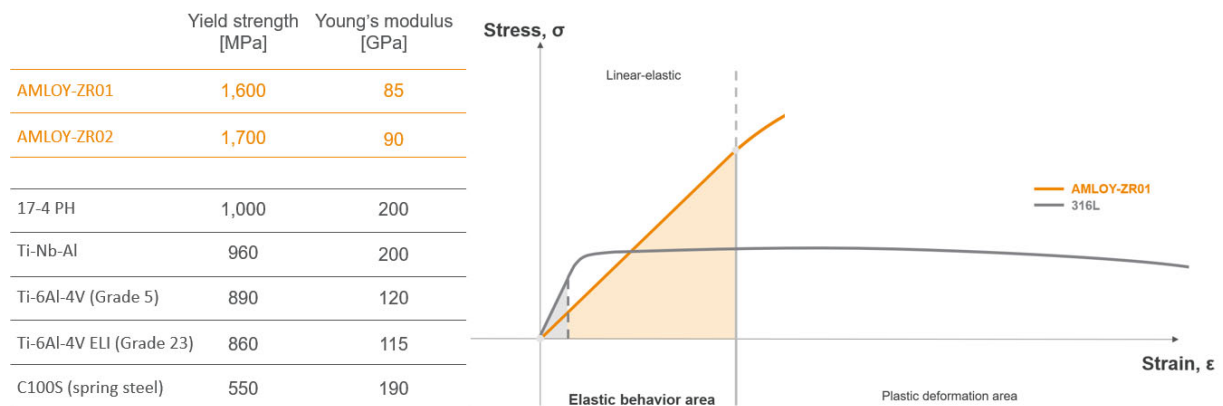
*valeska.melde@heraeus.com (Corresponding author identified by the superscript of *)

Keywords: Amorphous alloys, Bulk Metallic Glasses, Injection Molding, 3D Printing, Medical Technology, Robotics & Mechanics, Sensor Applications

Whether due to their exceptional combination of high strength and high elasticity in use as spring elements or in transmission applications, or due to their high corrosion resistance and even biocompatibility as medical sensors or long-term implants, amorphous alloys have been seen as a potential solution to many challenges in high-tech applications since their discovery. However, the challenging production of components from amorphous alloys, in a reproducible, high quality with as little post-processing as possible and in a cost-efficient way, has so far inhibited the use of this promising class of materials.

Heraeus AMLOY Technologies has managed to overcome this limitation as a fully integrated contract manufacturer along the value chain. With its own alloyed raw material range of amorphous alloys, AMLOY is able to mass-produce bulk metallic glass components reproducibly according to technical drawings using an adapted injection molding process and the additive LPBF process. The general quality controls by means of CT and optical measurement are also extended by application-related test rigs and thus the performance of components made of AMLOY alloys continues to be confirmed and improved.

Fig. 1: Mechanical performance of AMLOY alloys regarding strength and elasticity



In addition to the mechanical properties shown in Fig. 1, AMLOY has also succeeded in addressing markets and entering development partnerships that place high demands on material purity (medical technology), reproducible dimensional accuracy (sensor technology) and long-term stable performance (robotics & mechanics). AMLOY's consulting and support in the development process of the components also plays a decisive role here, successfully contributing its expertise in materials and manufacturing processes to design guidelines for improving component performance in the application environments.

In addition to the recent expansion of AMLOY's machine park, with its own and independently manufactured production equipment in injection molding, in the future, the use of AMLOY materials in near-net-shape manufactured components is expected to solve specific challenges in medical technology, robotics and sensor technology and improve performance, to continue to accelerate amorphous alloys from scientific innovation to an established manufacturing method.

Large-scale density fluctuations during structural transition in metallic glass forming liquid beyond medium range order

*F. Yang¹, N. Neuber², B. Adams², L. Kreuzer^{1,3}, L. Ruschel², M. Blankenburg⁴, R. Busch², A. Meyer¹

¹ Institut für Materialphysik im Weltraum, Deutsches Zentrum für Luft- und Raumfahrt, Cologne, 51170, Germany,

² Lehrstuhl für metallische Werkstoffe, Universität des Saarlandes, Saarbrücken 66123, Germany,

³ Heinz Maier-Leibnitz Zentrum (FRM II), TU München, Garching 85748, Germany,

⁴ Deutsches Elektronen-Synchrotron (DESY, Hamburg 22607, Germany

* fan.yang@dlr.de

Keywords: Liquid-liquid transition, SAXS/WAXS, in-situ synchrotron diffraction.

Phase transformation between two disordered structures i.e., the so-called polyamorphism, is a long-standing issue in the field of liquid and glass physics, still being intensively studied and debated. This kind of liquid-liquid (LL) transition was first suggested to be present in water [1]. Meanwhile, indications of the LL-transition have been found in oxide, semiconductor, and a number of metallic glass-forming melts [2-4], pointing to a rather general phenomenon. It has been proposed that such transitions can be interpreted as analogous to an order-disorder transition, with a diverging correlation length at the transition point and a lambda shaped heat capacity [2]. This scenario implies large impacts on the structural and dynamic properties of the melt, including diffusion or liquid viscosity, as well as the glass forming ability (GFA). However, the physical nature and microscopic mechanism of the LL-transition is still not well understood. For oxide and molecular liquids, the microscopic mechanism of the LL-transition can be often viewed structurally as a change of the bonding angle or the coordination of the structural units. Classical metallic bonding is, on the other hand, nondirectional. Thus, so far, changes of the medium-range order are considered to be relevant for the LL-transition in alloy melts [2,3]. Whether and how the observed LL-transition in metallic glass-forming liquids can be understood in accordance with the general picture together with other glass formers is still not clear.

Only recently, direct structural investigations on two well-known bulk metallic glass forming liquids, $Zr_{41.2}Ti_{13.8}Cu_{12.5}Ni_{10.0}Be_{22.5}$ and $Zr_{58.5}Cu_{15.6}Ni_{12.8}Al_{10.3}Nb_{2.8}$, show that the kinetics of the LL-transition are rather slow, which must involve long range, diffusion like mass transports [4]. Using a simultaneous SAXS/WAXS setup, combined with electrostatic levitation, we are now able to investigate in-situ structural changes in the undercooled liquid across the liquid-liquid transition region on a length scale well beyond the medium range order. We confirm the previous estimation of the occurrence of large-scale structural fluctuations on the order of nanometers close to the transition temperature. Depending on the temperature of the undercooled melt, such structural changes also act as a “precursor” of the crystallization of the undercooled liquid. The observed characteristic length scale is incompatible with a transition mechanism involving local structural changes only, as in the case of oxides or molecular liquids.

References:

[1] C. A. Angell, *Science* **319**, 582 (2008).

[2] S. Wei, F. Yang, J. Bednarčík, I. Kaban, O. Shuleshova, A. Meyer, and R. Busch, *Nature Comm.* **4**, 2083 (2013).

[3] M. Stolpe, I. Jonas, S. Wei, Z. Evenson, W. Hembree, F. Yang, A. Meyer, and R. Busch, *Phys. Rev. B* **93**, 014201 (2016).

[4] I. Jonas, F. Yang, A. Meyer, *Phys. Rev. Lett.* **123**, 055502 (2019).

Structure and dynamics in the no-man's land of phase-change materials

*Shuai Wei

Department of Chemistry, Aarhus University, Aarhus, Denmark

* shuai.wei@chem.au.dk

Keywords: phase-change materials, liquid-liquid transition, fragile-strong transition, metal-semiconductor transitions, X-ray/Neutron scattering, crystallizations.

Phase-change materials such as Ge-Sb-Te and Ge-Sb can be reversibly switched between amorphous and crystalline states within the timescale of nanoseconds. The switchable states can be used to encode information for data storage applications. While fast-switching rewritable nonvolatile memory units based on phase-change materials are promising technologies for future computer memory devices, an in-depth understanding of the physical factors that determine their success is still lacking(1, 2). Here we show the existence of a liquid-state metal-to-semiconductor transition, located not far below the melting point, T_m , as essential(1, 3–5). The metal-to-semiconductor transition is itself a consequence of atomic rearrangements that are involved in a high-density to low-density liquid-liquid transition and a fragile-to-strong transition in liquid viscosity. The latter controls both the speed of crystallization and the stabilization of the glass state(6), which are essential for the understanding of materials' switching behaviors. Furthermore, we demonstrate the direct structural evidence of such a liquid-liquid transition in the supercooled liquid state (no-man's land) of phase-change materials using femtosecond X-ray diffractions with X-ray free electron lasers. At last, we introduce a new parameter, the "metallicity". When T_m -scaled temperatures of known metal-to-semiconductor transitions of Group IV, V, and VI alloys are plotted against their metallicities, the curvilinear plot leads directly to the composition zone of all known phase-change materials and the temperature interval below T_m , which may provide guidance for tailoring the materials(1)

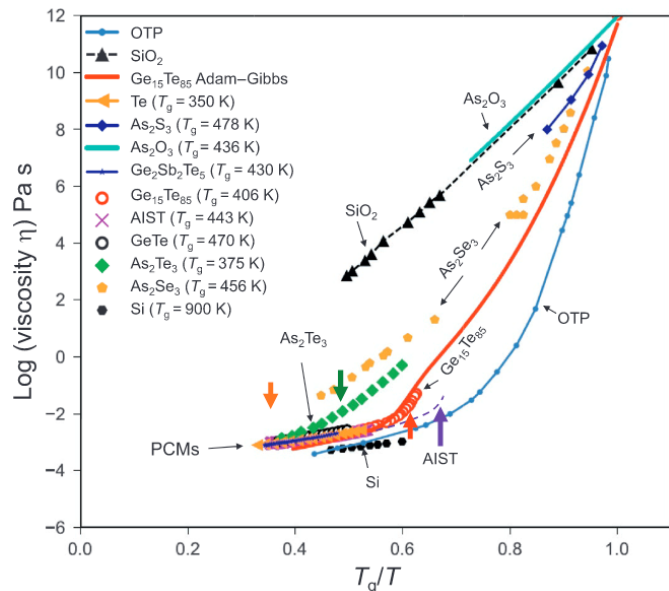


Fig. 1. Angell-plot of alloys based on group-VI, V, V. The double kink in the Adam-Gibbs fitting curve (red curve) reveals a fragile-strong transition. Taken from Ref.1.

References

1. S. Wei, P. Lucas, C. A. Angell, Phase-change materials: The view from the liquid phase and the metallicity parameter. *MRS Bulletin*. **44**, 691–698 (2019).
2. M. Wuttig, N. Yamada, Phase-change materials for rewritable data storage. *Nature Materials*. **6**, 824–32 (2007).
3. P. Zalden, F. Quirin, M. Schumacher, J. Siegel, S. Wei, A. Koc, M. Nicoul, M. Trigo, P. Andreasson, H. Enquist, M. J. Shu, T. Pardini, M. Chollet, D. Zhu, H. Lemke, I. Ronneberger, J. Larsson, A. M. Lindenberg, H. E. Fischer, S. Hau-Riege, D. A. Reis, R. Mazzarello, M. Wuttig, K. Sokolowski-Tinten, Femtosecond x-ray diffraction reveals a liquid–liquid phase transition in phase-change materials. *Science*. **364**, 1062–1067 (2019).
4. S. Wei, Z. Evenson, M. Stolpe, P. Lucas, C. A. Angell, Breakdown of the Stokes-Einstein relation above the melting temperature in a liquid phase-change material. *Science Advances*. **4**, eaat8632 (2018).
5. S. Wei, G. J. Coleman, P. Lucas, C. A. Angell, Glass Transitions, Semiconductor-Metal Transitions, and Fragilities in Ge-V-Te (V=As, Sb) Liquid Alloys: The Difference One Element Can Make. *Phys. Rev. Applied*. **7**, 034035 (2017).
6. S. Wei, P. Lucas, C. A. Angell, Phase change alloy viscosities down to T_g using Adam-Gibbs-equation fittings to excess entropy data: A fragile-to-strong transition. *J. Appl. Phys.* **118**, 034903 (2015).

Thermoplastic forming capacity of a ZrCoAl metallic glass for surface patterning

*[Loïcia Gaudilliere](mailto:loicia.gaudilliere@grenoble-inp.fr), Rémi Daudin, Jean-Jacques Blandin

Univ. Grenoble Alpes, SIMaP, Grenoble, F-38000, France

*loicia.gaudilliere@grenoble-inp.fr

Keywords: thermoplastic forming, surface patterning, ZrCoAl, crystallization, high temperature rheology

Metallic glasses (MG) are known for their great properties at room temperature (hardness, yield stress, elastic strain...) but are also interesting for their ability to be shaped at high temperature by thermoplastic forming (TPF) and surface patterning. Many studies were performed on precious MG such as Au-, Pd- or Pt-based compositions and due to their oxidation resistance, TPF can be done under air¹. Some Zr-based alloys are also reported for TPF, because of the existence of a supercooled liquid region (SLR) usually associated with Newtonian rheologies^{2,3}.

In the present work, the $Zr_{56}Co_{28}Al_{16}$ MG was chosen for its great potential for medical applications thanks to its good compromise between corrosion resistance and mechanical behaviour⁴. This work focuses on the high temperature rheology of this alloy with an emphasis concerning its thermal stability and the structural transformation processes occurring in the temperature range of the TPF window. Differential Scanning Calorimetry (DSC) (Fig. 1) reveals a limited SLR (leading to a lack of Newtonian regime and suggesting non-ideal conditions regarding TPF) and a two-stage crystallization behavior. Both X-Ray Diffraction and Transmission Electron Microscopy suggest that crystallization actually happens only around the second exothermic peak. Compression tests including strain rate jumps at different temperatures were performed and showed that an increase of the strain rate and/or the temperature may enhance the phase transformation kinetic. Finally, despite relatively high viscosities and a lack of Newtonian regime (resulting from the associated structural transformations), surface patternings were successfully performed.

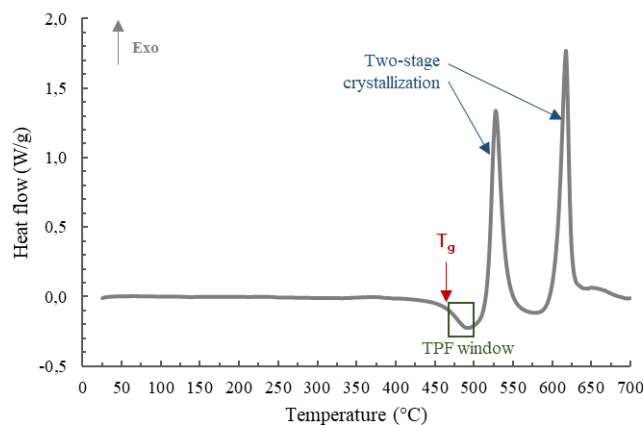


Fig. 1: DSC curve of the $Zr_{56}Co_{28}Al_{16}$ metallic glass

References

1. Hasan, M. *et al.*, Functionalization of Metallic Glasses through Hierarchical Patterning. *Nano Lett.* **15**, 963–968 (2015).
2. Li, N. *et al.* A thermoplastic forming map of a Zr-based bulk metallic glass. *Acta Mater.* **61**, 1921–1931 (2013).
3. He, J. J. *et al.* The precision replication of a microchannel mould by hot-embossing a Zr-based bulk metallic glass. *Intermetallics* **21**, 50–55 (2012).
4. Guérin, E. Processing and properties of Zr-Co-Al bulk metallic glass for biomedical applications, *Ph.D. Univ. Grenoble Alpes* (2022).

Shape memory effect in metallic glasses

*Tianding Xu¹, Xiao-Dong Wang², Jian-Zhong Jiang³

¹ *International Center for New-Structured Materials (ICNSM), Laboratory of New-Structured Materials, State Key Laboratory of Silicon Materials, and School of Materials Science and Engineering, Zhejiang University, Hangzhou, 310027, China.*

* xutd@zju.edu.cn

Keywords: atomic dynamics, metallic glass, X-ray photon correlation spectroscopy, shape memory effect.

Shape memory effect (SME), mainly present in crystalline Ti-Ni alloys, is basically missing in metallic glasses (MGs) that lack the long-range periodic order to characterize crystals. Here we report experimental results of SME in annealed MGs, in which the low-energy configuration state recovery is observed by both differential scanning calorimetry and X-ray photon correlation spectroscopy. We elucidate the origin of SME in MGs under the potential energy landscape framework, i.e., after annealing, the energy of MGs enters into a deep basin and atoms are located in the low-energy configuration state. Albeit deviating from their relative stable configurations by temperature changes, atoms in the annealed MGs tend to return to the low-energy atomic configurations along certain trajectories as pre-annealing temperature is approached. These results could extend the application of MGs as functional materials by directionally manipulating their energy states via annealing and rejuvenation.

References:

1) T. D. Xu, X. Wang and J. Jiang, *Matter*, 4 (2021): 3327.

Present address: Zhejiang University, Hangzhou, 310027, China

Role of Y content on glass-forming ability and soft magnetic properties of Co-Y-B metallic glasses

S. Ma, *M. Yao, *W. Zhang

Key Laboratory of Materials Modification by Laser, Ion, and Electron Beams (Ministry of Education), School of Materials Science and Engineering, Dalian University of Technology, Dalian, 116024, P.R.China

*yaoman@dlut.edu.cn (M. Yao), wzhang@dlut.edu.cn (W. Zhang).

Keywords: Co-based metallic glasses, glass-forming ability, soft magnetic property, *ab initio* molecular dynamics simulations, local atomic structures.

Co-based metallic glasses (MGs) have attracted great attention due to their excellent soft magnetic properties including high permeability, low coercivity (H_c), and near-zero magnetostriction, whereas the poor glass-forming ability (GFA) severely limits their applications and development [1-2]. To improve the GFA of Co-based MGs while maintaining superior soft magnetic properties, microalloying with appropriate elements is an effective method [3-4]. Recently, we found that the thermal stability and GFA of $\text{Co}_{75}\text{B}_{25}$ alloy are effectively enhanced with minor Y addition, accompanied by the improvement of magnetic softness. However, the influence mechanisms of Y content on GFA and magnetic behaviors remain unclear. Therefore, we employed *ab initio* molecular dynamics (AIMD) simulations and density functional theory (DFT) calculations to analyze the relationship between local atomic structures and properties.

The experimental results demonstrated that the addition of 3.5 at.% Y into $\text{Co}_{75}\text{B}_{25}$ alloy promotes the occurrence of glass transition (Fig. 1 (a)), and enlarges critical thickness t_c to 240 μm , lowers H_c to 1.5 A/m with saturated magnetic flux density B_s of 0.73 T. By calculating the local atomic structures (pair distribution function, coordination numbers, chemical short-range order, Voronoi polyhedron, structure factor, and the ratio of voids), dynamic behavior, electronic structure, magnetic moment, and magnetic anisotropy energy (MAE), it is revealed that the local atomic structures of Co-Y-B MGs are dominated by the B-centered prism units, and Y plays a vital role in the formation of the densely packed structures. The strongest chemical affinities between B-B, Co-Y, and B-Y pairs in $\text{Co}_{71.5}\text{Y}_{3.5}\text{B}_{25}$ alloy are the critical factor for enhancing GFA and magnetic softness (Fig. 1 (c)). In addition, we proposed a method to estimate the MAE of MGs, and the changes of H_c can be interpreted from the changes in MAE (Fig. 1 (b)). We expect that our findings will provide new insights into the mechanism of the microstructure-induced improvement of GFA and soft magnetic properties for Co-based MGs.

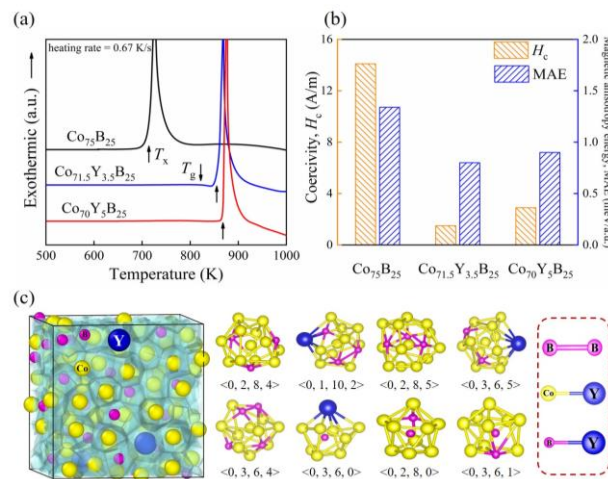


Fig. 1. (a) The differential scanning calorimetry curve, (b) coercivity and magnetic anisotropy energy, and (c) the typical Voronoi polyhedron of $\text{Co}_{75-x}\text{Y}_x\text{B}_{25}$ ($x = 0, 3.5, 5$) MGs.

References:

- 1) A. Inoue, B.L. Shen, H. Koshiba, H. Kato and A.R. Yavari, Nat. Mater. 2 (2003) 661-663.
- 2) A.H. Taghvaei, M. Stoica, K.G. Prashanth and J. Eckert, Acta Mater. 61 (2013) 6609-6621.
- 3) G.Q. Guo, L. Yang, S.Y. Wu, Q.S. Zeng, C.J. Sun and Y.G. Wang, Mater. Des. 103 (2016) 308-314.
- 4) H.K. Kim, J.P. Ahn, B.J. Lee, K.W. Park and J.C. Lee, Acta Mater. 157 (2018) 209-217.

Formation of a local structural order in the aluminum melt before crystallization

*V.B.Vorontsov.¹, V.K.Pershin²

1.Ural State University of Railway transport (USURT), Ykaterinburg, 620079, Russia, 2. Ural State University of Railway transport (USURT), Ykaterinburg, 620034, Russia, *metranpazh23-1@ya.ru *

Abstracts

Acoustic emission (AE) has been experimentally investigated with a decrease in the temperature of the aluminum melt in the temperature range of 860-660 °. A Fourier analysis of the amplitude-frequency spectrum of AE signals in the frequency range of 20 -200 kHz was carried out; periodically repeating signals with maximum intensity were established. It is assumed that the acoustic spectrum of signals is associated with structural rearrangements in the melt and reflects the transition from disorder to local order in liquid aluminum in the form of clusters. At the Table.1 presents the results of cluster modeling and compares the frequencies calculated theoretically with the frequencies determined experimentally. Below is a cluster model when the melt is cooled from a temperature of 860 °.

Tabl.1 The experimentally and theoretically calculated frequencies of cluster elements.

n	1	2	3	4	5	6	7
F							
kHz	127	63	42	32	25	21	18
теоретические							
F							
kHz	126	60	40	30	24	20	нет
экспериментальные							данных

Based on calculations frequency data, taken from the Table were used to build a cluster model.

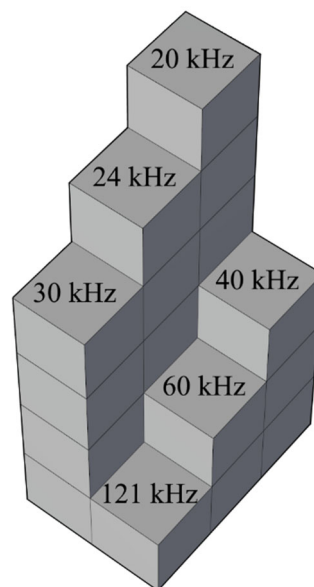


Fig.1 Model of an Al melt cluster during melt cooling from a temperature of 860°C. Based on the above, the concepts of the melt structure before crystallization as a partially ordered clusters discussed

Key words: Crystal structure, Melts, Gradient, Acoustic emission, Temperature.

Development of metal-metalloid high-entropy bulk metallic glasses with ultrahigh thermal stability and strength

*Yanhui Li¹, Wei Zhang¹

¹School of Materials Science and Engineering, Dalian University of Technology, Dalian 116024, China

*yhli@dlut.edu.cn

Keywords: High-entropy bulk metallic glass, Thermal stability, Crystallization behavior, Mechanical properties.

High-entropy alloys (HEAs) or called multi-principal component alloys have gained increasing attention in the field of advanced metallic materials over recent years due to their unique composition characteristic and excellent properties. The HEAs with a glassy structure, known as high-entropy bulk metallic glasses (HE-BMGs), have also been synthesized in some specific alloy systems, which provide an approach to design novel BMGs. We have successfully developed metal-metalloid type HE-BMGs in the alloy systems of Fe-Co-Ni-(B, Si, P, C) and Fe-Ni-Cr-Mo-(P, C, B), which exhibit larger supercooled liquid region, higher crystallization temperature (T_x), larger undercooling, and more sluggish crystallization process upon heating than the conventional metallic glasses in the same systems. In addition, the Fe-Co-Ni-(B, Si, P, C) and Fe-Ni-Cr-Mo-(P, C, B) HE-BMGs exhibit good soft magnetic properties and excellent corrosion resistance in acids and NaCl solutions, respectively. Recently, we added an appropriate amount of refractory metal (RM) into a FeCoNi(B, Si) alloy and synthesized new HE-BMGs with further enhanced glass-forming ability, thermal stability, and strength. The FeCoNiRM(B, Si) HE-BMGs possess high T_x and fracture strength up to 867 K and 4.2 GPa, respectively, which are superior among the reported HE-BMGs (Fig. 1).

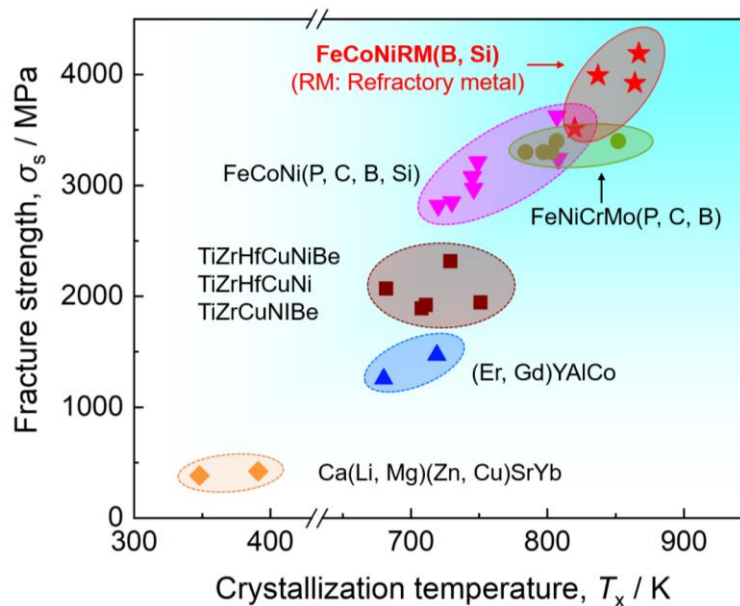


Fig. 1 Fracture strength versus crystallization temperature of FeCoNiRM(B, Si) and other typical HE-BMGs.

References:

- 1) T. Qi, Y. Li, A. Takeuchi, G. Xie, H. Miao, W. Zhang, *Intermetallics* 66, 8 (2015).
- 2) Y. Li, W. Zhang, T. Qi, *J. Alloys Compd.* 693, 25 (2017).
- 3) Y. Xu, Y. Li, Z. Zhu, W. Zhang, *J. Non-cryst. Solids* 487, 60 (2018).
- 4) Y. Li, S. Wang, X. Wang, M. Yin, W. Zhang, *J. Mater. Sci. Technol.* 43, 32 (2020).

Change of collective dynamics in supercooled glass-forming aluminium film

Dmitrii Fleita^{,1,2}, Genri Norman^{1,2,3}, Vasily Pisarev^{1,2,3}

¹HSE University, Moscow, 101000, Russia

²Joint Institute for High Temperatures of the Russian Academy of Sciences, Moscow, 125412, Russia

³Moscow Institute of Physics and Technology, Dolgoprudny, 41701, Russia

*fleyta.du@phystech.edu

Keywords: molecular dynamics, metastable states, spatio-temporal correlations, vitrification.

The thermodynamic functions of substance do not undergo any drastic changes in the point of phase transition, and despite its exceptional influence in some manner on the behavior of a substance, is not special for them [1]. Widely known, that any phase can exist, at least as metastable, and on the other side of the transition point; thermodynamic inequalities at this point are not violated within the relaxation time.

Preliminary analysis of metastable fluids [2] with use of the molecular dynamics simulations (MD) revealed features in the region of phase transitions for specific two-particle motion correlators [2, 3], and promising change in described collective dynamics of particles in various models of particle interactions was found.

In this particular work, the temporal behavior of motion correlators observed in deep supercooled state of aluminium film near glass-transition temperature [4, 5]. The analysis shows a change of dynamical structure (Fig.1a) till and during the relaxation processes of vitrification and gives vitrification temperature which consistent with volumetric (Fig.1b) and other analysis methods [6].

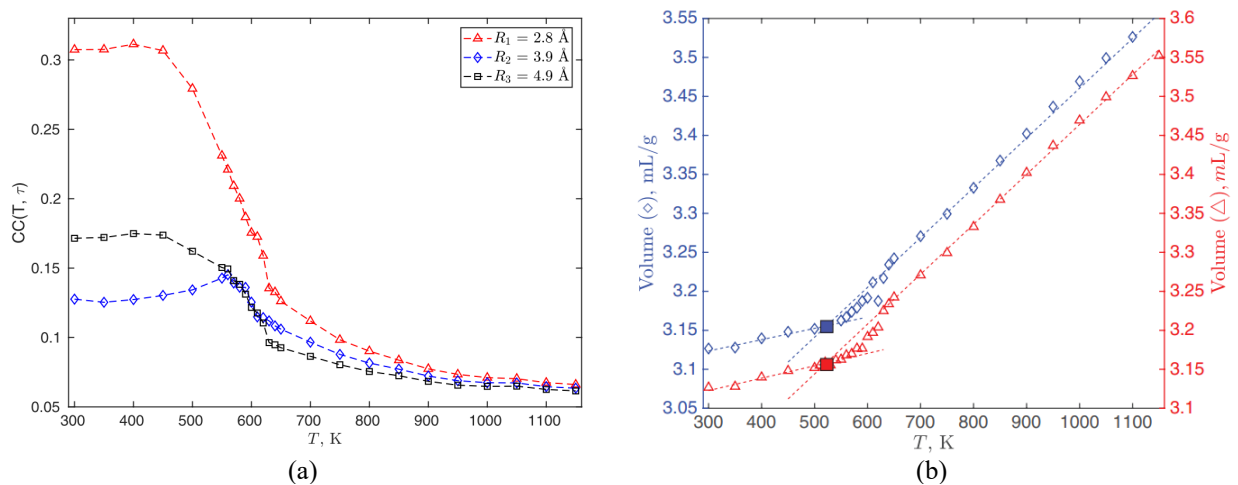


Figure 1. Temperature dependence of correlator $CC(T, \tau)$ for different diagnostic radius (left) and volume of film (right) for pure aluminium film after overcooling with rate in interval 10^{12} - 10^{14} Ks^{-1} . Both shows two transition temperatures 610 and 520 K, which detach different metastable states of supercooled liquid aluminium film.

This work was supported by the grant of the President of Russian Federation (project No. 17-79-20391). The authors acknowledge the JIHT RAS HPC and HSE University HPC Cluster "cHARISMa".

References:

- 1) L. Landau, E. Lifshitz, Statistical Physics (Course of Theoretical Physics Vol. 5) (Oxford: Butterworth-Heinemann) (1980).
- 2) D. Fleita, V. Pisarev and G. Norman, JETP Lett. **109**, p. 667 (2019)
- 3) V. Voloshin, G. Malenkov and Yu. Naberukhin, J. Struct. Chem. **54**, p. S233 (2013)
- 4) D. Fleita, V. Pisarev and G. Norman, J. Phys.: Conf. Ser. **1147**, p. 012015 (2019)
- 5) D. Fleita, G. Norman and V. Pisarev, J. Phys.: Condens. Matter **32**, p. 214009 (2020)
- 6) E. Kirova, G. Norman and V. Pisarev, Computational Materials Science **172**, p. 109367 (2020)

Atomic transport properties of $\text{Bi}_{1-x}\text{Zn}_x$ segregating alloys

Fysol Ibna Abbas^{1,2} and G. M. Bhuiyan^{1*}

¹Department of Theoretical Physics, University of Dhaka, Dhaka-1000, Bangladesh

²Department of electrical and electronic Engineering, City University, Dhaka-1216, Bangladesh

Abstract

Atomic transport properties namely the shear viscosity and diffusion coefficient for liquid $\text{Bi}_{1-x}\text{Zn}_x$ segregating alloys are theoretically investigated using the Rice-Allnatt theory. The interionic interaction is described by a widely used local pseudopotential. Temperature dependent behaviour of the mentioned transport properties is also investigated. The overall agreement of our theoretical results with the available experimental data is found to be good for the whole range of concentration. More interestingly, results clearly exhibit the segregating feature of bending of the viscosity profile near the critical concentration.

*gbhuiyan@du.ac.bd

Keywords: Segregating alloys, Rice-Allnatt theory, shear viscosity, diffusion coefficient.

High-Dimensional Neural Network Potentials for Simulations of Complex Systems

*[J. Behler](#)¹

¹Theoretische Chemie, Institut für Physikalische Chemie, Universität Göttingen, Göttingen, 37077, Germany

*joerg.behler@uni-goettingen.de

Keywords: Atomistic Simulations, Machine Learning Potentials, Molecular Dynamics

A lot of progress has been made in recent years in the development of machine learning potentials (MLPs) for atomistic simulations¹. While the first generation of MLPs relying on single feed-forward neural networks has been restricted to small molecules with only a few degrees of freedom, the second generation extended the applicability of MLPs to high-dimensional systems containing thousands of atoms by constructing the total energy as a sum of environment-dependent atomic energies. High-dimensional neural network potentials (HDNNP)² have been the first example of a second-generation MLP, and to date HDNNPs have been applied to many different types of systems. Long-range electrostatic interactions can be included in third-generation HDNNPs employing environment-dependent charges³, but only recently limitations related to the underlying locality approximation could be overcome by the introduction of fourth-generation HDNNPs⁴, which are able to describe non-local charge transfer and multiple charge states using a global charge equilibration step.

In this talk, the basic concepts of the different generations of HDNNPs will be briefly summarized, followed by a discussion of applications with a focus on solid-liquid interfaces. In particular, our recent work on the lithium intercalation compound $\text{Li}_x\text{Mn}_2\text{O}_4$, which is used as positive electrode material in lithium batteries, and its interface with water will be presented^{5,6}.

References:

- 1) J. Behler, *J. Chem. Phys.* 145, 170901 (2016).
- 2) J. Behler and M. Parrinello, *Phys. Rev. Lett.* 98, 146401 (2007).
- 3) N. Artrith, T. Morawietz, and J. Behler, *Phys. Rev. B* 83, 153101 (2011).
- 4) T. W. Ko, J. A. Finkler, S. Goedecker and J. Behler, *Nature Comm.* 12, 398 (2021).
- 5) M. Eckhoff, F. Schönewald, M. Risch, C. A. Volkert, P. E. Blöchl, and J. Behler, *Phys. Rev. B* 102, 164107 (2020).
- 6) M. Eckhoff and J. Behler, *J. Chem. Phys.* 155, 244703 (2021).

Structural inheritance and machine learning for materials design: from study of liquid to prediction crystals

Nikolay Chtchelkatchev^{1}, Roman Ryltsev^{2,1}

¹ Vereshchagin Institute for High Pressure Physics, RAS, 108840 Moscow, Troitsk, Russia

² Institute of Metallurgy, Ural Branch RAS, 620016 Ekaterinburg, Russia

*chtchelkatchev@hppi.troitsk.ru

Keywords: Neural networks, Structural inheritance, Ab initio simulation, Machine learning, Genetic algorithms, Compositional transferability.

The use of machine learning is a new paradigm in modern computational materials science [1-2]. One of the most promising and widely accepted techniques is using ab initio reference data on energies, forces, and stress tensors to develop machine learning interatomic potentials (MLIPs) with a flexible functional form which can effectively fit the potential energy surface of the particle system. This approach allows solving the principal problems of ab initio simulations: the effects of “small size” and “short time”, associated with difficulties in simulating sufficiently large supercells at long enough computational times. MLIPs can provide nearly ab initio accuracy with orders of magnitude less computational cost for systems composed of up to millions of particles.

One of the most challenging applications of MLIPs is design of new functional materials on top of classical molecular dynamics simulations. It requires developing accurate MLIPs, universal for ordered (crystal) and disordered systems (melts, supercooled liquids, glasses) in wide temperature and concentration ranges. This is a difficult task for materials design when possible ordered structures are not known.

We have found that MLIPs for multicomponent metallic alloys trained only on disordered configurations can accurately describe crystal structures even at low temperatures. Training MLIP on liquid configurations is straightforward: using certain algorithm we generate disordered configurations and find energy, interatomic forces and virials using DFT. Disordered systems require rather large supercells (we use 512 particle sells) that include a number of possible local structural configurations. Sampling enough the configurational space one can build representative training dataset.

We address MLIPs for multicomponent metallic melts taking the ternary Al-Cu-Ni ones as a convenient example [3]. It is shown that MLIP trained on liquid configurations demonstrates good compositional transferability, which extends far beyond compositional fluctuations in the training configurations. Using so trained MLIP we can describe not only liquid, but find with ab initio accuracy all stable and low-lying metastable crystal configurations of AlCuNi using a laptop and USPEX genetic algorithm. Fig.1 shows that MLIP trained on liquid quite well reproduce DFT equation of states for a crystal. The results obtained open up prospects for design multicomponent metallic alloys with MLIPs.

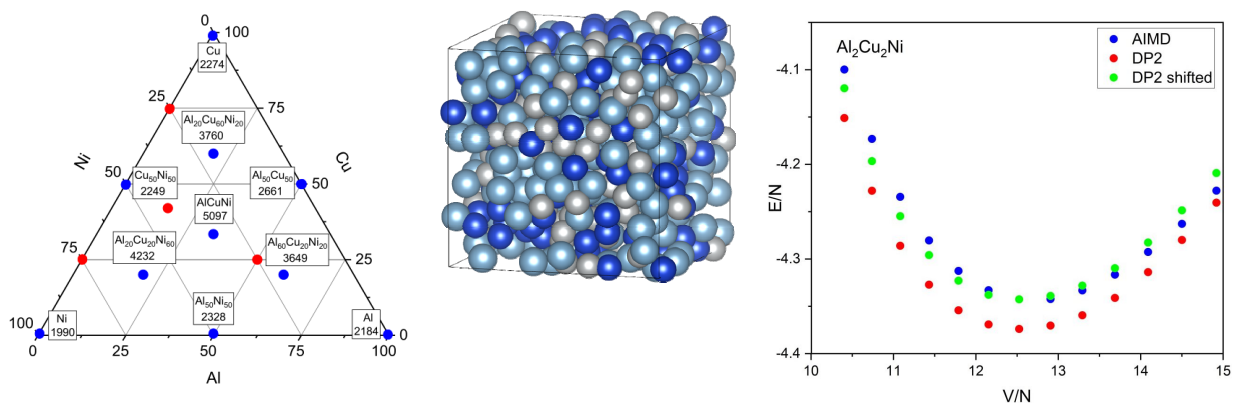


Figure 1. (Left) Ternary plot for Al-Cu-Ni system with the compositions included in the training dataset. (Middle) Snapshot of AlCuNi melt with 512 particles in the cell. (Right) Energy-volume relation obtained for Al₂Cu₂Ni crystal using MLIP (Dp2) trained on liquid configurations and AIMD DFT in VASP.

Support of Russian Science Foundation (#18-12-00438) is acknowledged.

References (Example: non-mandatory, 10 point):

[1] J. Behler and M. Parrinello, Phys. Rev. Lett. 98, 146401 (2007).

[2] L. Zhang, D.-Y. Lin, H. Wang, R. Car, and W. E, Phys. Rev. Materials 3, 023804 (2019).

[3] R.E. Ryltsev and N.M. Chtchelkatchev, J. Mol. Liq. 349, 118181 (2022).

Finite-temperature modeling of materials with first-principles accuracy

Michele Ceriotti

Institute of Materials, École Polytechnique Fédérale de Lausanne, Lausanne, Switzerland
michele.ceriotti@epfl.ch

When modeling materials and molecules at the atomic scale, achieving a realistic level of complexity and making quantitative predictions are usually conflicting goals. Data-driven techniques have made great strides towards enabling simulations of materials in realistic conditions with uncompromising accuracy. In this talk I will summarize the core concepts that have driven the extraordinarily fast progress of the field, discuss some of the most promising modeling techniques that combine physics-inspired and data-driven paradigms, indicate the most pressing open challenges, and present several applications to semiconductors and to metallic systems.

References

- 1) N. Lopanitsyna, C. Ben Mahmoud, and M. Ceriotti, *Phys. Rev. Materials* 5(4), 043802 (2021).
- 2) G. Imbalzano and M. Ceriotti, *Phys. Rev. Materials* 5(6), 063804 (2021).
- 3) F. Musil, A. Grisafi, A. P. Bartók, C. Ortner, G. Csányi, and M. Ceriotti, "Physics-Inspired Structural Representations for Molecules and Materials," *Chem. Rev.* 121(16), 9759–9815 (2021).

Composition Dependence of Melting Temperature of Rb-Na Alloy Using First-principles-based Thermodynamic Integration

*A. Irie, A. Koura, K. Shimamura, F. Shimojo[#]

Department of Physics of Kumamoto University, Kumamoto, 860-8555, Japan

*brauner.nacht@gmail.com

Keywords: Phase transition, Alkali metals, Thermodynamic integration, Ab initio simulation, Machine learning.

The melting point of alkali metal alloys depends non-linearly on the composition, and shows a minimum at a certain composition which is different for each combination of alkali metals [1]. For instance, it has been experimentally reported that $\text{Rb}_x\text{Na}_{1-x}$ alloy has the lowest melting point around $x = 0.8$ [2]. Due to these remarkable characteristics, alkali metal alloys have drawn attention for the application as high-performance coolants [3]. The purpose of this study is to theoretically clarify the microscopic origin of the minimum melting temperature, which is lower than those of simple substances. We have investigated the concentration dependence of melting points by using thermodynamic integration (TI) based on the first-principles molecular dynamics (FPMD) simulations. A non-empirical simulation model with high precision can be achieved using FPMD, but it is computationally demanding, making it difficult to apply FPMD to TI. Machine learning interatomic potentials (MLIP) obtained by training FPMD data with artificial neural networks have enough accuracy and low computational cost, and, therefore, contribute to overcoming this cost problem.

We estimated the melting temperatures of $\text{Rb}_x\text{Na}_{1-x}$ at $x = 0.0, 0.5, 0.8$ and 1.0 . The system consists of 128 atoms in total. Figure 1 shows the composition dependence of melting points of $\text{Rb}_x\text{Na}_{1-x}$ by numerical simulation and experiment [2] (black crosses). The red circles represent the results obtained by TI with MLIP based on FPMD with Γ point for Brillouin-zone sampling. The calculated melting points of $\text{Rb}_{0.5}\text{Na}_{0.5}$ are much lower than the experimental values. To take system-size effects into account, we performed FPMD simulations with $4k$ -point sampling, which corresponds to an electronic state calculation with an eight times larger system than the Γ point. The green squares represent the results of $4k$ -point sampling, and show that the melting temperatures of Na and $\text{Rb}_{0.5}\text{Na}_{0.5}$ are 20 K [4] and 65 K higher than those of the Γ point, respectively. We consider that the size effect on the melting temperature for the mixture is larger than pure Na because $\text{Rb}_{0.5}\text{Na}_{0.5}$ consists of only 64 atoms of each atomic species. Figure 2 shows Helmholtz free energies of the solid (black squares) and liquid (blue circles) phases of (a) Na and (b) $\text{Rb}_{0.5}\text{Na}_{0.5}$ as a function of the number of sampling k points. In pure Na, both the Helmholtz free energies of the solid and liquid phases decrease with increasing the number of k points from 1 to 4. In contrast, the Helmholtz free energy of the liquid phase of $\text{Rb}_{0.5}\text{Na}_{0.5}$ is almost independent of the number of sampling k points, while that of the solid phase has the same behavior as in pure Na. The k -point dependence of the Helmholtz free energy is mostly due to that of potential energy U , and the entropy S is nearly unrelated to the number of k points. It is quite characteristic that the potential energy of $\text{Rb}_{0.5}\text{Na}_{0.5}$ in the liquid phase remains unchanged when the number of k points changes.

In the presentation, we will discuss the dependence of physical quantities on the number of sampling k points in detail.

References:

- [1] X. Ren, *et al.*, *Calphad* **35**, 446 (2011).
- [2] J. R. Goates, *et al.*, *Trans. Faraday Soc.* **66**, 25 (1970).
- [3] Y. Gao, *et al.*, *Front. Energy* **8**, 49 (2014).
- [4] A. Irie, *et al.*, *J. Phys. Soc. Jpn.* **90**, 094603 (2021).

[#] Present address: Department of Physics, Kumamoto University 2-39-1 Kurokami, Chuo-ku, Kumamoto 860-8555, Japan.

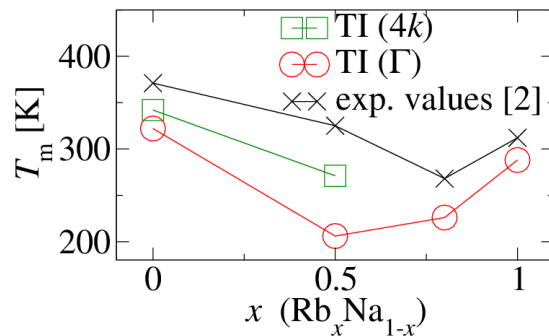


Fig. 1. Composition dependence of melting temperatures of $\text{Rb}_x\text{Na}_{1-x}$. The green squares and the red circles represent melting points sampling $4k$ and Γ points for Brillouin-zone integration, respectively. The black crosses correspond to experimental values [2].

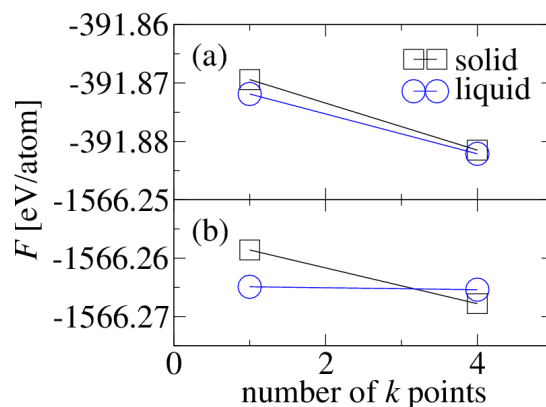


Fig. 2. The number dependence of k point sampling of (a) Na and (b) $\text{Rb}_{0.5}\text{Na}_{0.5}$. The black squares and the blue circles correspond to solid and liquid phase, respectively.

Response of the Free Energy Landscape to Temperature Modulation and Aging

*Takashi Odagaki^{1,2}

¹ Kyushu University, Fukuoka, 819-0395, Japan, ² Research Institute for Science Education, Inc., Kyoto, 603-8346, Japan

*t.odagaki@kb4.so-net.ne.jp

Keywords: Free energy landscape, Aging, Temperature modulation, Non-equilibrium system

The free-energy-landscape (FEL) approach is a theoretical frame work for non-equilibrium systems [1]. It provides unified understanding of dynamic and thermodynamic properties of super-cooled liquids including cooling-rate dependence of specific heat and time-temperature-transformation diagram, and it gives a solid foundation of the trapping diffusion model of glass transition [2] and the Adam-Gibbs relation [3,4]. The FEL is defined in the configurational space by the density function produced by fast motion of atoms and therefore depends on temperature in contrast to the potential energy landscape. Expressing the response of the FEL to a temperature modulation by relaxation of the FEL, I investigate the waiting time dependence of aging in various systems

Many non-equilibrium systems show a delayed response to a sudden perturbation and the delayed response is represented by a relaxation function. I first classify the aging into two types: Type I when the apparent relaxation time is always an increasing function of the waiting time t_w and type II when the apparent relaxation time can increase or decrease as a function of the waiting time t_w . I show that (1) the relaxation of the FEL manifests itself as type II aging and (2) the relaxation time of the FEL can be deduced from the waiting time dependence of the apparent relaxation time.

As examples, I first investigate the self-part of the intermediate scattering function (FSKT) for a random walk model and show that the delayed response of the FEL gives rise to type II aging. Figure 1 shows the time dependence of FSKT for various values of t_w when the temperature is increased ($T \uparrow$) or decreased ($T \downarrow$) suddenly at time $t = 0$. The relaxation time of FSKT is a decreasing function of t_w for T-up protocol and an increasing function of t_w for T-down protocol which is not seen in the KWW relaxation.

Next, I investigate the relaxation function and the susceptibility of a dielectric relaxation [5,6] and the massless Landau model under sudden modification of temperature. On the basis of the two-time relaxation function and the two-time instantaneous decay constant, I show that the aging in these systems belongs to type II aging when the free energy landscape responds to the temperature change with a delay [7].

References

- [1] T. Odagaki, J. Phys. Soc. Jpn. **86**, 082001 (2017).
- [2] T. Odagaki and Y. Hiwatari, Phys. Rev. A **41**, 929 (1990).
- [3] G. Adam and J. H. Gibbs, J. Chem. Phys. **43**, 139 (1965).
- [4] T. Odagaki, J. Phys. Soc. Jpn. to appear (2022).
- [5] K. Fukao and D. Tahara, Phys. Rev. E **80**, 051802 (2009).
- [6] T. Hecksher, N. B. Olsen, K. Niss, and J. C. Dyre, J. Chem. Phys. **133**, 174514 (2010).
- [7] T. Odagaki, Y. Saruyama and T. Ishida, J. Non-Cryst. Solids **558**, 119448 (2021).

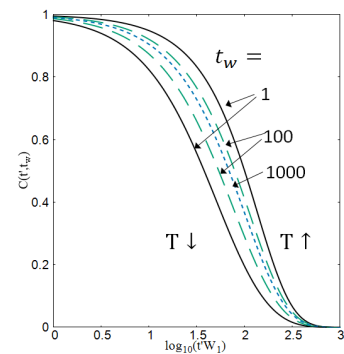


Fig. 1 Time dependence of FSKT for different waiting times when the temperature is increased or decreased suddenly at $t=0$.

New understanding of liquid thermodynamics, viscosity and its lower bounds

Kostya Trachenko

School of Physical and Chemical Sciences, Queen Mary University of London, United Kingdom
k.trachenko@qmul.ac.uk

Understanding most basic thermodynamic properties of the liquid state such as energy and heat capacity turned out to be a long-standing problem in physics [1]. Landau&Lifshitz textbook states that no general formulas can be derived for liquid thermodynamic functions because the interactions are both strong and system-specific. Phrased differently, liquids have no small parameter. Recent experimental and theoretical results open a new way to understand liquid thermodynamics on the basis of collective modes (phonons) as is done in the solid state theory. There are important differences between phonons in solids and liquids, and we have recently started to understand and quantify this difference. I will review collective modes in liquids including high-frequency solid-like transverse modes and will discuss how a gap in the reciprocal space emerges and develops in their spectrum [2,3]. This reduces the number of phonons with temperature, consistent with the experimental decrease of constant-volume specific heat with temperature [1]. I will discuss the implication of the above theory for fundamental understanding of liquids. I will also mention how this picture can be extended above the critical point where the recently proposed Frenkel line on the phase diagram separates liquid-like and gas-like states of supercritical dynamics [1,4]. I will subsequently describe how this leads to the theory of minimal quantum viscosity in terms of fundamental physical constants and will compare this minimum to the holographic bound [5]. The minimum of thermal diffusivity can be equally written as the same combination of fundamental constants, in agreement with experiments. I also mention an upper bound on the speed of sound in terms of fundamental constants following from a similar approach [6]. Finally, I will note that the kinematic viscosity of the quark-gluon plasma is surprisingly close to the kinematic viscosity of liquids at their minimum [7].

References:

- [1] K Trachenko and V Brazhkin, Collective modes and thermodynamics of the liquid state, Reports on Progress in Physics 79, 016502 (2016)
- [2] C Yang, M T Dove, V Brazhkin and K Trachenko, Physical Review Letters 118, 215502 (2017)
- [3] M Baggioli, M Vasin, V Brazhkin and K Trachenko, Physics Reports 865, 1 (2020)
- [4] C Cockrell, V Brazhkin and K Trachenko, Physics Reports 941, 1 (2021)
- [5] K Trachenko and V Brazhkin, Minimal quantum viscosity from fundamental physical constants, Science Adv. 6, eaba3747 (2020)
- [6] K Trachenko, B Monserrat, C Pickard and V Brazhkin, Science Adv. 6, eabc8662 (2020)
- [7] K Trachenko, V Brazhkin and M Baggioli, Similarity between the kinematic viscosity of quark-gluon plasma and liquids at the viscosity minimum, SciPost Phys 10, 118 (2021)

Thermodynamic and Structural Studies on Glass Transitions of Molecular Glasses

*O. Yamamuro¹, Y. Mizuno¹, Y. Zhao¹, H. Akiba¹, S. Tatsumi², S. Kohara³, K. Ohara⁴, Y. Kono⁵, N. Kondo⁵, M. G. Tucker⁶, M. T. McDonnell⁶

¹Institute for Solid State Physics, University of Tokyo, Kashiwa, Chiba 277-8581, Japan, ²Faculty of Material Science and Engineering, Kyoto Institute of Technology, Kyoto 606-8585, Japan, ³Research Center for Advanced Measurement and Characterization, National Institute for Materials Science (NIMS), Ibaraki 305-0047, Japan, ⁴Diffraction and Scattering Division, Japan Synchrotron Radiation Research Institute (JASRI), Hyogo 679-5198, Japan, ⁵Geodynamic Research Center, Ehime University, Matsuyama 790-8577, Japan, ⁶Spallation Neutron Source, Oak Ridge National Laboratory, Oak Ridge, TN 37831, USA

*yamamuro@issp.u-tokyo.ac.jp

Keywords: Glass, Liquid, Heat capacity, X-ray diffraction, Neutron diffraction, RMC modeling

Glass transition is one of the most important unsolved subjects in condensed matter physics. It is said that the history of the glass transition study started when Giauque found a heat capacity jump of glycerol in 1923 [1]. As shown in this example, thermodynamic experiments, e.g., heat capacity, thermal expansivity, etc., are the most direct approach to investigate the glass transition. For the last 20 years, we have measured the heat capacities of many simple molecular liquids to investigate the structures of liquids and glasses through the configurational entropy based on the Adam-Gibbs theory [2]. For very simple molecules, which crystallize readily on cooling, we used vapor deposition (VD) method at low temperature ($T < 10$ K) whose speed is estimated to be more than 10^7 Ks⁻¹. The VD procedure was performed by using an adiabatic calorimeter with which heat capacity was measured in situ. We found that the cooperative rearranging regions (CRRs) of liquids increase on cooling, especially below their melting temperatures, and reach 4-7 molecules at the glass transitions for many molecules including carbon tetrachloride (CCl₄), carbon disulphide (CS₂), propane (CH₃CH₂CH₃), and propene (CH₃CH=CH₂), which cannot be vitrified by usual liquid quenching [3,4].

Recently we are studying the short- and intermediate-range structure of simple molecular liquids and glasses by using X-ray and neutron diffraction techniques [5-7]. The simplicity of molecular structure is more important in diffraction works than in thermodynamic ones since the structure factor $S(Q)$, which is Fourier transformation of the pair distribution function, cannot provide definite information on intermolecular correlations for complicated molecules with many intra- and intermolecular atomic pairs with close atomic distances. Hence, we have constructed cryostats for both an in house X-ray diffractometer [5] and a high-energy X-ray diffractometer at BL04B2, SPring-8 [6]. By using these instruments, we have succeeded in forming the glasses of carbon dioxide, carbon disulphide, carbon tetrachloride, propane, propene, and toluene, and measured their X-ray diffraction data in a wide Q range of 0.2 to 25 Å⁻¹. Both CO₂ and CS₂ are rigid linear molecules while propane and propene are dog-leg molecules and toluene is a planar molecule. The diffraction data of their liquid states were also measured in a temperature range above their crystallization temperatures. Fig. 1 shows the reduced pair distribution functions of liquid and glassy CS₂ in a wide temperature range of 3-300 K. These data clearly indicate that the intermolecular correlation becomes gradually larger on cooling and drastically sharpened at a glassy state. On the basis of these data, we have performed molecular dynamics (MD) and reverse Monte Carlo (RMC) analyses. The results are quite consistent with the CRRs obtained by the thermodynamic works. In the presentation, we are going to show very recent diffraction data under high pressure up to 5 GPa.

References

- 1) G. E. Gibson and W. F. Giauque, *J. Am. Chem. Soc.* 45, 93 (1923).
- 2) G. Adam and J. H. Gibbs, *J. Chem. Phys.* 43, 139 (1965).
- 3) O. Yamamuro, et al., *J. Phys. Chem. B*, 102, 1605 (1998).
- 4) S. Tatsumi, S. Aso, O. Yamamuro, *Phys. Rev. Lett.* 109, 045701 (2012).
- 5) Y. Mizuno, M. Kofu, O. Yamamuro, *J. Phys. Soc. Jpn.*, 85, 124602 (2016).
- 6) Y. Mizuno, et al., *J. Chem. Phys.*, 156, 034503 (2022).
- 7) O. Yamamuro, et al, *Europhys. Lett.*, 63, 368 (2003).

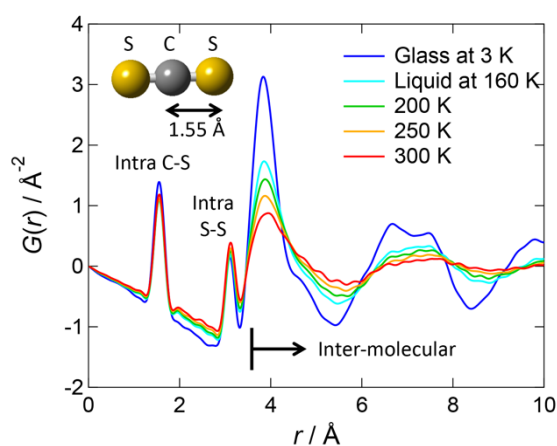


Fig. 1. Reduced pair distribution functions of CS₂

Poster Presentations

Abstracts

Determination of cooperatively rearranging regions in binary glass former

*Tomoko Mizuguchi¹, Takashi Odagaki²

¹ Faculty of Materials Science and Engineering, Kyoto Institute of Technology, Kyoto, 606-8585, Japan,

² Research Institute for Science Education Inc., Kyoto, 603-8346, Japan

* mizuguti@kit.ac.jp

Keywords: Cooperative rearranging regions, Configurational entropy, Molecular dynamics simulations, Glass, Kob-Andersen model

The dynamical slowing down in glassy system is attributed to the cooperative motion of particles. The Adam-Gibbs scenario is one of the theories focusing on the cooperative motion and can explain the divergence of viscosity at finite temperatures of glassy materials in a phenomenological way [1,2]. The central idea of this theory is to relate cooperatively rearranging regions (CRR) to configurational entropy. The CRR is defined as the minimum size of a space in which atoms can relax. The size of CRR has been determined in several ways, but distributed depending on experiments [3]. In this study, we carried out molecular dynamics (MD) simulations to determine the temperature dependence of CRR size and discuss the relationship between the CRR and configurational entropy.

We used Kob-Andersen Lennard-Jones (KALJ) model which has been widely used as a simple glass former of a binary alloy [4]. All simulations were performed using LAMMPS with a timestep of 0.005 in LJ units. The isothermal-isochoric (NVT) conditions at a density of 1.2 were realized using the Nose-Hoover thermostat. To determine the size of CRRs, we set up a space of spheres of various radii and fixed the atoms outside the spheres. We changed the radius of sphere and determined the minimum size of sphere in which atoms cannot relax in a sufficient time. Structural relaxation of atoms was observed by analyzing the bond break correlation [5]. The method measures the bonds between particles at $t=0$ can survive after time or not. Fig.1 shows the number of survival bonds at various radii of spheres at $T=2.0$ (normal liquid). As the radius decreases, the bonds are hard to break. Fig.2 shows the temperature dependence of the number of survival bonds with the radius $R=3.0$. At the high temperature of $T=2.0$, the number of bonds decreases rapidly. The rate of decrease becomes slow at $T=1.0$, but the bonds still breaks with time. At $T=0.5$, near the glass transition point, the bonds at $t=0$ hardly break after 500,000 timesteps, thus the number of bonds keeps the initial value. Namely, the atoms in the spherical area does not relax. We will discuss the size of CRRs in relation to the configurational entropy.

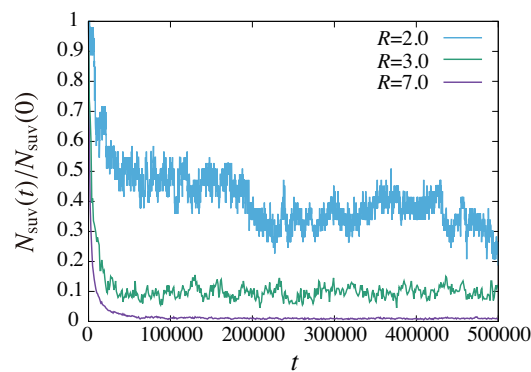


Fig. 1. The number of survival bonds between particles versus time at $T=2.0$ (normal liquid) as the radius of a mobile space R is changed.

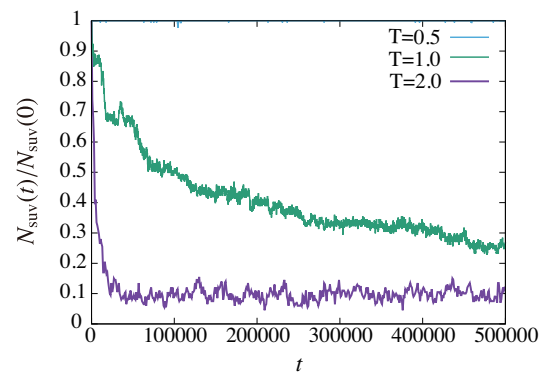


Fig. 2. The number of survival bonds between particles versus time at the radius of a mobile space $R=3.0$ as the temperature is changed.

References:

- 1) G. Adam and J. H. Gibbs, J. Chem. Phys. 43, 139 (1965).
- 2) T. Odagaki, J. Phys. Soc. Jpn. 91, 043602 (2022).
- 3) T. Kanaya, I. Tsukushi, K. Kaji, J. Bartos, and J. Kristiak, J. Phys. IV France 10, Pr7-317 (2000).
- 4) W. Kob and H. C. Andersen, Phys. Rev. E 51, 4626 (1995).
- 5) R. Yamamoto and A. Onuki, J. Phys. Soc. Jpn. 66, 2545 (1997).

Novel Experimental Scheme for Microscopic Study of Johari-Goldstein Process

Makina Saito^{1}, Yoshitaka Yoda², Makoto Seto³,

¹Tohoku University, Sendai, 980-8578, Japan, ²Japan Synchrotron Radiation Research Institute, Sayo, 679-5198, Japan, ³Kyoto University, Kumatori, 590-0494, Japan

*makina.saito.d6@tohoku.ac.jp

Keywords: Synchrotron radiation, Quasi-elastic scattering, Johari-Goldstein process, Glass transition

The Johari-Goldstein-(JG) process is widely observed in a variety of glass-forming systems and recognized as an intrinsic process in deeply supercooled and glassy states. In a deeply supercooled region, the JG process starts to be observed as its time scale branches from the time scale of microscopic diffusion process (α process) by cooling. The JG process appears on the high-frequency (shorter time scale) side compared with the α process. By further cooling, the temperature dependence of the JG relaxation time follows the Arrhenius law in supercooled state and even in glass state, where the α process almost freezes. Therefore, the JG process is often one of the main origins of the structural relaxation in glass and known to be the microscopic origin of some glass properties related to the structural relaxation such as stability of glass state and resistance for impact. Therefore, understanding the mechanism of the JG process is highly useful to effectively improve these glass properties.

Some experimental techniques such as dielectric relaxation spectroscopy and NMR, which are often used to study the JG process, have poor information on the spatial scale of the JG process. Here, inelastic and quasi-elastic scattering experiments allow us to determine the spatial scale of dynamics. In Fig. 1(A), we show the typical time and spatial scale of the α process and the JG process. In Fig. 1(B), time and spatial scales covered by some established inelastic and quasi-elastic scattering techniques such as inelastic X-ray scattering (IXS), quasi-elastic neutron scattering (QENS), neutron spin echo (NSE) techniques, are shown. As shown in the figures, the JG process is difficult to be directly observed by the conventional techniques. In addition to the experimental difficulty, the JG process is quite difficult to be observed by MD simulation because of its relatively slow time scale. Therefore, the microscopic picture of the JG process is largely uncertain.

Quasi-elastic gamma-ray scattering spectroscopy (QEGS) using multi-line Mössbauer time-domain interferometry (TDI) based on synchrotron radiation has been recently developed to the application level in SPring-8.¹⁾ Using this technique, microscopic motions can be observed by measuring intermediate scattering function in appropriate momentum-transfer (q) ranges corresponding to angstrom scales and in the time scales between nanosecond to sub-microsecond.^{1,2)} As shown in Fig. 1(A) and 1(B), TDI-based QEGS is very suitable for direct observation of the JG process because the method can access to the atomic/molecular scale dynamics in the time scale of 100 nanosecond, where the JG processes dominate the relaxations.

The JG process has not been observed in small molecular glass-forming systems by the conventional inelastic and quasi-elastic scattering techniques. Previously, we succeeded to observe the JG process in small molecules for *o*-terphenyl by using TDI-based QEGS.³⁾ In addition, we found the anomalous q dependence of the relaxation time of the intermediate scattering function whose relaxation is caused by the JG process.³⁾ TDI-based QEGS was also applied to polymeric glass former polybutadiene and the JG process was microscopically observed in polybutadiene.⁴⁾ Very recently, the JG process was revealed in glycerol, where the JG process has not been clearly observed by any methods, by using TDI-based QEGS.⁵⁾ These results suggest that the JG process exists in variety of glass forming systems and TDI-based QEGS is ideal tool to investigate the JG process.

We introduce summary of the studies on the JG process and recent upgrade of the TDI-QEGS experimental system at BL35XU. In addition, we discuss the new experimental scheme to directly reveal the microscopic behaviour of the JG process based on the experimental data such as the temperature and q dependences of the relaxation time obtained by using TDI-QEGS.

References:

- 1) M. Saito, R. Masuda, Y. Yoda, M. Seto, Sci. Rep. 7, 12558 (2017).
- 2) A. Q. R. Baron, H. Franz, A. Meyer, R. Ruffer, A. I. Chumakov, E. Burkel, W. Petry, Phys. Rev. Lett. 79, 2823 (1997).
- 3) M. Saito, S. Kitao, Y. Kobayashi, M. Kurokuzu, Y. Yoda, M. Seto, Phys. Rev. Lett. 109, 115705 (2012).
- 4) T. Kanaya, R. Inoue, M. Saito, M. Seto, Y. Yoda, J. Chem. Phys. 140, 144906 (2014).
- 5) M. Saito, M. Kurokuzu, Y. Yoda, and Makoto M. Seto, Phys. Rev. E 105, L012605 (2022).

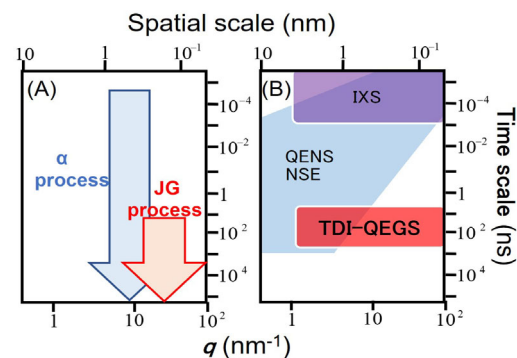


Fig. 1. (A) typical time and spatial scale of the diffusion process (α process) and the JG process. (B) time and spatial scales covered by some experimental techniques.

Configurational entropy of an isotropic monatomic glass

A. Ueno¹ and *T. Mizuguchi²

¹Graduate School of Science and Technology, Kyoto Institute of Technology, Kyoto, 606-8585, Japan

²Faculty of Materials Science and Engineering, Kyoto Institute of Technology, Kyoto, 606-8585, Japan

*mizuguti@kit.ac.jp

Keywords: Glass transition, Configurational entropy, Reversible scaling method, Adiabatic switching process, Lennard-Jones-Gauss potential

The glass transition is one of the major unsolved problems in condensed matter physics. A theoretical framework that can explain the glass transition in a unified manner does not yet exist, and various theories are currently being proposed. One of the most promising candidates is the theory based on the configurational entropy, which is the entropy corresponding to the number of atomic configurations. Various methods have been proposed to estimate the configurational entropy in computer simulations. In general, it is not easy to calculate only the configurational entropy, since the total entropy is composed of multiple contributions including configurational, mixing, harmonic vibrational, and non-harmonic vibrational components. Therefore, the relationship between the configurational entropy and the structure is still a central issue for the study of glass transition. To discuss this relationship quantitatively, we calculate the configurational entropy in simulations using a monatomic glass-forming model where the atoms interact each other isotropically.

We performed molecular dynamics simulations using Lennard-Jones-Gauss (LJG) potential [1] (Fig. 1). The general form of the effective two-body potential of alloys is an oscillatory potential consisting of a short-range repulsion term and a damping oscillation (Friedel oscillation) term. The LJG potential can be regarded as the cutoff of such an oscillatory potential at the second maximum [2]. First, we quenched from the melt at $T=2.5$ to $T=0.1$ and obtained a glassy state. Fig. 2 shows the temperature dependence of the potential energy during heating from the glassy state at $T=0.1$. We obtained the configurational entropy by calculating the free energy over a wide range of temperatures. The configurational entropy is defined as the total entropy minus the vibrational entropy. The free energy of the glass at any temperature was obtained by the reversible scaling (RS) method [3] using the glass at a temperature $T=0.1$ as the reference system, and the derivative of this free energy with respect to temperature is regarded as the vibrational entropy. The free energy of the liquid at any temperature was obtained by the RS method with the liquid at $T=2.5$ as the reference system, and the derivative of this free energy with respect to temperature is considered as the total entropy. The free energies at $T=0.1$ (glass) and $T=2.5$ (liquid), which are the references in the RS method, can be obtained by adiabatic switching process [4] using the Einstein crystal and the Uhlenbeck-Ford model, respectively.

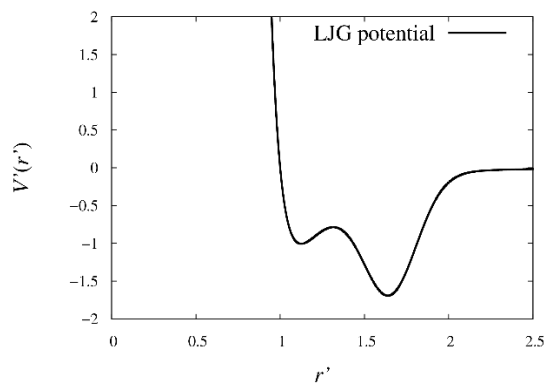


Fig. 1. The shape of LJG potential. All quantities are dimensionless in LJ units.

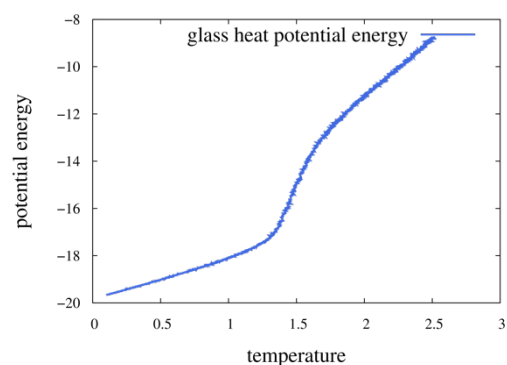


Fig. 2. Temperature Dependence of potential energy that was obtained by heating at rate $2 \times 10^{-6} \text{ step}^{-1}$ from $T=0.1$ to 2.5.

References:

- 1) M. Engel, H. R. Trebin, Phys. Rev. Let. 98(22), 225505 (2007).
- 2) V. Van. Hoang, T. Odagaki, Physica B Condens. Matter 403(21-22), 3910-3915 (2008)
- 3) M. de Koning, A. Antonelli, Phys. Rev. B 55(2), 735 (1997).
- 4) M.de Koning, A. Antonelli, S. Yip, Phys. Rev. Let. 83(20), 3973 (1999).

Anomaly of Linear Thermal Expansion Coefficient induced by rejuvenation treatment

*Tomoya OSHIKIRI¹, Masato OHNUMA¹, Motoki OHTA², Rui YAMADA³, Junji SAIDA⁴

¹Hokkaido University, Sapporo, 060-8628, Japan, ²Shimane University, NEXTA, Matsue, 690-8504, Japan,

³Tohoku University, IMR, Sendai, 980-8577, Japan, ⁴Tohoku University, FRIS, Sendai, 980-8578, Japan,

* ohnuma.masato@eng.hokudai.ac.jp

Keywords: Rejuvenation, Free Volume, Localized flow unit

Recently, we have shown that linear thermal expansion measurements using Thermo-Mechanical Analysis (TMA) can detect small length change due to the release of quenched-in strain even in the amorphous ribbons. Analysing anomaly of Linear Thermal Expansion Coefficient (LTEC) can give us the relationship between the mechanism of quenched-in strain and localized flow units¹⁾. Because LTEC is also sensitive to the volume change due to release of free volume, we applied TMA measurements before and after rejuvenation treatments in as-quenched and pre-treated Fe-Si-B amorphous ribbons. Sample size for TMA measurements is 15mm x 5mm x 0.02mm. As the rejuvenation treatments, samples are dipped into liquid nitrogen for 10 seconds and following by dipping into warm water for 10 seconds. These process were repeated 20 times for the one set of the rejuvenation treatment. Figure 1 shows the temperature dependence of LTEC with and without rejuvenation process. One set of LTEC measurement consists of four heating processes. The first one was the heating process with the heating rate of 20 K/min up to 300°C which is shown as black curves in the Fig.1. Then, the sample was cooled down to 80°C and again heated to 400°C as the second heating process which is shown by red curves. The difference between black and red is caused by the release of free volume in the temperature range below 300°C. Then the sample was cooled down again to 80°C and then heated to 550°C. Since the inflection point due to the invar effect of this alloy appears at 410°C, it is difficult to discuss the free volume release above this temperature. However, free volume release from 300 to 400°C appears as the difference between green and red curves. More than three times measurements have been performed to suppress the artifacts mainly due to vibration and slipping. Comparing the LTEC behavior between the ribbons, clear enhancement of the free volume release in the sample with rejuvenation treatments appear as shown by the circles in Fig.1. The effects of pre-treatment including annealing for releasing quenched-in strain or cold rolling will also be discussed in this presentation.

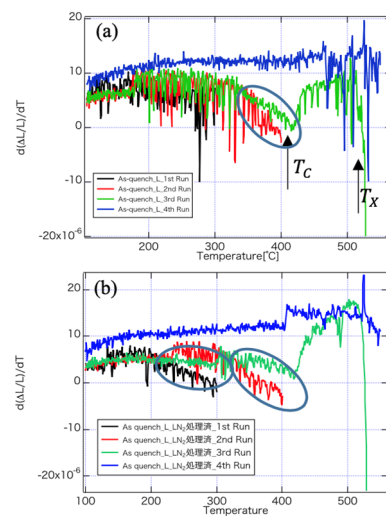


Fig.1 LTEC curves of Fe-Si-B as-quenched amorphous ribbons measured along the ribbon direction (a) before and (b) after the rejuvenation treatment. LTEC are obtained from the linear thermal expansion rate measured by TMA with the heating rate of 20 K/min. The color of the curves represents the heating process; black (1st heating up to 300°C, red: 2nd one up to 400°C, green 3rd one up to 550°C. Those are the curves for amorphous state. Since the crystallization occurs by the 3rd heating, the LTEC curve for the fourth heating represent the crystalline state. It shows relatively constant compare to other curves.

1) P.Kozikowski, M.Ohnuma, R.Hashimoto, K.Takano, G.Herzer, M.Kuhnt, C.Polak, Phys.Rev. Mater., 4(2020), #095604

The structural analysis of low-density liquid phosphorus using reverse Monte Carlo simulation

Takuya Nishioka, Hiroki Naruta, *Kazuhiro Fuchizaki

Department of Physics, Ehime University, Matsuyama, 790-8577, Japan

*fuchizak@phys.sci.ehime-u.ac.jp

Keywords: Liquid-liquid transition, Phosphorus, Reverse Monte Carlo simulation.

After the exciting discovery of phosphorus' liquid-liquid transition (LLT)¹⁾ at the beginning of this century, many substances undergoing an LLT have been identified. However, like phosphorus, substances exhibiting a transition between thermodynamically stable phases are still rare. Under these circumstances, sulfur may probably be a unique substance whose polyamorphic phase diagram, including the location of the (second) critical point, was unveiled.²⁾ Although phosphorus and sulfur are believed to transform from a molecular to polymerized liquid state on the pressure-induced LLT, the Clapeyron slope of phosphorus (sulfur) slope is negative (positive). The quantitative entropy difference between the low-density liquid (LDL) and high-density liquid (HDL) phases could explain the difference in the slope's sign. However, no structural analysis useable for the entropy estimation has been done to the authors' knowledge. Here, we show for the first time the three-dimensional atomic arrangement in phosphorus' LDL state with the help of reverse Monte Carlo (RMC) simulation.³⁾

The simulation requires the two indispensable inputs; the structure factor $S(k)$, given as a function of wavenumber k , and the liquid density ρ in question. Here, $S(k)$ at 0.77 GPa and 1040 °C (open circles in Fig. 1) was taken from Ref. 1, whereas $\rho=1.75$ g/cc resulted from the method given in Ref. 4. The other nontrivial input is an initial configuration. An aggregation of randomly oriented 2744 tetrahedrons was prepared using the molecular dynamics method developed for a system of SnI₄ molecules.⁵⁾

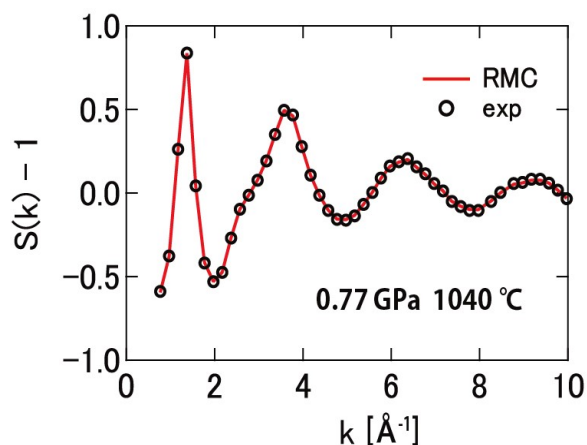


Fig. 1. The structure factors of LDL phosphorus used as input (circles) and resulted from the simulation (red line).

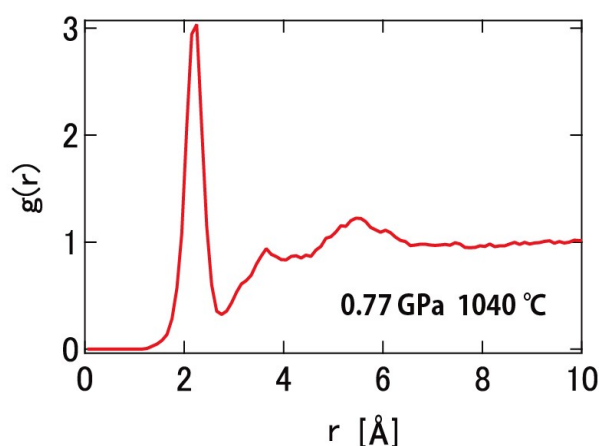


Fig. 2. The resulting radial distribution function plotted against radial distance.

Red lines in Figs. 1 and 2 are the resultant structure factor and radial distribution function. The former justifies the simulation result. As shown in Fig. 3, we visually confirmed that phosphorus atoms in LDL constitute regular tetrahedrons. The regularity was ensured by the sharpness of the first peak at 2.2(2) Å, showing the intramolecular P—P correlation.

References

- 1) Y. Katayama et al., Nature 403, 170 (2000).
- 2) L. Henry et al., Nature 584, 382 (2020).
- 3) O. Gereben and L. Pusztai, J. Comput. Chem. 33 2285 (2012).
- 4) T. Sakagami et al., J. Phys.: Condens. Matter 28, 395101 (2016).
- 5) S. Sugiyama et al., J. Chem. Phys. 112, 10379 (2000).

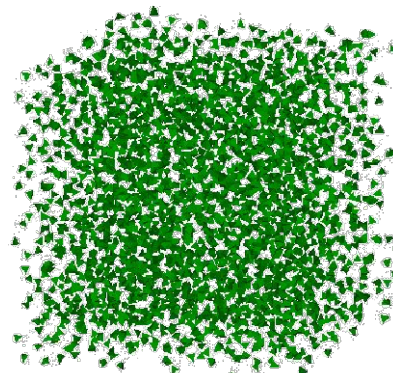


Fig. 3. A three-dimensional view for the resultant aggregate of P₄ molecules shown in green.

Local Structure of $\text{Ga}_{85.8}\text{In}_{14.2}$ eutectic liquid alloy and its pressure temperature melting line.

Yimin MIJITI¹, Aangela Trapananti¹, Lucie Nataf², Francois Baudelet², Toru Shinmei³, Tetsuo Irifune³, Jian Zhong Jiang⁴, Andrea Di Cicco^{1,*}

¹ School of Science and Technology, University of Camerino, Via Madonna delle Carceri 9, Camerino, MC 62032, Italy

² Synchrotron Soleil, L' Orme des Merisiers BP 48, Gif-sur-Yvette 91192, Cedex, France

³ Geodynamics Research Center Ehime University Matsuyama 790-8577, Japan

⁴ International Center for New-Structured Materials (ICNSM), Laboratory of New-Structured Materials, State Key Laboratory of Silicon Materials, and School of Materials Science and Engineering, Zhejiang University, Hangzhou 310027, P. R. China

[*andrea.dicicco@unicam.it](mailto:andrea.dicicco@unicam.it)

Keywords : EXAFS, XRD, Local structure, melting line, eutectic GaIn liquid alloy

The structure of the $\text{Ga}_{85.8}\text{In}_{14.2}$ eutectic liquid alloy is investigated both under ambient conditions and at high pressure/high temperature using X-ray absorption spectroscopy (XAS) and X-ray diffraction (XRD) techniques. The local structure of the liquid alloy at ambient conditions is analyzed using double-edge refinements of the XAS data. Solid-liquid phase transitions under high-pressure and high-temperature conditions are monitored by combined XAS and XRD measurements along several quasi-isobaric heating runs, allowing to draw a melting line up to 10 GPa. The established melting line is found to be slightly below the one of pure gallium (Ga) and to follow its trend as expected from the eutectic nature of the compound. A series of Ga *K*-edge X-ray absorption fine structure (XAFS) spectra measured at different pressures indicates the absence of large structural modifications at local Ga sites in the liquid within the investigated pressure and temperature range.

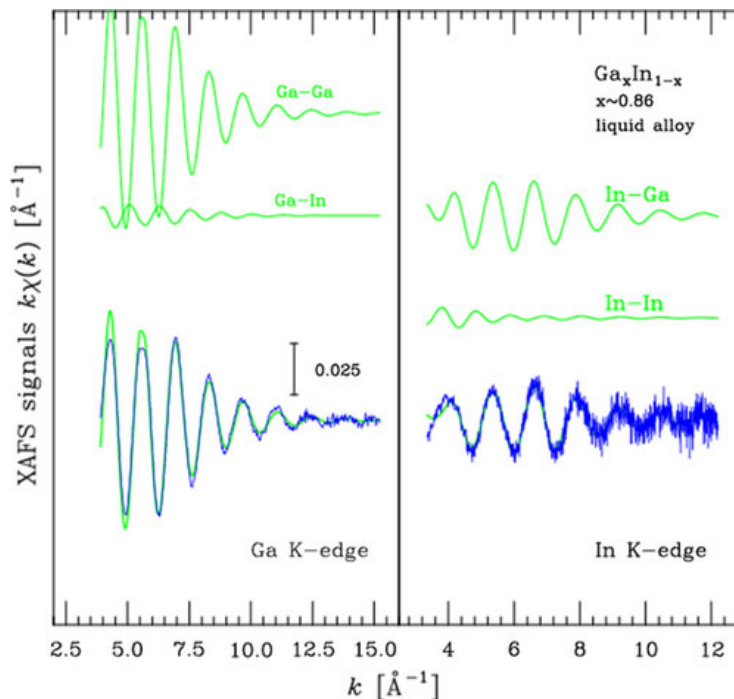


Figure: Best fit double-edge EXAFS refinement of the local structure of GaIn eutectic liquid alloy at ambient conditions.

Development of an Analysis Method for Liquid Electrolyte at a Lithium Electrode Interface using X-ray Total Reflection

*[Koji Kimura](#)¹, Kairi Fujii¹, Hisao Kiuchi^{2,†}, Kazuki Yoshii³, Tatsumi Hirano², Yasuhiro Takabayashi¹, Hikari Sakaebe³, and Kouichi Hayashi¹

¹Nagoya Institute of Technology, Gokiso, Nagoya, Aichi 466-8555, Japan ²Office of Society-Academia Collaboration for Innovation, Kyoto University, Gokasho, Uji, Kyoto 611-0011, Japan ³Research Institute of Electrochemical Energy (RIECEN), National Institute of Advanced Industrial Science and Technology (AIST) Ikeda, Osaka 563-8577, Japan

*kimura.koji@nitech.ac.jp

[†]Present address: Institute for Solid State Physics, The University of Tokyo, Kashiwa, Chiba 277-8581, Japan

Keywords: X-ray Total Reflection, Electrolyte, Battery, Synchrotron Radiation

Lithium metal batteries (LMBs) are regarded as promising candidates for post-lithium-ion batteries, because of their large theoretical capacity of 3860 mAhg^{-1} . LMBs are widely used as primary batteries but not as secondary batteries, because it is difficult to control the interfacial behavior between liquid electrolytes and the lithium-metal electrode during charging and discharging. So far, extensive studies have been performed to characterize the interfacial properties using various techniques such as the optical microscopy²⁾, electron microscopy^{3,4)}, and X-ray photoelectron spectroscopy⁴⁾. However, these studies have focused on the electrode-side of the interface, but not on the electrolyte-side. It is important to investigate the electrolyte-side of the interface in order to comprehensively understand the electrolyte/lithium interface.

In this study⁵⁾, we used an X-ray total reflection to investigate the electrolyte-side of the interface. Since the density of lithium ($\sim 0.5 \text{ g cm}^{-3}$) is lower than that of typical electrolytes ($> 1.0 \text{ g cm}^{-3}$), grazing incidence X-rays going through the electrolyte can be totally reflected by the electrolyte. Therefore, reflected X-rays from the electrolyte/lithium interface strongly reflect the electrolyte properties at the interface.

Reflected X-ray from the electrolyte/lithium interface was measured at BL28XU in SPring-8 using a specially designed cell, where a lithium deposition film on a SiC substrate was inserted. A mixture of propylene carbonate, 1 mol L^{-1} of LiPF_6 , and 50 ppm of H_2O was used as the electrolyte. The incident X-ray energy was 28 keV. Two dimensional CdTe detector was used for the measurements.

Figure 1 shows the two-dimensional image of the X-ray intensities measured at the incident angle of 0.035° . We can clearly observe a total reflection X-ray together with the direct beam, which demonstrates the occurrence of X-ray total reflection from the electrolyte-side of the electrolyte/lithium interface. Figure 2 shows the X-ray reflectivity curve. An abrupt drop of the reflected X-ray intensity is observed at 0.042° corresponding to the critical angle. This value is in good agreement with the calculated value of 0.039° , which further confirms the successful detection of the total reflection X-ray. In the presentation, details of the cell design and the application to the in-operando measurements will also be described.

This work was based on results obtained from projects, JPNP16001 and JPNP21006, commissioned by the New Energy and Industrial Technology Development Organization (NEDO).

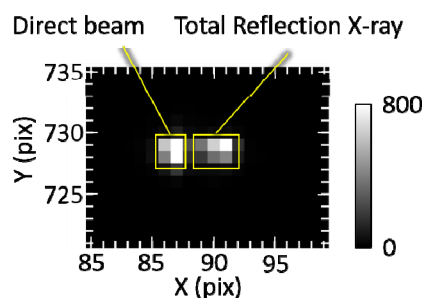


Fig. 1 Two-dimensional X-ray intensity from the electrolyte/lithium interface measured at the incident angle of 0.035° .

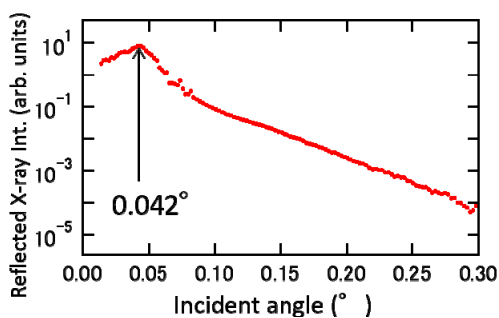


Fig. 2 X-ray reflectivity curve of the electrolyte/lithium interface.

References

- 1) X.-B. Cheng *et al.*, *Chem. Rev.* **117**, 10403 (2017).
- 2) H. Sano *et al.*, *Chem. Lett.* **42**, 77 (2013).
- 3) Y. Xu *et al.*, *ACS Nano* **14**, 8766 (2020).
- 4) T. Tsuda *et al.*, *Electrochim. Acta* **279**, 136 (2018).
- 5) K. Kimura *et al.*, *Chem. Lett.* **50**, 1526 (2021).

Structure of amorphous $\text{Mg}_{85}\text{Zn}_6\text{Y}_9$ alloy as a seed of a long-period stacking ordered structure

*Shinya Hosokawa¹, Jens Rüdiger Stellohorn,² Akihide Koura,³ Fuyuki Shimojo,³ Makoto Tokuda,⁴ Akira Yoshiasa,⁴ Nils Blanc,⁵ Nathalie Boudet,⁵ Hiroshi Okuda,⁶ Michiaki Yamasaki,^{7,8} Yoshihito Kawamura^{7,8}

¹ Institute of Industrial Nanomaterials, Kumamoto University, Kumamoto 860-8555, Japan, ² Department of Applied Chemistry, Hiroshima University, Higashi-Hiroshima 739-8527, Japan, ³ Department of Physics, Kumamoto University, Kumamoto 860-8555, Japan, ⁴ Department of Earth and Environmental Sciences, Kumamoto University, Kumamoto 860-8555, Japan, ⁵ Institut Néel, Centre National de la Recherche Scientifique (CNRS)/University of Grenoble Alpes, 38042 Grenoble Cedex 9, France, ⁶ Department of Materials Science and Engineering, Kyoto University, Kyoto 606-8501, Japan, ⁷ Department of Materials Science, Kumamoto University, Kumamoto 860-8555, Japan, ⁸ Magnesium Research Center, Kumamoto University, Kumamoto 860-8555, Japan
*shhosokawa@kumamoto-u.ac.jp

Keywords: Mg alloys, Partial structure, Anomalous X-ray scattering, XAFS, Reverse Monte Carlo modeling

For recent twenty years, Mg alloys containing Zn and rare-earth impurities discovered by Kawamura et al. [1], which is the so-called KUMADAI Magnesium (denoting the Kumamoto University Magnesium), have achieved much attention owing to their potential for applications as new structural materials. As well known, pure Mg is flammable and chemically active as well as the strength and ductility are very poor. By adding small amounts of Zn and Y impurities, however, Mg becomes non-flammable and shows high thermal stability [2]. Moreover, these alloys exhibit superior mechanical properties, such as a tensile yield strength of about 600 MPa and an elongation of about 8% at room temperature [1,2]. Due to such excellent properties together with an ease of recycling, these Mg alloys are promising as next-generation structural materials, such as for bodies of subways or even aircrafts.

These properties are found to be based on the formation of a long-period stacking ordered (LPSO) phase with a $L1_2$ type (fragments of *fcc* structure) Zn_6Y_8 clusters, which was observed by a high-angle annular dark-field scanning transmission electron microscopy observations [3]. Okuda et al. [4] investigated the phase transition process of amorphous-to-crystal states in the $\text{Mg}_{85}\text{Zn}_6\text{Y}_8$ alloy by using small angle x-ray scattering, and observed a hierarchical transition process; the clustering of the impurity atoms occurs first, and the spatial rearrangement of the clusters induces secondary, leading to two-dimensional order of the $L1_2$ clusters. To obtain proof of the existence of the clusters in the amorphous phase, Hosokawa et al. carried out Y $3d$ core-level photo emission experiments, and the obtained spectrum shows three doublets and one on them coincide well in binding energy with that of polycrystalline $\text{Mg}_{85}\text{Zn}_6\text{Y}_8$ alloy having mostly 100% of the LPSO phase [5]. Therefore, some fragments of the clusters are expected to exist even in the amorphous phase.

In this study, we carried out anomalous x-ray scattering (AXS) measurements at BM02 of the ESRF and x-ray absorption fine structure (XAFS) experiments at BL9C of the PF-KEK close to the Zn and Y K edges to acquire direct structural information. The obtained experimental data were analyzed by using reverse Monte Carlo (RMC) modeling to obtain partial structure factors, $S_{ij}(Q)$, partial pair distribution functions, $g_{ij}(r)$, and the corresponding three-dimensional atomic configurations. An ab initio molecular dynamics calculation was, furthermore, performed to compare the simulated structures with the experiments.

A large number of the Zn-Zn and Y-Y correlations were found in the first-neighboring shell region unlike the crystal configurations of the $L1_2$ clusters; however, the Zn-Y heteropolar bondings are preferable rather than the Zn-Zn and Y-Y homopolar bondings in the amorphous phase, which can be considered as the seeds of the crystalline $L1_2$ clusters. A charge transfer from Y to other elements is expected from the estimated atomic radius of Y. However, a large fraction of the $L1_2$ cluster fragments are not observed in contrast to the previous conclusion without the XAFS data in the RMC analysis [6].

References:

- 1) Y. Kawamura, K. Hayashi, A. Inoue, and T. Masumoto, *Mater. Trans.* 42, 1172 (2001).
- 2) Y. Kawamura, T. Kasahara, S. Izumi, and M. Yamasaki, *Scr. Mater.* 55, 453 (2006).
- 3) E. Abe, A. Ono, T. Itoi, M. Yamasaki, and Y. Kawamura, *Philos. Mag. Lett.* 91, 690 (2011).
- 4) H. Okuda, M. Yamasaki, Y. Kawamura, M. Tabuchi, and H. Kimizuka, *Sci. Rep.* 5, 14186 (2015).
- 5) S. Hosokawa, J. R. Stellohorn, B. Paulus, K. Maruyama, K. Kobayashi, H. Okuda, M. Yamasaki, Y. Kawamura, and H. Sato, *J. Alloys Compd.* 764, 431 (2018)
- 6) S. Hosokawa, J. R. Stellohorn, B. D. Klee, W.-C. Pilgrim, H. Okuda, M. Yamasaki, Y. Kawamura, N. Blanc, and N. Boudet, *Appl. Phys. Express* 11, 071402 (2018).

Collective dynamics of liquid sulfur across the polymerization transition temperature probed by inelastic x-ray scattering

*Shinya Hosokawa¹, Yoshinori Katayama², Satoshi Tsutsui³, Alfred Q. R. Baron^{4,3}

¹ Institute of Industrial Nanomaterials, Kumamoto University, Kumamoto 860-8555, Japan, ² Kansai Photon Science Institute, National Institutes for Quantum Science and Technology, Sayo 679-5148, Japan, ³ Japan Synchrotron Radiation Research Institute (JASRI), Sayo 679-5198, Japan, ⁴ Materials Dynamics Laboratory, RIKEN SPring-8 Center, Sayo 679-5148, Japan

*shhosokawa@kumamoto-u.ac.jp

Keywords: Molecular liquid, Phonon dispersion, Diffusion, Inelastic X-ray scattering.

The so-called λ transition in liquid sulfur occurs at about 159°C, which is attributed to the formation of long chain molecules by breaks and polymerizations of eight-membered sulfur rings at low temperatures. Inelastic x-ray scattering (IXS) experiments on liquid sulfur were carried out at BL35XU of the SPring-8 [1], below and above the polymerization temperature (140 and 180°C, respectively) to investigate collective dynamics of this unique molecular liquid showing a liquid-liquid phase transition. The obtained IXS spectra were analyzed by using a damped harmonic oscillator (DHO) model [2] with a Lorentzian quasielastic peak.

Figure 1 shows the dispersion relations of the longitudinal acoustic (LA) excitation modes at 140°C (empty circles) and 180°C (solid triangles) obtained from the DHO model. The solid and dashed lines indicate the dispersions of the hydrodynamic limits obtained from ultrasonic sound velocity data [3]. Only slight differences are observed in the excitation energies, ω_Q , although the macroscopic shear viscosity is very different across the λ transition temperature, T_λ . Note that the so-called positive dispersion of dynamic sound velocity are observed by about 40% for both the phases. The width of the LA modes does not change mostly when crossing T_λ .

Figure 2 shows the width (half-width at half maximum, HWHM) of the central quasielastic peaks, Γ_0 . As seen in the figure, the Γ_0 values at $Q < 6 \text{ nm}^{-1}$ beyond T_λ are narrower than those below T_λ . This result indicates that the diffusion of sulfur atoms is distinct at the correlation length of more than the molecule size of S_8 rings. A generalized Langevin formalism with a memory function [4] will be applied to obtain microscopic thermodynamic parameters. The results will be discussed by comparing a previous IXS experiment [5].

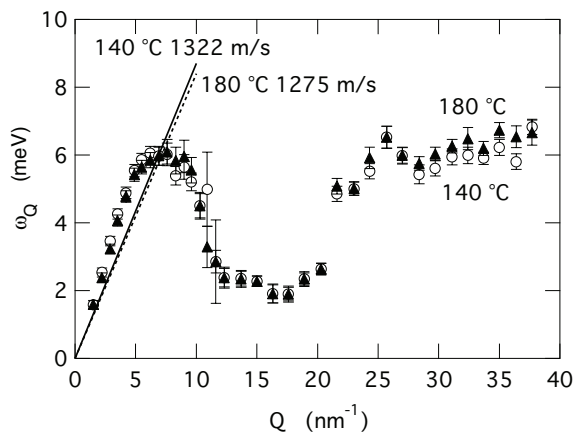


Fig. 1. Dispersion relations of the LA excitation modes at 140 (empty circles) and 180°C (solid triangles). The solid and dashed lines indicate the dispersions of the hydrodynamic limits obtained from ultrasonic sound velocity data [2].

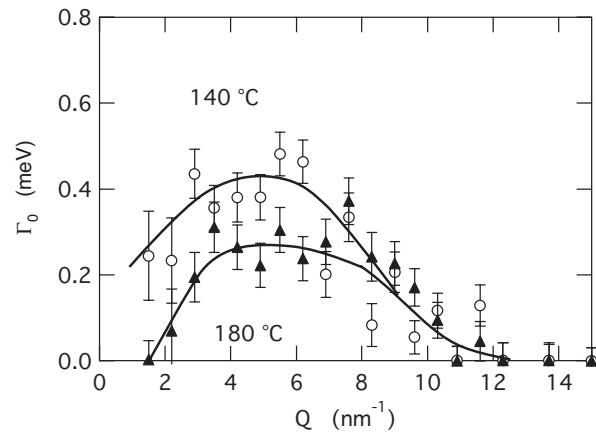


Fig. 2. HWHM of the quasielastic peak at 140 (empty circles) and 180°C (solid triangles). The solid curves are the guide for eyes.

References:

- 1) A. Q. R. Baron et al., *J. Phys. Chem. Solids* 61, 461 (2000).
- 2) B. Fåk and B. Dorner, *Physica B* 234–236, 1107 (1997).
- 3) V. F. Kozhevnikov, J. M. Viner, and P. C. Tayler, *Phys. Rev. B* 64, 214109 (2001).
- 4) J. P. Boon and S. Yip, *Molecular hydrodynamics* (McGraw-Hill, New York, 1980).
- 5) G. Monaco et al., *Phys. Rev. Lett.* 95, 255502 (2005).

Phonon dynamics of liquid Hg probed by inelastic x-ray scattering

*Shinya Hosokawa¹, Masanori Inui², Yukio Kajihara², Ayano Chiba³, Satoshi Tsutsui⁴, Alfred Q. R. Baron^{5,4}

¹Institute of Industrial Nanomaterials, Kumamoto University, Kumamoto 860-8555, Japan, ²Graduate School of Advanced Science and Engineering, Hiroshima University, Higashi-Hiroshima 739-8521, Japan, ³Department of Physics, Keio University, Yokohama 223-8522, Japan, ⁴Japan Synchrotron Radiation Research Institute (JASRI), Sayo 679-5198, Japan, ⁵Materials Dynamics Laboratory, RIKEN SPring-8 Center, Sayo 679-5148, Japan
*shhosokawa@kumamoto-u.ac.jp

Keywords: Liquid metals, Phonon dispersion, Inelastic X-ray scattering

In 2002, an inelastic x-ray scattering (IXS) measurement on liquid Hg was carried out at room temperature [1] as one of the pioneering IXS studies on liquid heavy metals. For this experiment, an in-line IXS spectrometer with a resolution of 2.2 meV was used at APS, and the statistical quality was insufficient. Only the longitudinal acoustic (LA) modes could be obtained. The so-called *positive* dispersion, i.e., larger excitation energies beyond the hydrodynamic prediction at small Q values, was observed by about 20%, which was similar to those in other liquid metals [2]. However, the indication of extra excitation modes was hardly detected due to an insufficient data quality.

In 2009, we found an indication of transverse acoustic (TA) phonon modes in liquid Ga in addition to the usual LA modes [3] by IXS with much higher statistical quality [4]. We also detected the TA signals in liquid Sn [5], Zn [6], and transition metals of Fe and Cu [6]. We analyzed the IXS data using current correlation functions, which are in good agreement with results of an *ab initio* molecular dynamics simulation [5]. Thereby, the theoretical LA and TA data show a mixing effect, i.e., mixtures of two excitation branches of quasi-LA and -TA contributions, and the experimental data are always very similar to the theoretical LA result.

Based on these experimental and theoretical understandings, we recall liquid Hg to examine if such an extra excitation mode exists in liquid heavy metals. IXS experiments were carried out at BL35XU of the SPring-8 using a high-resolution IXS spectrometer with an energy of about 1.5 meV and an incident x-ray intensity of more than one order of magnitude [4]. Liquid Hg sample was contained in a single crystal sapphire cell with a sample thickness of about 0.02 mm and an x-ray window thickness of 0.2 mm [7].

Figure 1 shows IXS intensities of liquid Hg at the selected Q values, where extra excitation modes may be clearly observed, i.e., including the quasi-first and -second Brillouin zone border. As seen in the figure, shoulders are observed at 8-10 meV depending on Q , which are surely the LA excitation modes. Compared with the IXS data on liquid light metals [2], the IXS signals have quite different features. Further analyses are now in progress, and the results will be shown in the presentation.

References:

- 1) S. Hosokawa et al., J. Non-Cryst. Solids 312-314, 163 (2002).
- 2) T. Scopigno, G. Ruocco, and F. Sette, Rev. Mod. Phys. 77, 881 (2005).
- 3) S. Hosokawa et al., Phys. Rev. Lett. 102, 105502 (2009).
- 4) A. Q. R. Baron et al., J. Phys. Chem. Solids 61, 461 (2000).
- 5) S. Hosokawa et al., J. Phys.: Condens. Matter 25, 112101 (2013).
- 6) S. Hosokawa et al., J. Phys.: Condens. Matter 27, 194104 (2015).
- 7) K. Tamura, M. Inui, and S. Hosokawa, Rev. Sci. Instrum. 70, 144 (1999).

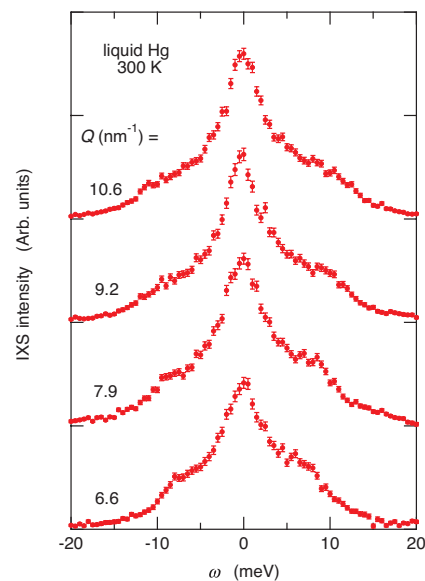


Fig. 1. IXS intensities of liquid Hg at selected Q values.

Inelastic x-ray scattering experiments for liquid GeCu_2Te_3 *M. Inui¹, S. Hosokawa², S. Tsutsui³, Y. Nakajima⁴, K. Matsuda⁴, and A.Q.R. Baron^{5,3}¹ Graduate School of Advanced Science and Engineering, Hiroshima University, Higashi-Hiroshima, Hiroshima 739-8521, Japan, ² Institute of Industrial Nanomaterials, Kumamoto University, Kumamoto 860-8555, Japan, ³ Japan Synchrotron Radiation Research Institute (JASRI), Sayo-cho, Hyogo 679-5198, Japan,⁴ Department of Physics, Kumamoto University, Kumamoto 860-8555, Japan, ⁵ Materials Dynamics Laboratory, RIKEN SPring-8 Center, Sayo, Hyogo 679-5148, Japan

* masinui@hiroshima-u.ac.jp

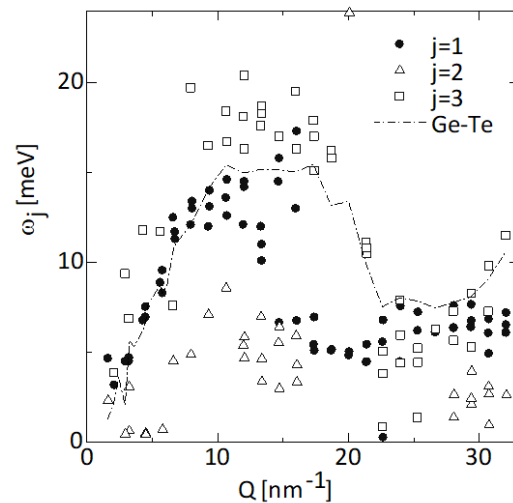
Keywords: atomic dynamics, inelastic X-ray scattering, liquid GeCu_2Te_3 , longitudinal acoustic excitation

Fast phase-change materials (PCMs) such as ternary $\text{Ge}_2\text{Sb}_2\text{Te}_5$ have been intensively investigated for the last two decades since the fast phase change phenomena between crystalline and amorphous states were utilized in nonvolatile memory [1]. PCMs for memory devices show strong optical contrast between the crystalline and amorphous states and its origin has been related to the difference in bonding properties between them. Besides $\text{Ge}_2\text{Sb}_2\text{Te}_5$, GeCu_2Te_3 was found to be another candidate of PCMs [2,3]. In the memory device, an amorphous bit is formed by rapid quenching a liquid spot made by laser beam irradiation. Hence, to investigate atomic dynamics in the liquid phase is important to understand fast crystallization in PCMs. So far we have carried out inelastic x-ray scattering (IXS) measurements for liquid $\text{Ge}_2\text{Sb}_2\text{Te}_5$ to obtain dynamic structure factor $S(Q, E)$, where Q and E are momentum and energy transfer, respectively. We found that high energy excitation in $S(Q, E)$ behaves like optical mode with the excitation energy approaching to approximately 20 meV at $Q=0$ [4]. In this study, we have carried out IXS measurements for liquid GeCu_2Te_3 to investigate Q dependence of excitation energies.

IXS measurements were conducted using high-resolution inelastic x-ray scattering spectrometer at BL35XU/SPring-8 in Japan. The IXS spectra at $2 < Q < 33 \text{ nm}^{-1}$ were obtained with the energy resolution of approximately 1.5 meV. After background subtraction, we could obtain $S(Q, E)$ of liquid GeCu_2Te_3 at 803 K. $S(Q, E)$ was deconvoluted with a model function composed of a Lorentzian and damped harmonic oscillator (DHO) functions. Fig.1 shows the excitation energies obtained by a model function of 3-DHO components as a function of Q before averaging the results at similar Q values. The excitation energies of DHO functions disperse with Q and the main component (black circles) is assigned as the longitudinal acoustic mode, which disperses with Q similarly to liquid GeTe denoted by a chain curve [5]. Lower excitation energies (open triangles) below the longitudinal acoustic ones appear at $Q > 3 \text{ nm}^{-1}$ and they do not show strong dispersion staying at approximately 5 meV at $5 < Q < 15 \text{ nm}^{-1}$. Interestingly, the longitudinal acoustic excitation energy exhibits bifurcation at $10 < Q < 20 \text{ nm}^{-1}$, similarly to liquid $\text{Ge}_2\text{Sb}_2\text{Te}_5$. However, higher excitation energy (open squares) does not show the optical mode-like behavior that was observed in liquid $\text{Ge}_2\text{Sb}_2\text{Te}_5$.

References:

- 1) S. R. Ovshinsky, Phys. Rev. Lett. **21**, 1450 (1968).
- 2) Y. Sutou et al., Acta Mater. **60**, 872 (2012).
- 3) T. Kamada et al., Thin Solid Films **520**, 4389 (2012).
- 4) M. Inui et al., Phys. Rev. B **104**, 064202 (2021).
- 5) M. Inui et al., Phys. Rev. B **97**, 174203 (2018)

Fig.1 Excitation energies in liquid GeCu_2Te_3 at 803 K.

Q-gap behavior of low energy excitations in liquid Sb and liquid Bi observed by inelastic x-ray scattering measurements

*M. Inui¹, Y. Kajihara¹, S. Hosokawa^{2,#1}, A. Chiba³, Y. Nakajima², K. Matsuda², J. R. Stellhorn¹, T. Hagiya^{4,#2}, D. Ishikawa⁵, H. Uchiyama⁵, S. Tsutsui⁵ and A. Q. R. Baron^{6,5},

¹ Graduate School of Advanced Science and Engineering, Hiroshima University, Higashi-Hiroshima, Hiroshima 739-8521, Japan, ² Department of Physics, Kumamoto University, Kumamoto 860-8555, Japan, ³ Department of Physics, Keio University, Yokohama 223-8522, Japan, ⁴ Graduate School of Science, Kyoto University, Kyoto 606-8502, Japan, ⁵ Japan Synchrotron Radiation Research Institute (JASRI), Sayo-cho, Hyogo 679-5198, Japan, ⁶ Materials Dynamics Laboratory, RIKEN SPring-8 Center, Sayo, Hyogo 679-5148, Japan

* masinui@hiroshima-u.ac.jp

Keywords: atomic dynamics, transverse acoustic excitation, inelastic X-ray scattering, liquid Sb, liquid Bi

The dynamic structure factor $S(Q, E)$, where Q and E are momentum and energy transfer, respectively, has been obtained for liquid Sb [1] and liquid Bi [2], using inelastic x-ray scattering (IXS) at SPring-8 in Japan. $S(Q, E)$ was deconvoluted by a model function composed of a Lorentzian and the damped harmonic oscillators. We have obtained lower excitation energy besides the longitudinal acoustic excitation in $S(Q, E)$ of these liquids. The longitudinal acoustic excitation energy experimentally obtained was in fairly good agreement with that predicted by ab initio molecular dynamics (AIMD) simulations [3,4,5]. Fig.1 shows the dispersion relation in liquid Sb at 973 K. The excitation energy of the longitudinal acoustic mode in liquid Sb (squares) exhibits flat-topped Q dependence as predicted by an AIMD simulation (a magenta curve) [5]. When we analyzed the data using a modified damped harmonic oscillator model function, it was clarified that the lower excitation energy (triangles) below the longitudinal acoustic excitation shows Q -gap behavior. The triangles at $4 < Q < 10 \text{ nm}^{-1}$ were fitted with a theoretical equation $\omega(Q)^2 = c_T^2 Q^2 - 1/(4\tau_M^2)$, where $\omega(Q)$, c_T , and τ_M are the excitation energy, transverse acoustic sound speed and Maxwell relaxation time, respectively. The broken curve in Fig.1 denotes the optimized one and the results show a Q gap of 4.7 nm^{-1} . The crosses in Fig.1, the simulated transverse acoustic excitation energy, lie in a lower energy region compared to the triangles, and similar fits gave a Q gap of 1.4 nm^{-1} . We speculate that the difference between IXS and AIMD arises from that IXS observes the transverse acoustic energy in the longitudinal $S(Q, E)$ whereas the simulation can predict the excitation energy in the purely transverse $S(Q, E)$. From the viscosity estimated from the Q -gap experimentally obtained, nevertheless, it is inferred that the lower energy excitation arises from the transverse acoustic excitation in the liquids.

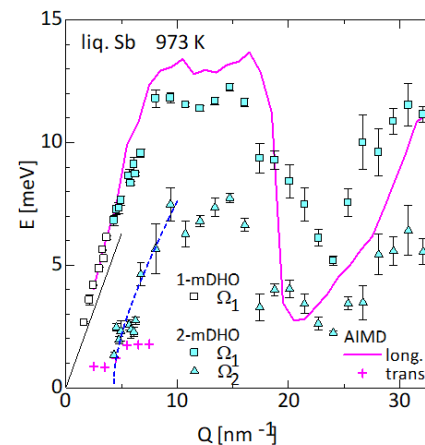


Fig.1 The optimised excitation energies of the inelastic components for liquid Sb. Also shown are the longitudinal (magenta curve) and transverse (crosses) acoustic excitation energies obtained by AIMD. The ultrasonic sound speed (black line) is 1910 m s^{-1} .

References:

- 1) M. Inui et al., J. Phys.: Condens. Matter **33** 475101 (2021).
- 2) M. Inui et al., Phys. Rev. B **92**, 054206 (2015).
- 3) J. Souto et al., Phys. Rev. B **81**, 134201 (2010).
- 4) M. Ropo et al., J. Chem. Phys. **145**, 184502 (2016).
- 5) R. O. Jones et al., J. Chem. Phys. **146**, 194502 (2017).

#1 Present address: Institute of Industrial Nanomaterials, Kumamoto University, Kumamoto 860-8555, Japan.

#2 Present address: Metal Powder Technology Department, Sanyo Special Steel Co., Ltd., Himeji, Hyogo 672-8677, Japan.

Phonon dispersion curves in the type-I crystalline and molten clathrate compound $\text{Eu}_8\text{Ga}_{16}\text{Ge}_{30}$

Takumi Hasegawa¹, *Masanori Inui¹, Takahiro Onimaru¹, Yukio Kajihara¹, Shinya Hosokawa^{2,#1}, Yoichi Nakajima², Kazuhiro Matsuda^{3,#2}, Toshiro Takabatake¹, Satoshi Hiroi⁴, Hiroshi Uchiyama⁴ and Satoshi Tsutsui^{4,5}

¹ Graduate School of Advanced Science and Engineering, Hiroshima University, Higashi-Hiroshima, 739-8521, Japan,

² Department of Physics, Kumamoto University, Kumamoto 860-8555, Japan,

³ Graduate School of Science, Kyoto University, Kyoto 606-8502, Japan,

⁴ Japan Synchrotron Radiation Research Institute (JASRI), Sayo-cho, Hyogo 679-5198, Japan,

⁵ Institute of Quantum Beam Science, Graduate School of Science and Engineering, Ibaraki University, Hitachi, Ibaraki 316-8511, Japan.

* masinui@hiroshima-u.ac.jp

Keywords: Inelastic X-ray scattering, thermoelectric material, clathrate compounds, phonon dispersion, ab initio molecular dynamics simulation

Intermetallic clathrate has been expected as a candidate for high-performance new thermoelectric materials since the concept of phonon glass-electron crystal was proposed [1]. Among various clathrate compounds, the type-VIII modification of $\text{Ba}_8\text{Ga}_{16}\text{Sn}_{30}$ exhibits preferable thermoelectric performance [2,3]. To design a suitable preparing route for the intended modification, it is important to know the properties in the liquid state. We have studied static and dynamic structures in molten clathrate compound $\text{Ba}_8\text{Ga}_{16}\text{Sn}_{30}$ to investigate clusters in the liquid state [4]. The pair distribution function in liquid $\text{Ba}_8\text{Ga}_{16}\text{Sn}_{30}$ suggests shorter and longer interatomic distances in the first coordination shell corresponding to (Ga, Sn)-(Ga, Sn) and Ba-(Ga, Sn) correlations, respectively. The dynamic structure factor of liquid $\text{Ba}_8\text{Ga}_{16}\text{Sn}_{30}$ obtained by inelastic x-ray scattering (IXS) exhibits the longitudinal acoustic excitations with a peak profile, and another excitation at a lower energy. The lower excitation energy in the liquid state was higher than a vibrational energy arising from a rattling motion of a guest atom in the solid state. The result suggests that the host-guest interaction in a solid $\text{Ba}_8\text{Ga}_{16}\text{Sn}_{30}$ clathrate is strengthened on melting.

In this study, we have carried out IXS measurements of type-I crystalline and liquid $\text{Eu}_8\text{Ga}_{16}\text{Ge}_{30}$ to compare phonon dispersions between crystalline and liquid states. IXS measurements with the energy resolution of approximately 1.5 meV were conducted using a high-resolution IXS spectrometer at BL35XU/SPRING-8 in Japan. IXS spectra of type-I clathrate $\text{Eu}_8\text{Ga}_{16}\text{Ge}_{30}$ were measured at the ambient conditions using a single crystal piece. As molten $\text{Eu}_8\text{Ga}_{16}\text{Ge}_{30}$ at 993 K was found to react with sapphire, the molten sample was sandwiched with glassy carbon in a sapphire cell. Ab initio phonon calculations based on the density functional perturbation theory were carried out for type-I crystalline $\text{Eu}_8\text{Ga}_{16}\text{Ge}_{30}$. The IXS spectra estimated from the calculated phonon modes are shown in Fig.1 as a color map, where the symbols in Fig.1 denote the excitation energies obtained from IXS spectra. The symbols fairly well agree with the simulated curves. The dynamics structure factor in liquid $\text{Eu}_8\text{Ga}_{16}\text{Ge}_{30}$ exhibits the inelastic excitations of the longitudinal acoustic mode that disperses faster than the energy simulated for type I crystalline form.

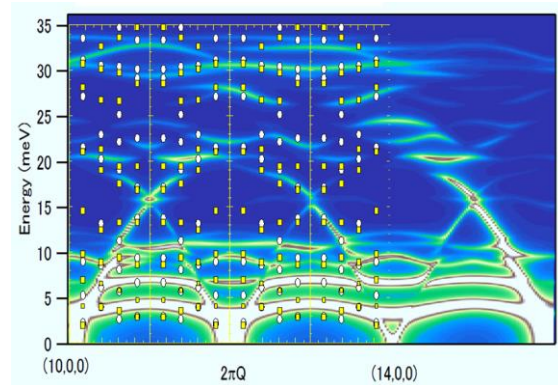


Fig.1 Phonon dispersion of type I clathrate compound $\text{Eu}_8\text{Ga}_{16}\text{Ge}_{30}$. Bright curves denote simulated phonon excitations and yellow and white symbols are excitation energies obtained by IXS.

References :

- 1) G. A. Slack, New materials and performance limits for thermoelectric cooling CRC Handbook of Thermoelectrics, ed. D. M. Rowe (Boca Raton, FL: CRC Press) p 407 (1995).
 - 2) K. Suekuni et al., Phys. Rev. B **77**, 235119 (2008).
 - 3) Y. Saiga et al., J. Alloys Compd. **507**, 1 (2010).
 - 4) M. Inui et al., J. Phys.: Condens. Matter **30**, 455101 (2018).
- #1 Present address: Institute of Industrial Nanomaterials, Kumamoto University, Kumamoto 860-8555, Japan.
 #2 Present address: Department of Physics, Kumamoto University, Kumamoto 860-8555, Japan.

Density response function of valence electrons in liquid Li

*Kazuhiro Matsuda¹, Toru Hagiya^{2, #}, Koji Kimura³, Masanori Inui⁴, Yukio Kajihara⁴, Nozomu Hiraoka⁵

¹ Department of Physics, Kumamoto University, Kumamoto 860-8555, Japan, ² Graduate School of Science, Kyoto University, Kyoto 606-8502, Japan, ³ Department of Physical Science and Engineering, Nagoya Institute of Technology, Nagoya 466-8555, Japan, ⁴ Graduate School of Advanced Science and Engineering, Hiroshima University, Higashi-Hiroshima, Hiroshima 739-8521, Japan, ⁵ National Synchrotron Radiation Research Center, Hsinchu 30076, Taiwan

*kaz-matsuda@kumamoto-u.ac.jp

Keywords : Liquid metals, Electronic states, Inelastic X-ray scattering, X-ray Raman scattering

The static density response function of electrons provides a unified view in describing the screening effects in metals. In the electron gas, the derivative of the density response function exhibits logarithmic divergence, which is responsible for the Friedel oscillation. Theoretical investigations have been made to calculate it in high accuracy, including the effects of exchange correlations ¹), but it has been difficult to confirm the theoretical calculations experimentally. Recent inelastic x-ray scattering (IXS) techniques using synchrotron radiation allow us to determine the density response function ²). In principle, dynamical structure factors can be related by the fluctuation dissipation theorem to the imaginary part of response function, and Kramers-Kronig transform of the dynamic structure factor leads to the real part of response function. In the present study, IXS experiments were performed on solid and liquid Li ³). Valence electrons of Li are well described by the electron gas model and suitable for the investigation of screening in simple metals. The measurements were performed at the beamline BL12XU at SPring-8. IXS spectra were collected in the momentum transfer of 0.30 - 3.47 Å⁻¹ and in the energy range of 0 to 350 eV. Density response function was constructed that can be compared with a theoretical model.

References:

- 1) G. Giuliani and G. Vignale, *Quantum Theory of the Electron Liquid* (Cambridge University Press, Cambridge) 2005.
- 2) P. Abbamonte et al, Phys. Rev. Lett. 92, 23740 (2004).
- 3) Toru Hagiya, Kazuhiro Matsuda, Nozomu Hiraoka, Yukio Kajihara, Koji Kimura, and Masanori Inui, Phys. Rev. B 102, 054208 (2020).

[#]Present address: Metal Powder Technology Department, Sanyo Special Steel Co., Ltd., Himeji, Hyogo 672-8677, Japan

Relationship Between Liquid Dynamics and Potential Energy Landscape

Franz Demmel¹ Louis Hennet² Noel Jakse^{3,*}

¹ISIS Facility, Rutherford Appleton Laboratory, Didcot OX11 0QX, UK.

²ICMN, CNRS and University of Orleans, 45071 Orléans, France.

³Université Grenoble-Alpes, CNRS, Grenoble INP, SIMaP, F-38000 Grenoble, France.

* noel.jakse@grenoble-inp.fr

Keywords: Potential Energy Landscape, Ab initio simulation, Molecular dynamics, Entropy scaling law, Machine Learning.

Understanding evolution of dynamic properties in stable and undercooled liquids as well as their interplay with their structural features represents an important and still open issue. Cooling a liquid will decrease the fluidity of a particle and the mobility of the neighboring particles, resulting in an increase of the viscosity until the system comes to an arrest. This process with a concomitant slowing down of collective particle rearrangements might already start deep inside the liquid state. By considering the Lennard-Jones potential [1] as a generic model and Aluminium [2] a typical liquid metal, it is shown that such a behavior takes its roots in the characteristics of the potential energy landscape which provides an attractive picture for these dramatic changes. The similarity found in dynamics of these two systems as well as with other monatomic liquid metals suggests a universal dynamic crossover above the melting point. The possible correlation with the excess entropy scaling law for diffusion is discussed.

[1] A. Saliou , P. Jarry , and N. Jakse, Phys. Rev E **104**, 044128 (2021).

[2] F. Demmel, L. Hennet , and N. Jakse, Sci. Rep. (Nature) **11**, 11815 (2021).

Selecting atomic fingerprints for high-dimensional neural network potentials: adaptive group lasso approach

*J. Sandberg^{1,2,3}, E. Devijver⁴, T. Voigtmann^{2,3}, N. Jakse¹

¹ Université Grenoble Alpes, CNRS, Grenoble INP, SIMaP, F-38000 Grenoble, France

² Institut für Materialphysik im Weltraum, Deutsches Zentrum für Luft- und Raumfahrt (DLR), 51170 Köln, Germany

³ Department of Physics, Heinrich-Heine-Universität Düsseldorf, Universitätsstraße 1, 40225 Düsseldorf, Germany

⁴ Université Grenoble Alpes, CNRS, Grenoble INP, LIG, F-38000 Grenoble, France

*johannes.sandberg@grenoble-inp.fr

Keywords: Molecular Dynamics, Ab initio simulation, Machine learning, Aluminium, Atomic fingerprints, Interatomic potentials

Interatomic potentials based on machine learning have developed into a widespread and powerful method of material science, opening up for ab initio quality simulations at a computational cost near that of classical force-fields. In commonly used approaches such as Behler-Parinello high-dimensional neural network potentials [1] and SNAP [2], among others, an intermediate set of atomic descriptors is used to represent the atomic environment in lieu of directly feeding atomic positions into the potential. An important component of any such approach is to select an appropriate set of atomic descriptors, with a bad choice potentially rendering the final potential unusable.

In this work we apply variable selection techniques to the Behler-Parinello high-dimension neural network potential framework in order to automatically select optimal subsets of atomic descriptors from much larger sets. This removes the need for the developer of the potential to manually select the set of descriptors based on physical intuition and guesswork, while allowing for computationally faster, more interpretable, and potentially more accurate potentials. We present a complete approach to the selection of atomic descriptors for high-dimensional neural network potentials, based on the adaptive group-lasso [3]. Although the approach is general, our work is largely focused on aluminium, owing to its important real-world applications and the existence of high-quality experimental data against which to evaluate the final potential [4]. This also allow us to build upon our recent study applying a machine learning potential for aluminium to the exploration of solidification phenomena [5].

Future work will be focused on applying the method to multi-component systems. Each added species will increase the number of descriptors needed, with variable selection being a promising approach to partly counteract this added cost. A further line of research will be to explore the introduction of higher level physical information into the training procedure, with the long term aim of studying the link between low-level properties of the potential and high-level macroscopic material properties of aluminium and its alloys.

References:

- 1) J. Behler and M. Parrinello, Phys. Rev. Lett. 98, 146401 (2007)
- 2) A.. Thompson et al., J. Comput. Phys. 285, 316 (2015)
- 3) V. C. Dinh and L. S. Ho, NeurIPS, 33, 2420 (2020)
- 4) H. L. Peng et al., Phys. Rev. B 100, 104202 (2019)
- 5) N. Jakse et al., arXiv:2201.01370, (2022), submitted

GeO₂ glass structure from neural network potential molecular dynamics –dependence of intermediate-range order on density functional approximation

*Kenta Matsutani¹, Shusuke Kasamatsu², Takeshi Usuki²

¹ Graduate School of Science and Engineering, Yamagata University, Yamagata, 990-8560, Japan, ² Faculty of Science, Yamagata University, Yamagata, 990-8560, Japan

*s203002m@st.yamagata-u.ac.jp

Keywords: Density functional theory, Neural network potential, Glass structure, Intermediate-range order

The compaction mechanism of oxides glasses under high pressure has been a topic of high interest in geoscience with the ultimate aim of understanding the nature of Earth's interior, and GeO₂ glass has been a subject of study in this regard as an analogue to silicate glasses. Although average local structures are relatively well understood^[1], there has been little progress in understanding the intermediate-range structure, which has been suggested to play a key role in the compaction mechanism under pressure.

Many classical and first-principles molecular dynamics (FPMD)^[2] studies have been performed to tackle this issue. Classical MD relies on empirical data and gives widely varying results depending on the parameterization. FPMD, on the other hand, is computationally expensive; it is virtually impossible to explore intermediate-range order due to the small number of atoms it can handle. Another issue is the accuracy of the approximations used in FPMD; standard approximations such as generalized gradient approximation (GGA) neglect the nonlocal dispersion interaction, which has been suggested to be important for reproducing the pressure-induced structural transition^[3]. Although more accurate approximations are available, they are even more computationally intensive and cannot be used directly for long-time simulation of glassy systems. In this work, we address these issues using neural network potential molecular dynamics (NNP-MD)^[4], where FPMD data is fitted with a machine-learning potential to enable large-scale and long-time molecular dynamics simulations with FPMD accuracy.

We employ VASP^[5] code for generating the training data set using three different approximation: the standard GGA-PBE, vdW-DF2-B86R^[6] which contains nonlocal correlation, and HSE06^[7] which corrects the delocalization error in GGA but is ~100 times more costly. A melt-quench process was simulated using FPMD using GGA-PBE and vdW-DF2-B86R with a 96-atom model to obtain glass structure from crystal. The glass and crystal structure under isotropic pressure were also simulated. The training dataset was then extracted from these simulation trajectories, which finally contains 1850 structures and their total energies. The training data for HSE06-based NNP was collected by recalculating the structures contained in the training data of the GGA-PBE. We employed SIMPLE-NN^[8] code for construction of neural network potential from the training dataset. The constructed NNPs were used for melt-quench glass formation and compaction simulations using LAMMPS code on 3240-atom supercell, which are clearly beyond the reach of FPMD.

Total structure factors obtained from our NNP-MD glass structures are shown in figure 1. The GGA-PBE result is in decent agreement with experiment, although the peak position at high k side is shifted to low k side and the peak intensity at $k = 1.5 \text{ \AA}^{-1}$ is slightly underestimated. The discrepancy in the high k region comes from usual GGA-PBE trend to overestimate covalent bond lengths. The low k peak at 1.5 \AA^{-1} implies intermediate-range order in the glass network. The vdW-DF2-B86R showed a larger deviation from experiment, which was surprising since we expected an improvement due to inclusion of nonlocal interactions. HSE06, the most expensive approximation examined here, yields almost perfect agreement for the bond length and best agreement in the low- k intensity. Moreover, only HSE06 could reproduce the preservation of the four-fold Ge-O coordination up to 4 GPa observed in experiment. In summary, NNP technology enabled large scale MD simulation of glass formation with HSE06 accuracy, which turned out to be imperative for accurate description of the pressure-induced structural transition in this prototypical glass network.

References

- 1) P. S. Salmon et al., Phys. Rev. Lett. 96, 235502 (2006).
- 2) X. F. Zhu et al., Phys. B: Condens. Matter 404 4178 (2009)
- 3) D. Marrocchelli et al., Mol Phys. 107 443 (2009)
- 4) J. Behler et al., Phys. Rev. Lett., 98 146401 (2007)
- 5) G. Kresse et al., Phys. Rev. B 52 11169 (1996)
- 6) I. Hamada, Phys. Rev. B 89 121103(R) (2014)
- 7) A. V. Krugau et al., J. Chem. Phys., 125 224106 (2006)
- 8) K. Lee et al., Comput. Phys. Commun. 242 95-103 (2019)

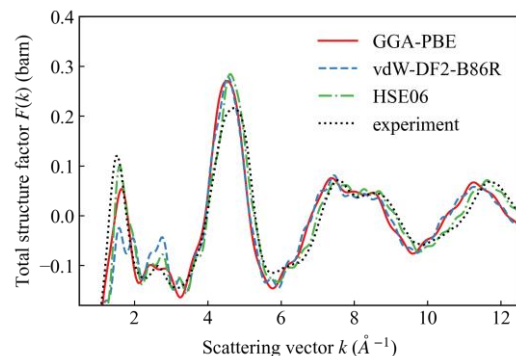


Fig. 1. Each total structure factors were obtained from NNP-MD and experiment^[1].

Optical properties of molten pure copper by density functional theory

*Susumu Kato¹, Shota Ono², Atsushi Sunahara³, Yuji Sato⁴, Masahiro Tsukamoto⁴

¹ Research Institute for Advanced Electronics and Photonics, National Institute of Advanced Industrial Science and Technology (AIST), Tsukuba, 305-8568, Japan, ² Department of Electrical, Electronic and Computer Engineering, Gifu University, Gifu, 501-1193, Japan, ³ Center for Materials Under eXtreme Environment (CMUXE), School of Nuclear Engineering, Purdue University, West Lafayette, 47907, USA, ⁴ Joining and Welding Research Institute (JWRI), Osaka University, Ibaraki, 567-0047, Japan

* s.kato@aist.go.jp

Keywords: Liquid metal, Density-functional theory, Joint density-of-state, Dielectric function,

Copper is widely used in automobile batteries, motors, and so on due to high electric conductivity. The welding of copper, which is a highly infrared-light-reflective material, is performed with blue and green lasers in addition to an infrared laser¹⁻³. Quality of the laser welding is determined by the absorptivity, which strongly depends on the laser wavelength and temperature.

Optical properties of pure copper have been a subject of many studies since the 1950's⁴⁻⁹. Some pioneering studies of electronic structure in liquid have been carried out using ab initio simulations¹⁰⁻¹¹. Optical properties of high-temperature solid and liquid copper in the visible light were not so clear in comparison with them in the infrared light¹²⁻¹⁴.

In this paper, the optical properties of molten pure copper investigated by the Density Functional Theory (DFT) using QUANTUM ESPRESSO package¹⁵. We used the pseudopotentials Cu.pbe-dn-rrkjus_psl.1.0.0.UPF from the QUANTUM ESPRESSO pseudopotential data base. The electron density of states (DOS) in face-centered cubic and liquid copper are shown in Figures 1(a) and (b). The density of 7.99 g/cc is chosen at the melting temperature of copper. The simulations were performed on a supercell containing 32 atoms and its size was (7.5Å)³.

The change of the absorptivity at the phase transition is considered using the joint density of states and complex dielectric constant obtained from DTF.

References (Example: non-mandatory, 10 point):

- 1) Y. Sato et al., Appl. Surf. Sci. 480, pp. 861–867 (2019).
- 2) S. Grabmann et al., Procedia CIRP 94, pp. 582–586 (2020).
- 3) M. Hummel et al., J Adv Join Process 1, 100012 (2020).
- 4) L.G. Schulz, J. Opt. Soc. Am. 44, pp.357–362 (1954). L.G. Schulz and F.R. Tangherlini, J. Opt. Soc. Am. 44, pp. 362–368 (1954).
- 5) S. Roberts, Phys. Rev. 118, pp.1509–1518 (1960).
- 6) G.P. Pells and M. Shiga, J. Phys, C 2, 1835–1846 (1969).
- 7) P.B. Johnson and R.W. Christy, Phys. Rev. B 6, pp.4370–4379 (1972). P.B. Johnson and R.W. Christy, Phys Rev B 11, pp.1315–1323 (1975).
- 9) D.J. Nash and J.R. Sambles, J. Mod. Opt. 42, pp.1639–1647 (1995).
- 10) E.G. Maksimov et al., J. Phys. F: Met. Phys. 18, pp.833–849 (1988)
- 11) A. Pasquarello et al., Phys. Rev. Lett. 69, pp.1982–1985 (1992).
- 12) J.C. Miller, Phil. Mag. 20, pp.1115–1132 (1969).
- 13) N. R. Comins, Phil. Mag. 25, pp.817–831 (1972).
- 14) K. Ujihara, J. Appl. Phys. 43, pp.2376–2383 (1972).
- 15) P. Giannozzi et al., J. Phys. Condens. Matter 21, 395502 (19pp) (2009). P. Giannozzi et al., J. Phys.: Condens. Matter 29, 465901 (2017). Giannozzi, P. et al., J. Chem. Phys. 152, 154105 (2020).

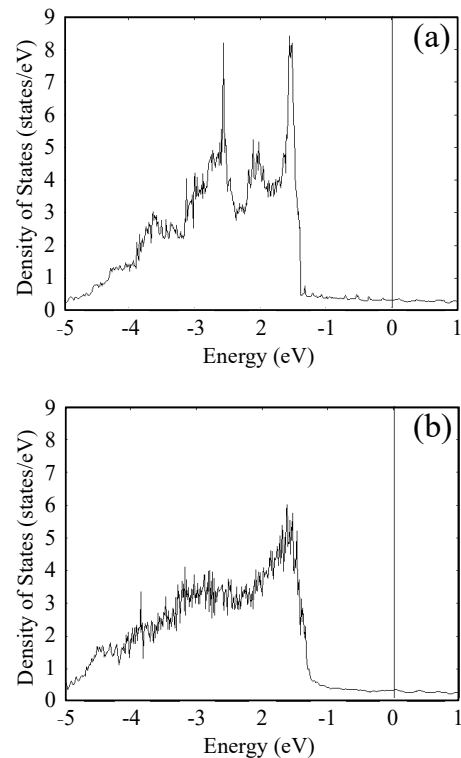


Fig. 1. Electron density of states (DOS) in (a) face-centered cubic and (b) liquid copper.

Development and optimization of sulfur-containing novel Ti-based Bulk Metallic Glasses and the correlation between primary crystalline phases, thermal stability and mechanical properties

*Lucas Matthias Ruschel¹, Bastian Adam¹, Oliver Gross², Nico Neuber¹, Maximilian Frey¹, Ralf Busch¹

¹Chair of Metallic Materials, Saarland University, 66123 Saarbrücken, Germany

²Amorphous Metal Solutions GmbH, 66424 Homburg, Germany

*lucas.ruschel@uni-saarland.de

Keywords: Bulk metallic glass, Titanium alloys, Mechanical properties, Thermal stability, Sulfur, Phase transformation

Amorphous metals possess a disordered atomic structure which is responsible for their high strength and elasticity in comparison to their crystalline counterparts. Recently, our group reported on the bulk glass formation in the Ti-Ni-S and Ti-Ni-Cu-S system [1], [2]. As sulfur addition is very effective in both systems, its influence on the $Ti_{33.4}Zr_{33.3}Cu_{33.3}$ eutectic composition in terms of glass forming ability, thermal stability and mechanical properties was investigated by conventional X-ray diffraction, differential scanning calorimetry and three-point beam bending experiments. A novel bulk glass forming region with a critical casting diameter of 4 mm was found in the quaternary Ti-Zr-Cu-S system, however, brittle fracture behavior was predominant. Various alloying strategies were employed to improve mechanical properties and a compositional transition from brittle to ductile has been found (e.g. for $Ti_{36}Zr_{33.5}Cu_{24.5}S_6$). A change of the primary precipitating phases from a C14 Laves (Frank-Kasper structure) to an intermetallic (Ti, Zr)₂Cu phase (and vice versa) can be observed, as well as a stabilization/destabilization of the glass transition. The origin of a thermally unstable behavior resides in the easy formation of the icosahedral phase upon heating, which is structurally close to the supposedly predominant icosahedral short-range order in the amorphous state. The systematic study carried out in this work indicates a strong correlation between primary crystallizing phase and thermal stability with the mechanical properties in Ti-based bulk glass forming alloys. The transition from the Laves to the intermetallic phase resulted in a distinct glass transition and ultimately improved mechanical properties with ductility in bending. It is assumed that this enhancement is directly related to the destabilization of the icosahedral short-range order in the amorphous structure.

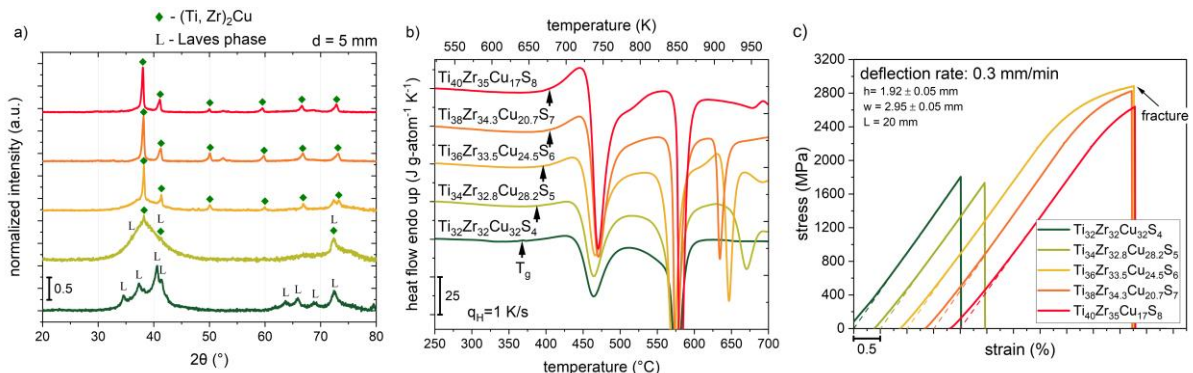


Figure 1 (a) XRD patterns of 5 mm partially crystalline samples. The primary precipitating phase is changing from a C14 Laves phase to the intermetallic (Ti, Zr)₂Cu phase. (b) In addition, the thermal stability of fully amorphous samples increases as the icosahedral phase (first exothermic event) is pushed to higher temperatures. (c) The change in primary phase and stabilization of the glass transition indicate a destabilized icosahedral short-range order, ultimately lead to a ductile fracture behavior in 3-point beam bending.

References:

- 1) Gross, O. et al, *Journal of Physics: Condensed Matter*, 84(20), 4029–4031 (2020)
- 2) A. Kuball et al., *J. Alloys Compd.*, vol. 790, pp. 337–346, Jun. (2019)

Structural analysis of etidronate disodium

*H. Shimakura¹, T. Hashizuka², and K. Ohara³

¹NUPALS, Niigata-shi, 956-8603, Japan, ²Dainippon Sumitomo Pharma Co., Ltd., Osaka, 554-0022, Japan,

³Japan Synchrotron Radiation Research Institute (JASRI), Sayo, Hyogo 679-5198, Japan

Keywords: RMC, MD simulation, Medical supplies

Generally, for low-molecular-weight pharmaceuticals, the active pharmaceutical ingredient (API) has been formulated as a solid (crystal) formulation from the viewpoint of drug stability and homogeneity. On the other hand, amorphous formulations of the API are increasingly being developed for difficult-to-water-soluble drugs, transdermal drugs, liposome formulations, and other products. However, amorphous formulations need to be investigated in detail due to the high risks associated with crystal transition and stability.

This study is a structural study of the amorphous molecular structure of disodium etidronate (Didronel), which is currently marketed as an active pharmaceutical ingredient in an amorphous state. It has been found that the stability and molecular shape of the amorphous state varies depending on the generation method. With the increase in the number of pharmaceuticals in the form, methods for evaluating the stability of these amorphous drug products have been developed not only by conventional thermal analysis and long-term stability testing, but also by predicting physical stability based on molecular mobility [1], and there is a need to establish a method that can be used for many amorphous drug products.

Figure 1 shows the structure factors $S(Q)$ of disodium etidronate tetrahydrate and anhydride crystals and the structure factor calculated based on the tetrahydrate crystal structure reported by Barnett et al. The tetrahydrate crystals measured in this study show almost the same spectra as the structure reported by them.

Figure 2 shows the reduced pair distribution function $G(r)$ for the disodium etidronate tetrahydrate and anhydride crystals, showing that there is slight change in the peaks associated with molecular geometry at distances below 4.0 Å, indicating that the structure of the etidronate molecule remains unchanged. On the other hand, in the region corresponding to the intermolecular distance, above 4.0 Å, differences between the tetrahydrate and anhydride crystals are apparent. In particular, the anhydride crystal shows a peak at 4.0-5.0 Å, indicating that there is a difference in the arrangement of etidronic acid molecules.

In my poster, we will mention to structural comparisons of them in crystals and amorphous.

References:

[1] E. Yonemochi, *Cryobiology and Cryotechnology*, **51** (2005) 25

[2] B. L. Barnett, L. C. Strickland, *Acta Crystallographica, Section B* **35** (1979) 1212

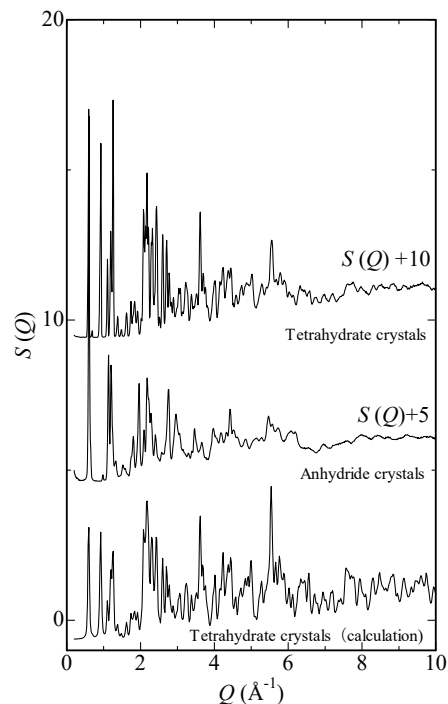


Fig.1 Structure factors of etidronate II sodium tetrahydrate crystals and anhydride crystals obtained experimentally and calculated from the structure reported by Barnett et al.

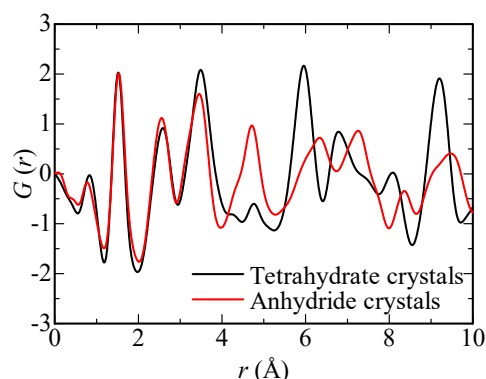


Fig.2 Reduced pair distribution function of etidronate II sodium tetrahydrate crystals and anhydride crystals

Topological analysis for α -AgI

*S. Tahara¹, H. Shimakura², and T. Fukami¹

¹Univ. of the Ryukyus, Nishihara-cho, 903-0213, Japan, ²NUPALS, Niigata-shi, 956-8603, Japan

Keywords: Superionic conductor, MD simulation, persistent homology analysis, Structure.

AgI is well known as a superionic conductor in the high temperature solid (α) phase where Ag ions can migrate through interstitial sites of b.c.c sublattice of I ions.¹⁾ In the case of typical salts such as RbCl, the first neighboring distance of cation-cation correlation is the almost same as that of anion-anion in both solid and liquid phases, however the first neighboring distance of Ag-Ag in AgI is anomalously close.²⁾ The anomalous Ag-Ag correlation in α - and molten AgI has been studied by several methods, for example reverse Monte Carlo method³⁻⁴⁾, classical MD simulations,⁵⁾ and *ab initio* MD simulations⁶⁾. The mechanism of Ag conduction is discussed from the viewpoint of the one-dimensional stream of Ag ions³⁻⁴⁾ and the cooperation between Ag and I ions⁶⁾. The observation of the first sharp diffraction peak at $Q = 1 \text{ \AA}^{-1}$ in the total structure factor for AgI and the partial structural factor of Ag-Ag are interpreted to be due to such an anomalous distribution of Ag ions. In order to reproduce such an anomalous Ag distribution by classical MD simulation, the polarizable ion model (PIM) which incorporates the polarization effect of anions by a self-consistent algorithm is important⁵⁾.

In the present study, we carried out the classical MD simulation for α -AgI at 573 K with PIM and analyzed the atomic configurations by means of persistent homology analysis method which is new geometrical mathematics method. Figure 1 shows that the 1-dimensional persistence diagram (PD) for Ag distribution for rigid ion model (RIM) and PIM simulations. Obviously, the PD distribution spreads due to the anion polarization, indicating that the two-dimensional polygons found in the distribution of Ag ions are diversified. In the presentation, we will report on the details of PD analysis, including 2-dimensional PD.

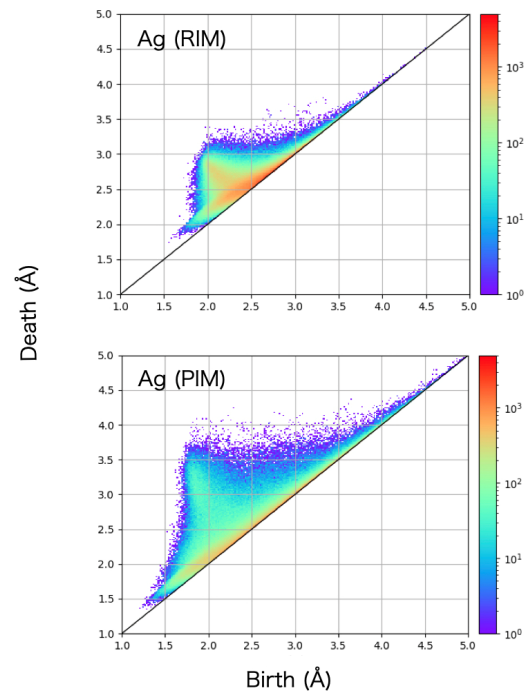


Fig.1 1-dimensional PD for Ag distribution in α -AgI at 573 K of RIM and PIM simulations.

References:

- 1) C. Tubandt and E. Lorentz, Z. Phys. Chem. 87, 513 (1914).
- 2) Y. Tsuchiya, J. Phys. C: Solid State Phys. 20, 5001 (1987).
- 3) Y. Kawakita, S. Tahara, H. Fujii, S. Kohara, and S. Takeda, J. Phys.:Condens. Matter 19, 335201 (2007).
- 4) S. Tahara, H. Ueno, K. Ohara, Y. Kawakita, S. Kohara, S. Ohno and S. Takeda, J. Phys.: Condens. Matter 23, 235102 (2011).
- 5) V. Bitrián and J. Trullás, J. Phys. Chem. B 112, 1718 (2008).
- 6) F. Shimojo, T. Inoue, M. Aniya, T. Sugahara, and Y. Miyata, J. Phys. Soc. Japan 75, 114602 (2006).

Glass transition temperature of nickel based binary alloys and its interparticle dynamics features

Dmitrii Fleita^{,1,2}

¹HSE University, Moscow, 101000, Russia

²Joint Institute for High Temperatures of the Russian Academy of Sciences, Moscow, 125412, Russia

*fleyta.du@phystech.edu

Keywords: molecular dynamics, metastable states, spatio-temporal correlations, vitrification.

Particle transport processes in dense melts are governed by highly cooperative phenomena. This makes available to predict their physical properties based on their structural-temporal properties.

We discuss the dependence of self- and inter-diffusion and collective coefficients on temperature and composition of melts. Earlier it was shown that certain spatio-temporal characteristics reflect the processes of transfer and glass transition [1]. The analysis of the behavior of the glass transition temperature is compared with experimental data for similar systems [2,3]. The analysis of interparticle interactions demonstrates a similar dependence of partial functions on the percentage composition of alloys found earlier in experiment [4] and MD simulation [5], reaching saturation with a change in the qualitative nature of the collective transfer of melt particles.

This work was supported by the grant of the President of Russian Federation (project No. 17-79-20391). The authors acknowledge the JIHT RAS HPC and HSE University HPC Cluster "CHARISMa".

References:

- 1) D. Fleita, G. Norman and V. Pisarev, *J. Phys.: Condens. Matter* **32**, p. 214009 (2020)
- 2) P. Kuhn, J. Horbach, F. Kargl, A. Meyer and T. Voigtmann, *Phys. Rev. B* **90**, p. 024309 (2014)
- 3) B. Nowak, D. Holland-Moritz, F. Yang, Th. Voigtmann, Z. Evenson, T.C. Hansen and A. Meyer, *Phys. Rev. B* **96**, p. 054201 (2017)
- 4) B. Nowak, D. Holland-Moritz, F. Yang, Th. Voigtmann, T. Kordel, T.C. Hansen and A. Meyer, *Phys. Rev. Mat.* **1**, p. 025603 (2017)
- 5) D. Fleita, G. Norman and V. Pisarev, *J. Phys.: Conf. Ser.* **1147**, p. 012015 (2017)

Local density fluctuation realized in Nb-Ni amorphous alloys

*T. Kawamata¹, N. Takehara¹, R. Kuroda¹, K. Sugiyama¹

¹Institute of Material Research, Tohoku University, 980-8577, Japan
kawamata@tohoku.ac.jp

Keywords: Amorphous alloy, Anomalous X-ray scattering, Reverse Monte-Carlo simulation.

The details of short and medium-range ordered structures realized in amorphous alloys are associated with their interesting material properties such as high GFA and high strength. For the understanding the fine structure of amorphous alloys, AXS-RMC, which is a combination of anomalous X-ray scattering (AXS) and RMC-simulation, could be counted as one of the powerful analytical tools¹. In this study, we report on the unique geometrical features with respect to the nearest neighbor pairs and the diversification of short-range ordered structures observed in Nb-Ni amorphous alloys².

Nb-Ni amorphous alloys were prepared by a copper single roll rapid quenching method. The anomalous X-ray scattering measurements were performed at the beam line BL-7C, high energy accelerator research organization (Tsukuba, Japan). In the present AXS analysis, X-ray diffraction measurement using two different energies were carried out at the Nb and Ni *K* edges. RMC analysis was performed using the environmental structure information obtained by the AXS as a constraint, and a three-dimensional amorphous structure model (RMC-model) was created so as to reproduce the environmental structure information around the constituent elements. The DRP (Dense Random packing of hard sphere) -model was used as the initial model for the RMC simulation.

As an example, the result of RMC simulation for Nb₆₀Ni₄₀ amorphous alloy is shown in Fig. 1. The DRP-model reproduces the fundamental features of the ordinary ($Q_i(Q)$) and environmental interference functions ($\Delta Q_{i\text{Nb}}(Q)$ and $\Delta Q_{i\text{Ni}}(Q)$) obtained from the experiments, however the fine oscillation profiles such as the split observed at the second peak at about 50 nm⁻¹ for every $Q_i(Q)$ s could not be reproduced well. On the other hand, the RMC-model is able to reproduce the details of both the ordinary and environmental interference functions. This fact indicates that RMC-model created by AXS-RMC method allows to discuss the structural role of constituent elements in Nb-Ni amorphous alloy. Fig. 2 shows the Nb-Nb partial distribution functions, $g(r)$ s calculated from DRP and RMC-models of Nb-Ni amorphous alloys. The $g(r)$ s calculated from DRP-model show similar shape in the nearest neighbor region for all alloy compositions, indicating single peaks near the sum of Goldschmidt radius for Nb (0.294nm). On the other hand, the present AXS-RMC analysis suggests the characteristic Nb-Nb correlations with a harmony of short (0.250 nm) and long (0.320 nm) distances. The subsequent CNA (common neighbor analysis) with respect to the Nb-Nb correlations revealed the unique CN structures of [666]_{CN} and [433]_{CN}. The former [666]_{CN} structure is associated well with dense tetrahedral packing and developed in the Nb-Nb correlations on the short-range region (0.240 nm to 0.280 nm). The latter [433]_{CN} structure represents the correlations developing on the long-range side (0.310 nm to 0.340 nm), which is associated with low-density octahedral filling. In other words, the variation of Nb-Nb pairs observed at the nearest neighbor region is attributed to the fluctuation of local density in Nb-Ni amorphous alloys, which could not be explained by DRP-model.

1) T. Kawamata, T. Muto and K. Sugiyama, Mater. Trans. 62, 20 (2021).

2) L. Xia, W. H. Li, S. S. Fang, B.C. Wei and Y. D. Dong, J. Appl. Phys. 99, 026103 (2006).

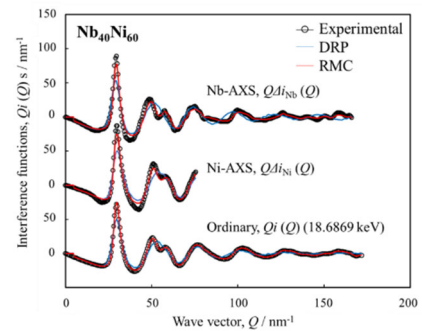


Fig. 1 Ordinary and environmental interference functions of Nb₄₀Ni₆₀ amorphous alloy calculated from DRP and RMC-model.

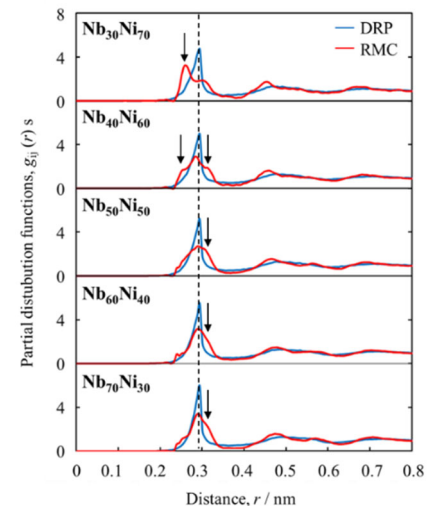


Fig. 2 Nb-Nb partial distribution functions, $g(r)$ s of DRP and RMC-models for Nb-Ni amorphous alloys. Vertical dotted lines in this figure indicate sum of Goldschmidt radius for Nb atoms.

Unsupervised topological learning of crystal nucleation in pure metals

Sébastien Becker^{1,2}, Emilie Devijver², Rémi Molinier³, *Noel Jakse¹

¹ Université Grenoble-Alpes, CNRS, Grenoble INP, SIMaP, F-38000 Grenoble, France.

² Université Grenoble-Alpes, CNRS, Grenoble INP, LIG, F-38000 Grenoble, France.

³ Université Grenoble-Alpes, CNRS, IF, F-38000 Grenoble, France.

* noel.jakse@grenoble-inp.fr

Keywords: Atomic structures, Molecular dynamics, Homogeneous nucleation, Topological data analysis, Machine learning.

Crystal nucleation in liquids is a fundamental process that we experience daily in nature (e.g., formation of ice) or through the human industry and creation of materials. Such a phenomenon is initiated at atomic scales that are still experimentally inaccessible, making the understanding of the underlying physics challenging. Thus, large-scale atomic-level simulations have been shown to provide a powerful way to investigate detailed information at such small spacetime levels [1]. From this perspective, we propose an unsupervised machine learning method [2] for the autonomous structural analysis of materials based on original topological descriptors of local atomic structures computed from persistent homology [3, 4]. From this protocol [5], a model is learned in course of nucleation in order to identify, without *a priori* on a system, clusters of atomic structures which arise in the process. This method has been applied to investigate several molecular dynamics configurations up to 10 million atoms undergoing homogeneous nucleation at the nose of the time-temperature-transformation curves of four pure metals chosen for the variety of their crystalline phase [6]; namely: Tantalum (Ta) and Zirconium (Zr) for body-centered cubic, Aluminium (Al) as face-centered cubic and Magnesium (Mg) for hexagonal close-packed. Precursors of the crystalline orders are highlighted as emerging from low fivefold symmetry regions in structural heterogeneities of the supercooled liquids and a general behavior for all the nuclei and embryos shows a concurrent emergence of the translational and orientational orderings. This unsupervised learning approach more generally opens the route to further investigation of atomic level structure-dependent phenomena.

[1] G. C. Sosso, J. Chen, S. J. Cox, M. Fitzner, P. Pedevilla, A. Zen, and A. Michaelides, *Chem. Rev.* **116**, 7078 (2016).

[2] M. Ceriotti, *J. Chem. Phys.* **150**, 150901 (2019).

[3] H. Edelsbrunner, D. Letscher, and A. Zomorodian, *Discrete Comput Geom* **28**, 511 (2002).

[4] A. Zomorodian and G. Carlsson, *Discrete Comput Geom* **33**, 249 (2005).

[5] S. Becker, E. Devijver, R. Molinier, and N. Jakse (*Phys. Rev. E*, accepted 2022).

[6] S. Becker, E. Devijver, R. Molinier, and N. Jakse, *Sci. Rep. (Nature)* **12**, 3195 (2022).